To the Graduate Council:

I am submitting herewith a thesis written by John K. Foster entitled "Development of a Computational Model of the Gas Dynamic and Ablation Effects in Plasma Armature Railguns." I have examined the final copy of this thesis for form and content and recommend that it be accepted in partial fulfillment of the requirements for the degree of Master of Science, with a major in Aerospace Engineering.

Dr. Roger Crawford, Major Professor

We have read this thesis and
recommend its acceptance:

Accepted for the Council:

Associate Vice Chancellor
and Dean of the Graduate School

STATEMENT OF PERMISSION TO USE

In presenting this thesis in partial fulfillment of the requirements for a Master's degree at the University of Tennessee Space Institute, I agree that the Library shall make it available to borrowers under rules of the Library. Brief quotations from this thesis are allowable without special permission, provided that accurate acknowledgement of the source is made.

Permission for extensive quotation from or reproduction of this thesis may be granted by my major professor, or in his absence, by the head of the Interlibrary Services when, in the opinion of either, the proposed use of the material is for scholarly purposes. Any copying or use of the material in this thesis for financial gain shall not be allowed without my written permission.

Signature John K. Foster

Date January 5, 1993

DEVELOPMENT OF A COMPUTATIONAL MODEL OF THE GAS DYNAMIC AND ABLATION EFFECTS IN PLASMA ARMATURE RAILGUNS

A Thesis

Presented for the

Master of Science

Aerospace Engineering

The University of Tennessee, Knoxville

John K. Foster

May 1993

Acknowledgements

The author would like to take this opportunity to thank several individuals for their assistance in my endeavor. I would like to express my appreciation to my faculty advisor, Dr. Roger Crawford, for his patience and assistance during the preparation of this thesis. I would like to thank both Dr. Crawford and Dr. Dennis Keefer for allowing me to assist them on the railgun project at UTSI. I would like to thank Dr. Vakili and Dr. Peters for serving on my faculty committee and the interest they exhibited in my work.

I want to thank the technical staff of the Center for Laser Application, especially Bruce Hill and Newton Wright, for their dedication to the railgun program and the help they provided to me as I worked. I also want to thank my fellow graduate students, Jaime Taylor and John Wise, for their assistance in data acquisition and analysis. I especially want to thank Jaime for his insight into the problem of railgun ablation. The amount of help he provided cannot be overstated.

Abstract

Railgun performance has not reached the expected level as originally indicated by electromagnetic theory. That is, projectile exit velocities do not approach the extremely high velocities that ideal analysis indicated   Various researchers re-examined railgun theory, and attempted to determine ways of improving railgun performance.

Research at the University of Tennessee Space Institute has been conducted to explore the causes of that decrease in performance. Ablation in the railgun bore has been identified as a factor in the reduction of peak expected performance. However, some experimental data indicated that some ablation effects, primarily the electrothermal interaction of the expanding ablated material and the driving gas, actually increased performance under certain conditions.

The purpose of this thesis is to describe the effort undertaken to identify some of the effects that ablation imposes on the performance of railguns, and to describe the computer model created to simulate these effects. This computer model included routines which accounted for the gas dynamics of the injector's driving gas through use of the (1)time-dependent method of characteristics, (2) the electromagnetic forces occurring within the electric arc armature, (3) the rate of ablation of material from the wall, and (4) the electrothermal interaction between each of these. A description is made of each routine's impact on the simulation, and each routine's importance to the calculation procedure is identified.

This effort concluded that the electrothermal interaction which occurred in each shot caused the driving potential of the injector light gas to increase, thereby increasing the force attributable to the light gas. This increase in force caused the railgun to produce velocities higher than were expected.

DEDICATION

I would like to dedicate this thesis to my beautiful wife, Norma, for all the love and support she has given to me during my years at UTSI. All the patience she showed to me during those long, frustrating nights of homework, computer typing, and thesis preparation were appreciated more than she will ever realize. May we share a long, prosperous, healthy, and happy life together along with our beautiful new baby, Rachel.

TABLE OF CONTENTS

LIST OF FIGURES

LIST OF TABLES

NOMENCLATURE

a ....Speed of Sound behind Wave (m/s)

A_{cs} ....Bore Cross Sectional Area (m^2)

C_1 ....Capacitance of inner rail circuit (f)

C_2 ....Capacitance of outer rail circuit (f)

C_f ....Coefficient of Friction of Gas

C_{farm} ....Coefficient of Friction of Armature

C_p ....Constant Pressure Specific Heat of Gas (J/kg°K)

C_{pa} ....Specific Heat of Ablated Material (J/kg°K)

C_{parm} ....Specific Heat of Armature Material (J/kg°K)

D ....Diameter of Bore (m)

dP ....Differential of Pressure across Wave (Pa)

dP_z ....Differential of Pressure across Ablation Region Interface(Pa)

E_{dis} ....Energy Dissipated into the Ablated Material (J)

$E_{rad\,(Abl)}$ ....Radiated Energy Transferred from the Ablated Material (J)

$E_{rad\,(Arm)}$ ....Radiated Energy Transferred from the Armature (J)

f_d ....Viscous Drag of the Driving or In-bore Gas (N)

F_D ....Viscous Drag of the Armature (N)

F_L ....Total Electromagnetic Force (N)

I_1 ....Inner rail current (A)

I_2 ....Outer rail current (A)

I_E ....Electrode current (A)

J ....Square Impulse Current

k ....Coefficient of Rail Coupling

k_1 ....Empirical Ablation Parameter

k_1 ....Empirical Ablation Parameter

k_2 ....Empirical Ablation Parameter

k_3 ....Empirical Ablation Parameter

L'_1 ....Inductance/length of inner rail (H/m)

L'_2 ....Inductance/length of outer rail (H/m)

L_1 ....Inductance of Inner rail due to Projectile Position.(H)

L_{abl} ....Length of Ablation Region (m)

L_{arm} ....Length of Armature (m)

LGG ....Light Gas Gun (m)

L_{LGG} ....Length of Light Gas Gun (m)

L_{O1} ....Inductance of inner rails (H)

L_p ....Length of Projectile (m)

L_{RG} ....Length of Railgun (m)

L_{T1} ....Total Inductance of Inner Rail (H)

L_{T2} ....Total Inductance of Outer Rail (H)

M'_{12} ....Mutual Inductance/Length of the rails (H/m)

M_{12} ....Mutual Inductance of the rails (H)

m_a ....Total Mass of Ablated Material (kg)

m_{arm} ....Mass of Armature (kg)

MAVIS ....Magnetic Velocity Induction Sensor

m_p ....Projectile Mass (kg)

P ....Gas Pressure (Pa)

PT1 ....Pressure Transducer #1

PT2 ....Pressure Transducer #2

R ....Gas Constant ($m^2/(s^2\ °K)$)

R_1 ....Resistance of inner rail circuit (Ohms)

R_2 ....Resistance of outer rail circuit (Ohms)

Q..................................Transported Charge

Re_D ....Reynold's Number based on bore Diameter

R_u ....Universal Gas Constant (Nm/(kgmol °K))

S..................................Characteristic Temperature of Light Gas (K)

T..................................Temperature of Gas (K)

T_0 ....Reference Temperature for Light Gas (K)

t..................................Time (s)

T_a ....Temperature of ablation region (K)

T_{abl} ....Temperature of ablated material (K)

t_{cb1} ....Crowbar Time for inner rail circuit (s)

t_{cb2} ....Crowbar Time for outer rail circuit (s)

t_d ....Delay time between PT1 initiation and fusing (s)

t_{fire} ....Time between firing of outer and inner rails (s)

t_{fuse} ....Time when projectile passes X_{PT1} (s)

u..................................Velocity of Gas (m/s)

V_a ....Armature Voltage (V)

V_b ....Breech Voltage (V)

V_{01} ....Initial Voltage charge on inner rail circuit (V)

V_{02} ....Initial Voltage charge on outer rail circuit (V)

V_{C1} ....Voltage charge on inner rail circuit (V)

V_{C2} ....Voltage charge on outer rail circuit (V)

V_{fire} ....Firing Voltage (V)

V_{O11} ....Empirical Constant for Voltage Model

V_p ....Projectile Velocity (m/s)

V_{sw} ....Velocity of Shock Wave (m/s)

V_w ....Velocity of Wave (m/s)

V_z ....Velocity of Ablation Region/Neutral Gas Interface (m/s)

W.................................Molecular weight (kg/kgmol)

x_p ....Position of Projectile (m)

X_{PT1} ....X Location of PT1 Pressure Probe (m)

X_{PT2} ....X Location of PT2 Pressure Probe (m)

x_w ....Position of Wave (m)

x_z ....Position of Ablation Region/Neutral Gas Interface (m/s)

α ....Ablation Coefficient (g/MJ)

β ....Fraction of Armature Power Dissipated into Ablation Region

γ ....Ratio of Specific Heats

ε ....Emissivity of Bore

η ....Shape Parameter for Empirical Pressure Model

θ ....Experimental Decay Constant for Empirical Pressure Model

λ ....Fraction of ablated mass added to the Armature

ω ....Shape Parameter for Empirical Pressure Model

Ω_{arm} ....Resistance of Armature(Ohms)

ρ ....Density of Gas behind Projectile (kg/m^3)

ρ_a ....Density of Ablated Material (kg/m^3)

ρ_{arm} ....Density of Armature Material (kg/m^3)

ρ_E ....Density of Electrode Material (kg/m^3)

I. INTRODUCTION

Hypervelocity projectiles have recently received high priority within the defense community especially when considering the Strategic Defense Initiative's requirement for the interception and destruction of enemy missiles and warheads in space with kinetic kill weaponry. Of the several concepts under consideration, plasma armature railguns presently offered the most potential, but several problems existed which affect railgun performance, and their physical nature was not fully understood.

Electromagnetic theory predicted for a simple railgun that the Lorentz force, F_L, created by the passage of a current through the armature behind the projectile was given by the equation:

$$F_L = \frac{1}{2} L' I^2, \tag{1}$$

where L' was the self-inductance per unit length of the rail and I was the armature current.[7] Therefore, as current increased through the armature, Lorentz force increased, and projectile acceleration increased. However, the theoretical velocities predicted by this analysis were never reached because of several loss mechanisms that were associated with railgun operation.

Several researchers looked into the problems associated with the operation of railguns. Parker[1] identified several problems with plasma armature railguns which include the following: 1) viscous drag, 2) momentum loss from the ablated material, and 3) arc restrike into the region behind the projectile. Aigner[2] discussed the possible causes of ablation and attempted to determine the performance degradation that it induced. Pyatt and McNab[3] discussed some of the limiting effects in railgun performance including radiation and convective heat trasnsfer. Rolader and Batteh[4] identified the effects of in-bore gas on the performance of railguns and offered a simplified model of these effects.

Batteh[5] also indicated that some transient phenomena, such as damped oscillation of the armature length, are caused by the addition of ablated material into the armature. He asserted that an understanding of these transient phenomena was important to the overall understanding of the railgun performance.

However, little effort had been concentrated on the interaction of the ablated material with the driving gas from the injector mechanism. Research conducted at the University of Tennessee Space Institute indicated that even though ablation did have an impact on performance caused by secondary arc restrike, the electrothermal interaction of the ablation region and driving gas caused an increase in railgun performance.[6,7]

It is generally accepted that in order to improve the performance of plasma armature railguns, the effects of ablation has to be understood. An effort is currently underway to examine these electrothermal effects in order to gain a better understanding of the physical nature of the ablation process, and its interaction with electrothermal pressure.

The purpose of this thesis is to describe the development of a one-dimensional, time dependent computational model which was developed to simulate the gas dynamic and ablation effects which occur during railgun operation. First, experimental evidence of the effects of ablation is presented. Second, the model's governing equations for the gas dynamics, electromagnetics, and projectile motion are discussed . Next, the simulation is compared to experimental data acquired at the UTSI railgun facility. Finally, the validity of the railgun model and future considerations are discussed.

Background

Railguns had been investigated since the early 1900's when the Norwegian physicist, Kristian Birkeland[9], built the first railgun device. Projectiles with solid

Solid Armature Railgun

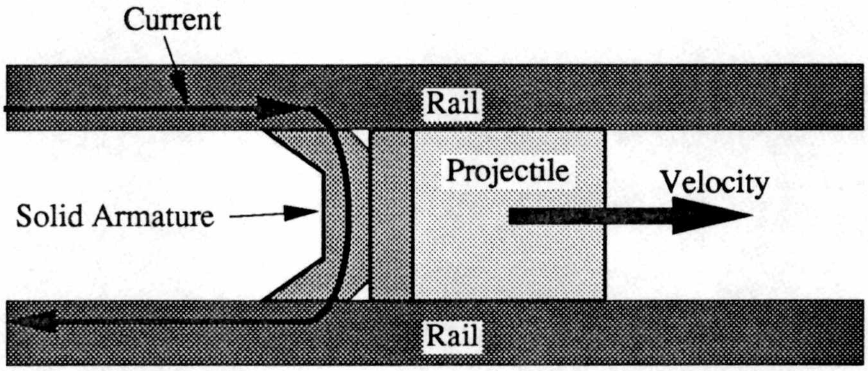

- **Large Armature Mass**
- **Low Power Levels Only (Limited by Armature's Melting Point)**
- **Loss of Contact with rail at high velocities**

Plasma Armature

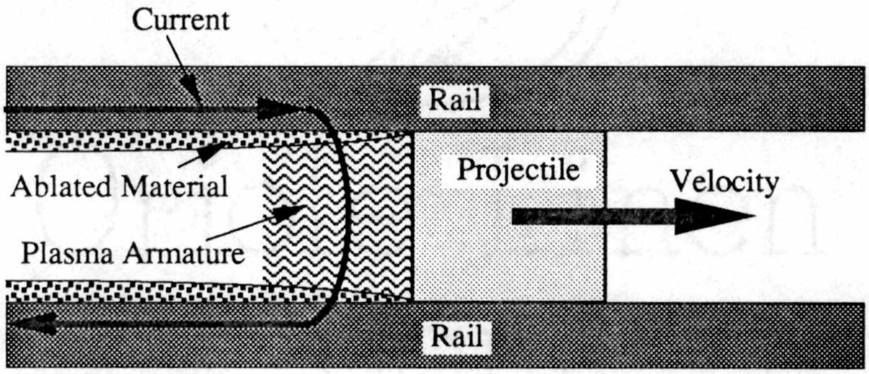

- **Low Armature Mass**
- **Armature Accomodates High Power Levels**
- **Plasma Maintains Contact with Rails**
- **Rail Erosion and Ablation Occur at High Power Levels**

Figure 1. Comparison of Solid and Plasma Armatures in Railguns

armatures could only be accelerated to velocities barely over 3 km/s, and interest in these types of devices soon faded. However, railguns recently received renewed interest with the advent of the plasma armature railgun. Figure 1 shows both the solid and plasma armatures during operation of the railgun.

Plasma armatures offered a tremendous increase in performance as compared to the solid armatures because of the substantial increase in power which can be transmitted through the plasma armature and the low armature mass.[5] Whereas solid armatures were limited by their melting point, plasma armatures theoretically had no limit to the amount of power which could be transmitted. This fact produced much optimism within the electromagnetic research community because plasma armatures offered theoretical projectile exit velocities in excess of 30 km/s.[1]

However, after over 20 years of research, this theoretical performance has yet to be achieved. Few railgun facilites have been able to produce repeatable performance with velocities greater than 6-10 km/s without the implementation of hypervelocity injectors, such as a two stage light gas injector.[10]

Previous Studies of Ablation

Work performed at the Los Alamos National Laboratory under the direction of J. V. Parker indicated that the primary culprit in performance loss was ablation from the rail surface into the railgun bore.[1] Very high power levels existed within the armature which maintained plasma temperatures well above 10000°K. These high temperatures created high radiation[1] and convective heat transfer rates[3] which cause the rail material to vaporize when the armature came into contact with the rail surface. If the temperatures were high enough, some of this rail vapor was ionized and added to the plasma armature. This, in essence, increased the effective projectile mass thereby decreasing acceleration, according to the theory.[1] However experimental data of the armature length indicated that the armature mass was very small and nearly constant for most cases.[11]

Another primary impact of ablation was identified to be viscous drag. According to Parker, the armature underwent intense turbulent flow with very thin boundary layers caused by MHD (Magnetohydrodynamic) effects. This resulted in a relatively high drag force. As ablation products entered the armature, the armature's mass increased thus increasing the viscous drag.[1] This theory of viscous drag being proportional to the rate of ablation has not been validated by computational or experimental methods.[11]

Parker proposed that since the ablated material mixed with the neutral gas, this caused large viscous and momentum losses in the driving gas flow. He theorized that if the projectile continued to be accelerated by the electromagnetic Lorentz forces, and if the driving gas was slowed by the momentum and viscous losses, a low density region was formed behind the plasma armature, thereby negating any driving gas pressure forces on the back of the projectile.[1] However, this theory has not been proven experimentally.[11]

Parker conceded that in low velocity railgun shots (Vexit < 2 km/s), the driving gases were "still able to push against the plasma armature."[12] Still, he did not take any electrothermal expansion of the armature into account or its possible impact on performance.

S. Aigner, working at the Technical University of Munich, studied ablation effects for several years and reached several conclusions.[2] First, he believed that the primary ablation effect depended upon what he termed the transported charge, Q, where:

$$Q = \int I_E \, dt \,. \tag{2}$$

According to his theory, the energy dissipated by this effect was the product of this transported charge and the plasma voltage.

Furthermore, Aigner believed that a secondary effect of ablation, termed the square impulse current, J, where:

$$J = \int I_E^2 \, dt \,. \tag{3}$$

This square impulse current was considered to be responsible for the sputtering of rail material within the bore.[2]

Using these two parameters, Q and J, Aigner developed a formulation for the mass of the ablated material, $m_a(t)$, given by:

$$m_a(t) = \rho_E \, k_1 \left[\int_0^t I(t)_E \, dt \right]^{k_2} \left[\int_0^t I(t)_E^2 \, dt \right]^{k_3} , \tag{4}$$

where ρ_e was the density of the rail material and k_1, k_2, and k_3 were empirically derived ablation parameters. By changing the various k terms, Aigner was able to curve fit the data he obtained in his attempt to find the magnitude of the various effects.[2]

In his analysis, Aigner assumed that all ablation occurred within the armature and was accelerated with the plasma by the Lorentz forces, thereby causing all of the ablation to become effective accelerated mass. This assumption inferred that ablation had only a negative impact on performance. First, momentum losses occurred when the ablated material was accelerated from rest to the velocity of the armature. Second, according to Newton's Law of Motion, the increased mass decreased the projectile acceleration.[2]

In his study, Aigner made no attempt to account for the electrothermal expansion of the ablated material or its interaction with the injector's driving gas. No mention was made of the particular injector mechanism used, and in the equation of motion, driving gas pressure terms were ignored, altogether.

However, electrothermal expansion of the armature and ablated material recently began to receive more attention from railgun investigators. Experimental evidence indicated that the mass ablated from the wall surface was not entrained by the armature and that the ablated material did not accumulate within the armature. It was theorized that the ablated material was accelerated by the armature creating a momentum loss. However, since the experimental data indicated that the armature maintained a constant length throughout most of the bore, the ablated material was eventually lost by the armature. The ablated material was then able to proceed rearward and interact with the driving gas. This interaction caused an increase in the pressure within the driving gas thus increasing the total force accelerating the projectile down the railgun bore.[6,11]

Ikuta[13] proposed a concept which operated on principles very similar to those identified in this theory. He called his concept an Ablation Mass Driver (AMD). In this concept, an electric current was passed continuously through the projectile's rear surface. This current caused material to be ablated off the projectile, and the material was expelled and expanded toward the rear, producing thrust. Almost all of the driving force was provided by the ablation process. Although the AMD was significantly different in design and concept from the railgun, it still gave support to the theory that some ablation effects within the railgun actually provided an increase in performance. Since ablation in the railgun is not negligible, this potential increase could not be ignored.

II. EXPERIMENTAL EVIDENCE

The evidence that ablation occurred within the railgun was very apparent. Inspection of the railgun bore usually revealed that some modes of rail and insulation erosion had occurred. The tremendous power levels and high radiation fluxes that existed within the armature were high enough to vaporize the rail material and insulation. However, the effects of ablation on railgun performance and especially the behavior of the railgun's gas dynamics were not well understood.

Researchers at UTSI performed an experimental study of several railgun configurations. During this study, several electrothermal effects were noticed, and an effort was made to identify the various electrothermal effects on railgun performance. By examining the experimental data, it was hoped that an understanding of these effects could be established, and a computer model to simulate these effects could be developed.

UTSI Railgun Facility

For the past four years, researchers at the UTSI railgun facility, shown in figure 2, have studied the MHD and electrothermal behavior of railguns in an attempt to gain a greater understanding of the complex physical nature associated with plasma armatures.[6] Various railgun configurations, including square bore, round bore, conventional, and augmented arrangements, were used to focus on several aspects of plasma armature physics.

The current configuration, a transaugmented railgun, was designed to investigate the effects of increasing the magnetic field through augmentation instead of just increasing the armature current. This railgun was designed so that it could easily be modified to fire as either a conventional or augmented railgun.[7]

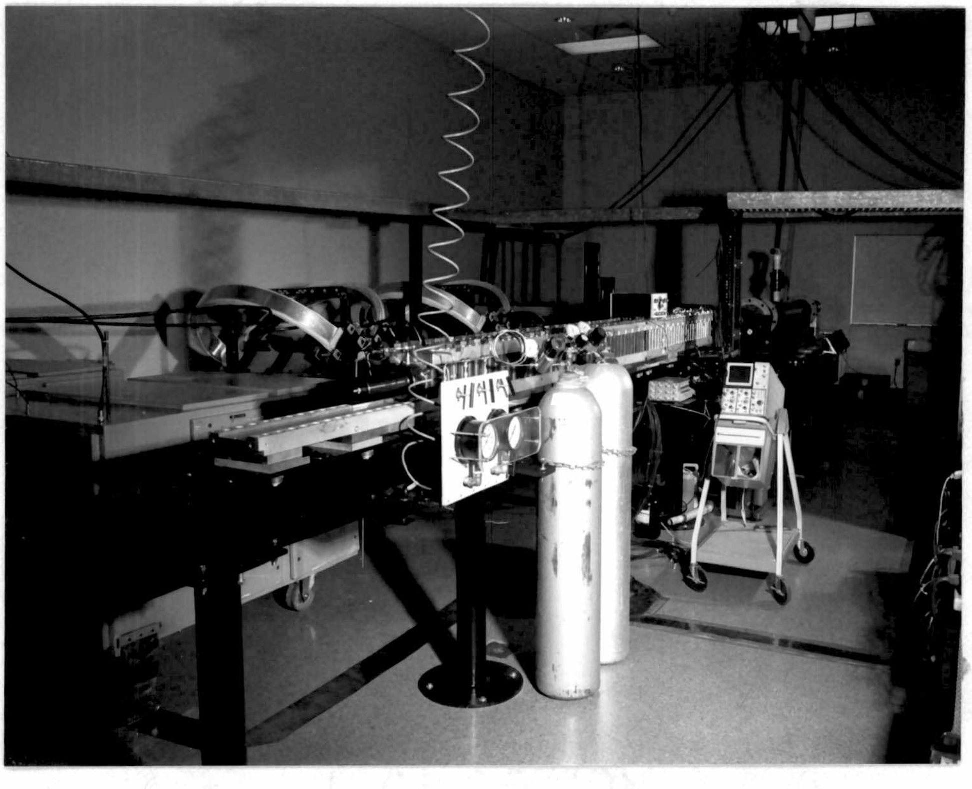

Figure 2. UTSI Railgun Facility

The conventional railgun configuration consisted of two parallel copper rails which were shorted by the plasma as it proceeded down the bore. The magnetic field was created by the inductance loop made by the circuit. The trans-augmented included a second set of parallel rails which were place outside the original rails and were on a separate cicuit. The second loop increased the magnetic field without increasing the current on the inner rails.

The cross-section of the internal bore structure and a cross-section of the overall structure of the transaugmented railgun are shown in figures 3 and 4, respectively. A schematic showing the instrumentation used on the railgun is shown in figure 5.

Rogowski coils were used to measure the time rate of change of the magnetic fields around each of the rails. From these measurements, values for the time rate of change of the current, dI/dt, were determined. Voltage measurements were made in the breech and muzzle to determine the voltage across the inner rail.[7]

A series of magnetic field sensing probes, or B-dot probes, was placed .1 m apart down the entire length of the railgun. These B-dot probes detected the position of the projectile by the magnetic field induced by the rail current or the armature current as it proceeded down the bore. From the position data from the B-dot probes, velocity was determined. The exit velocity of the projectile was measured by a magnetic velocity induction sensor (MAVIS) located within the catch tank.

A light gas gun (LGG) was used to inject the projectile at a high velocity into the railgun. The LGG reservoir was carefully pressurized to 3200 PSI with Helium for each of the railgun shots in order to provide a consistent injection velocity for every shot.

The injection velocity was determined using data obtained from the two pressure transducers, PT1 and PT2, located at the end of the light gas gun. Since the distance between the pressure probes was known, 40 mm, the velocity was found by dividing this distance by the Δt between the sensing time of the two probes.

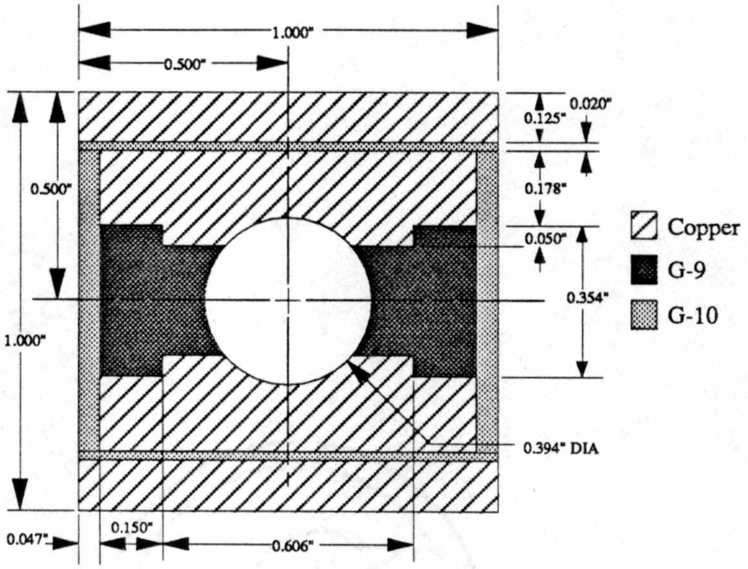

Figure 3. Transaugmented Railgun Bore Cross Section

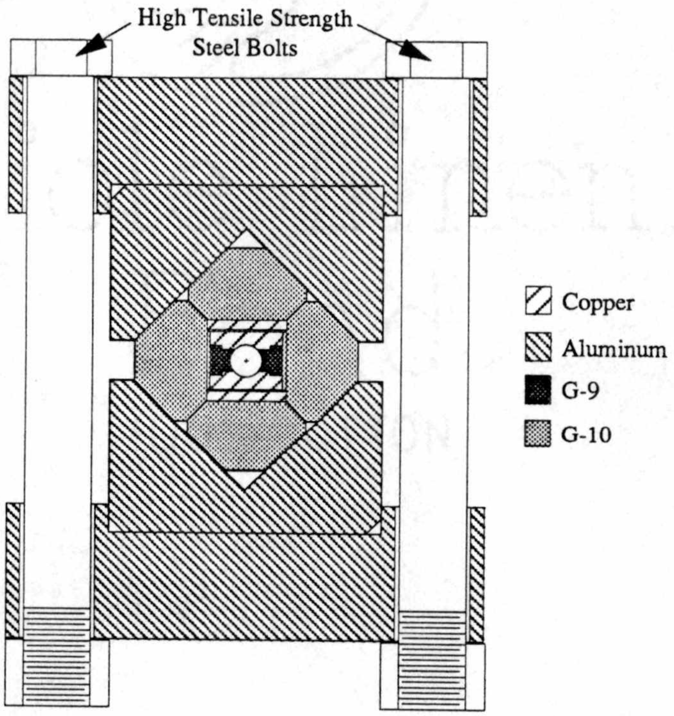

Figure 4. Overall Cross Section of UTSI Transaugmented Railgun

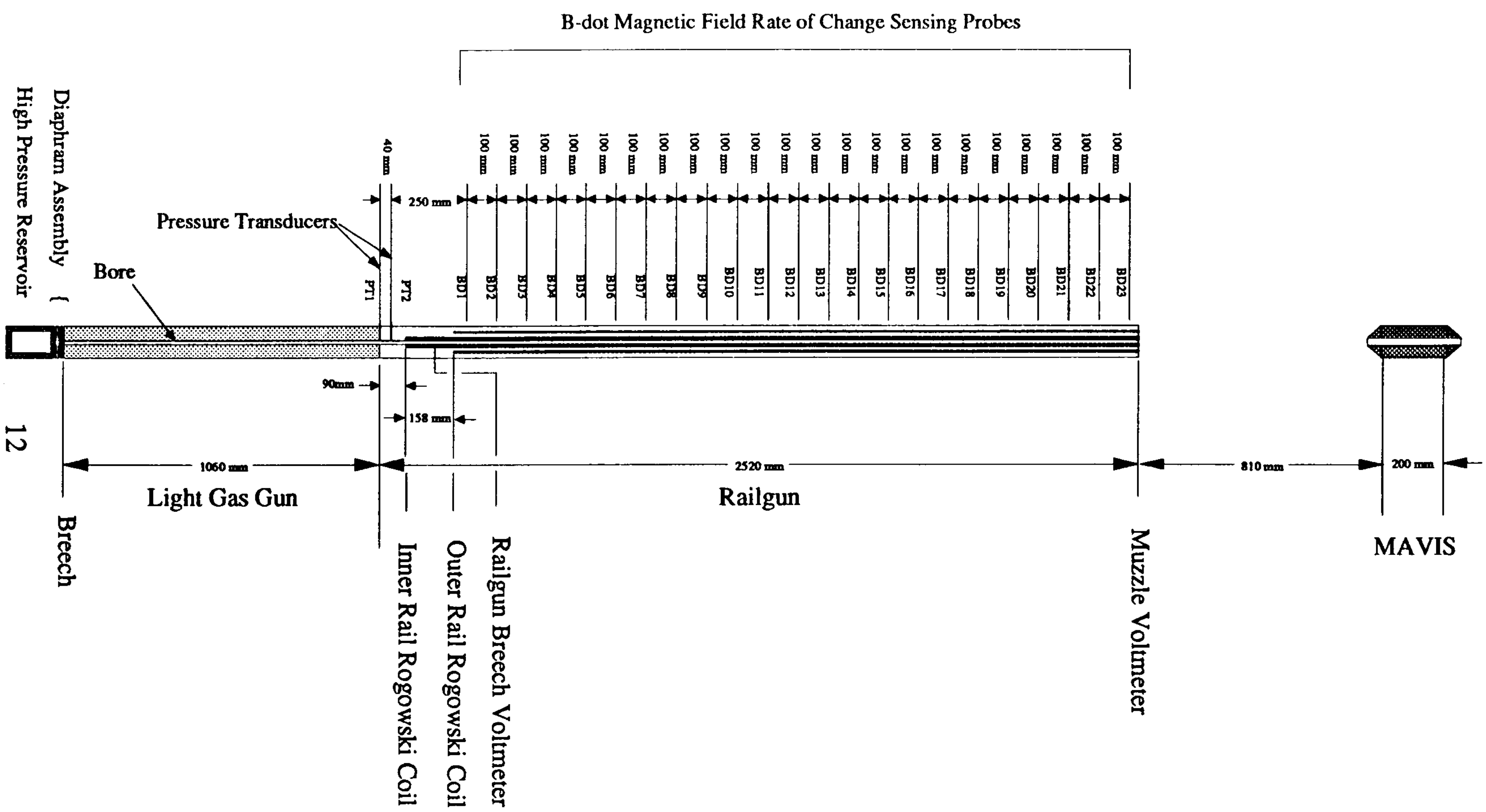

Figure 5. Schematic of UTSI Railgun Instrumentation

Evidence in Velocity Measurements

Projectile velocity during acceleration was derived from the shot's B-dot signal plot. Figure 6 shows a representative B-dot vs. time plot for a 70 kA conventional shot. The distance between each of the B-dot probes was a constant 100 mm. Therefore, when the B-dot probe senses the passing of an armature, the armature's position as a function of time was also known. By differentiating this position function, the velocity could be determined.[7]

An interesting effect was discovered which stemmed from the procedure used to clean and prepare the railgun. After the first series of shots in the round bore railgun, the gun bore was lapped and then cleaned with kerosene to remove the oil based, aluminum oxide lapping agent. However, it was evident that a residue of kerosene remained on the bore surface even after pumping the bore down to vacuum. This residual film of kerosene was considered to be an undesirable attribute during the first series of shots. Therefore, the kerosene was replaced by acetone since it evaporated much more readily from the bore wall. Table 1 shows pertinent data associated with those particular shots.

Cleaning Solvent	Peak Rail Current (MA) @ time (ms)	Peak Augment Current (MA) @ time (ms)	Muzzle Velocity (km/s)
Kerosene	.106 @ .353	0	2.476
Acetone	.105 @ .368	0	2.258
Kerosene	.104 @ .353	.108 @ .269	3.046
Acetone	.105 @ .368	.107 @ .388	3.085

Table 1. Data from UTSI Railgun for Kerosene and Acetone cleaned Shots

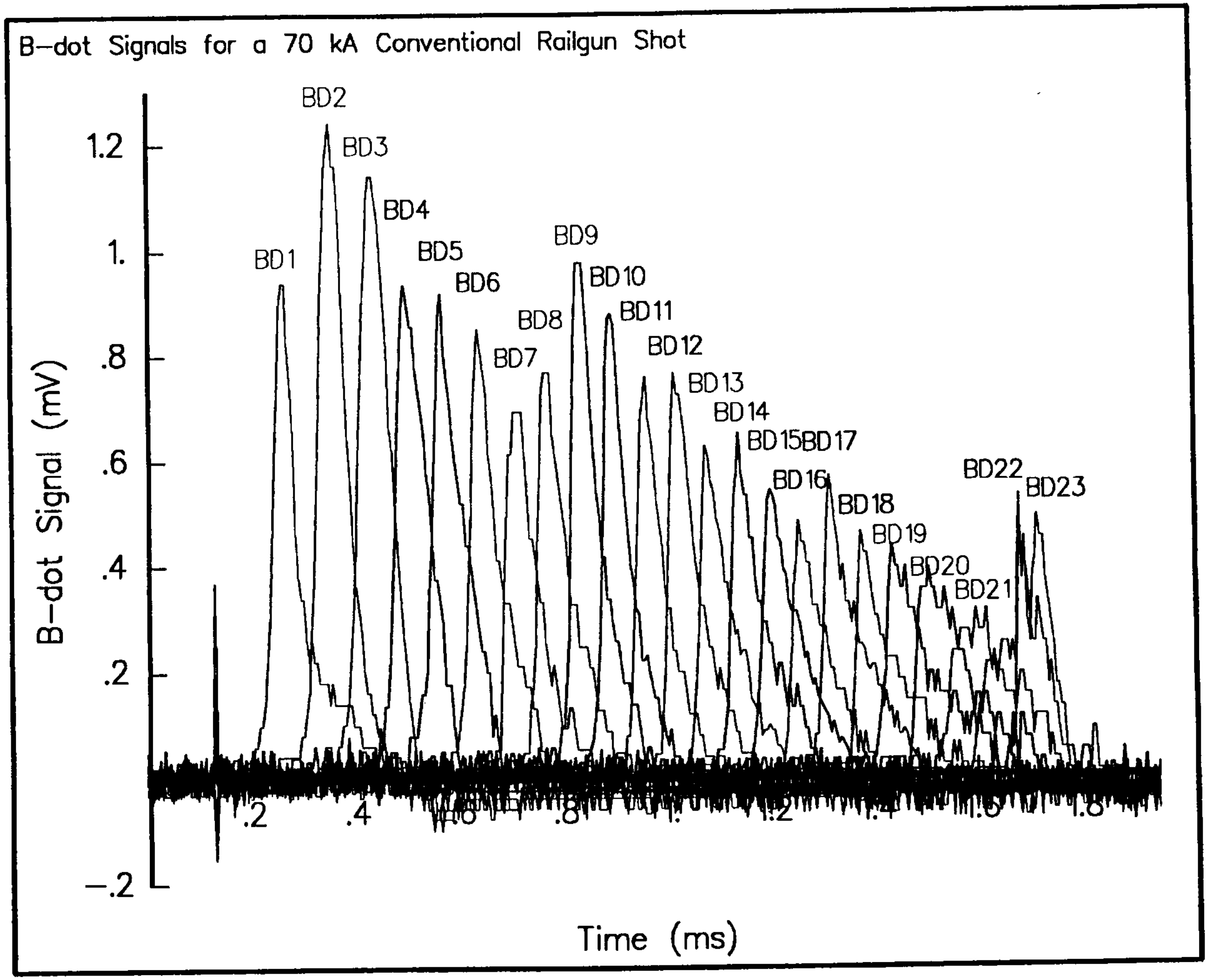

Figure 6. Representative B-dot Signal for a 70kA Conventional Railgun Shot

The series of shots was repeated in order to obtain data for a clean shot. Figure 7 shows a velocity plot of both conventional and augmented shots for both the kerosene-cleaned and acetone-cleaned cases.

As can be seen in the figure, the velocity of the kerosene-cleaned cases were higher through most of the bore for both cases. It was concluded that as the armature proceeded down the bore, the kerosene residue was vaporized off the rails and insulation and interacted with the driving gas. This interaction appeared to cause an increase in pressure in the driving gas which increased the driving force on the projectile.

However, the figure also indicated the effects of another phenomena associated with the kerosene residue. The kerosene vapor from the rail wall tended to enhance the formation of secondary arcs as indicated by the B-dot signals for those particular shots, and as can be seen in the comparison of the augmented cases, projectile acceleration in the kerosene case tended to decrease toward the end of the railgun. This eventually resulted in the acetone-cleaned shot having a higher exit velocity, as shown in the table.

Still the initial increase in velocity caused by the vaporization of the kerosene residue showed that material coming off the rail and interacting with the driving gas could significantly enhance the railgun's performance. Therefore, increase in driving pressure from the electrothermal effects must be considered in any careful analysis of railgun performance.

Evidence in Pressure Measurements

The pressure of the driving gas proceeding down the bore behind the projectile could be determined by examining the data obtained from the second pressure transducer, PT2. Figure 8 shows a representative pressure versus time plot for a 67 kA conventional

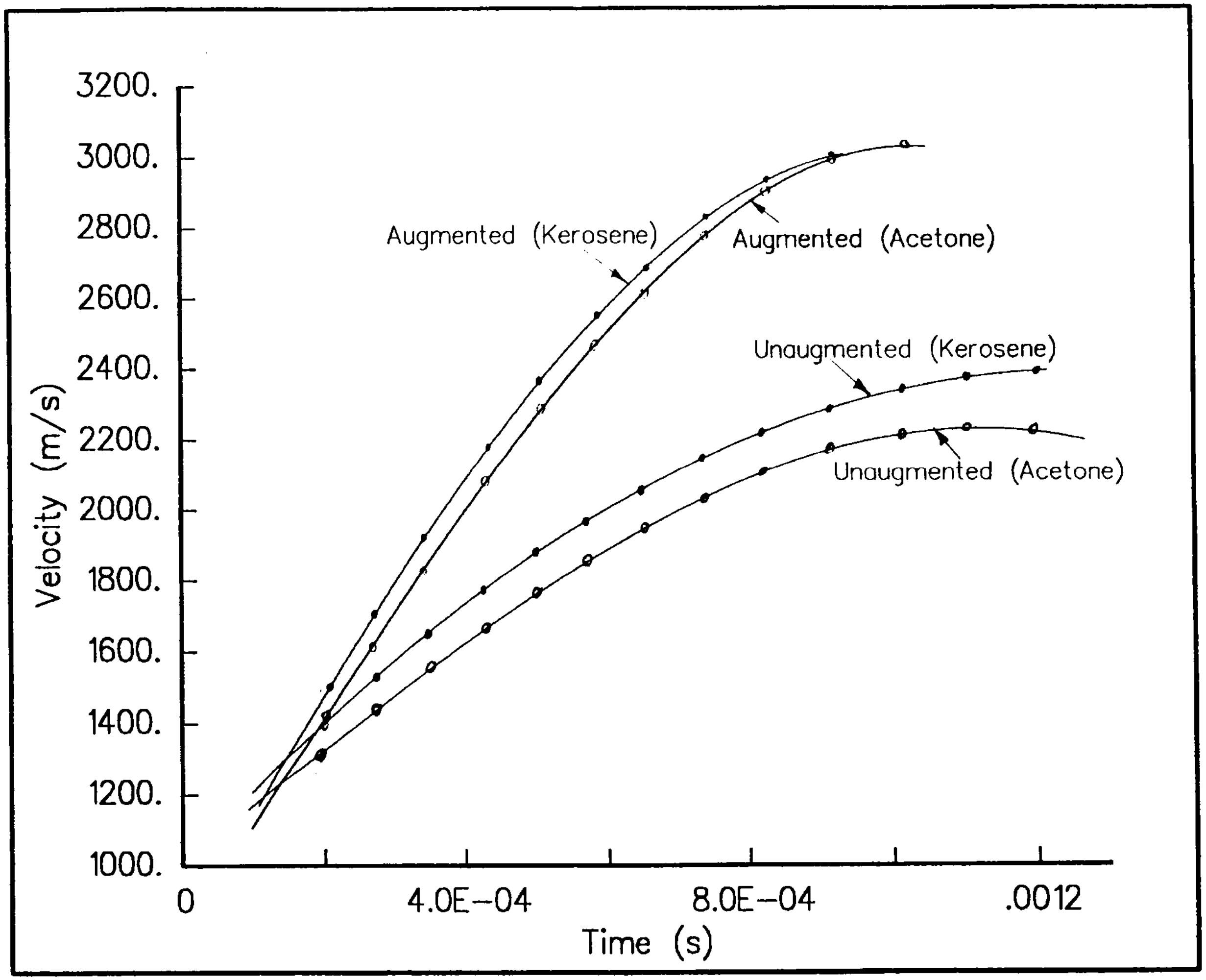

Figure 7. Comparison of Velocity Data for Kerosene and Acetone Cleaned Shots

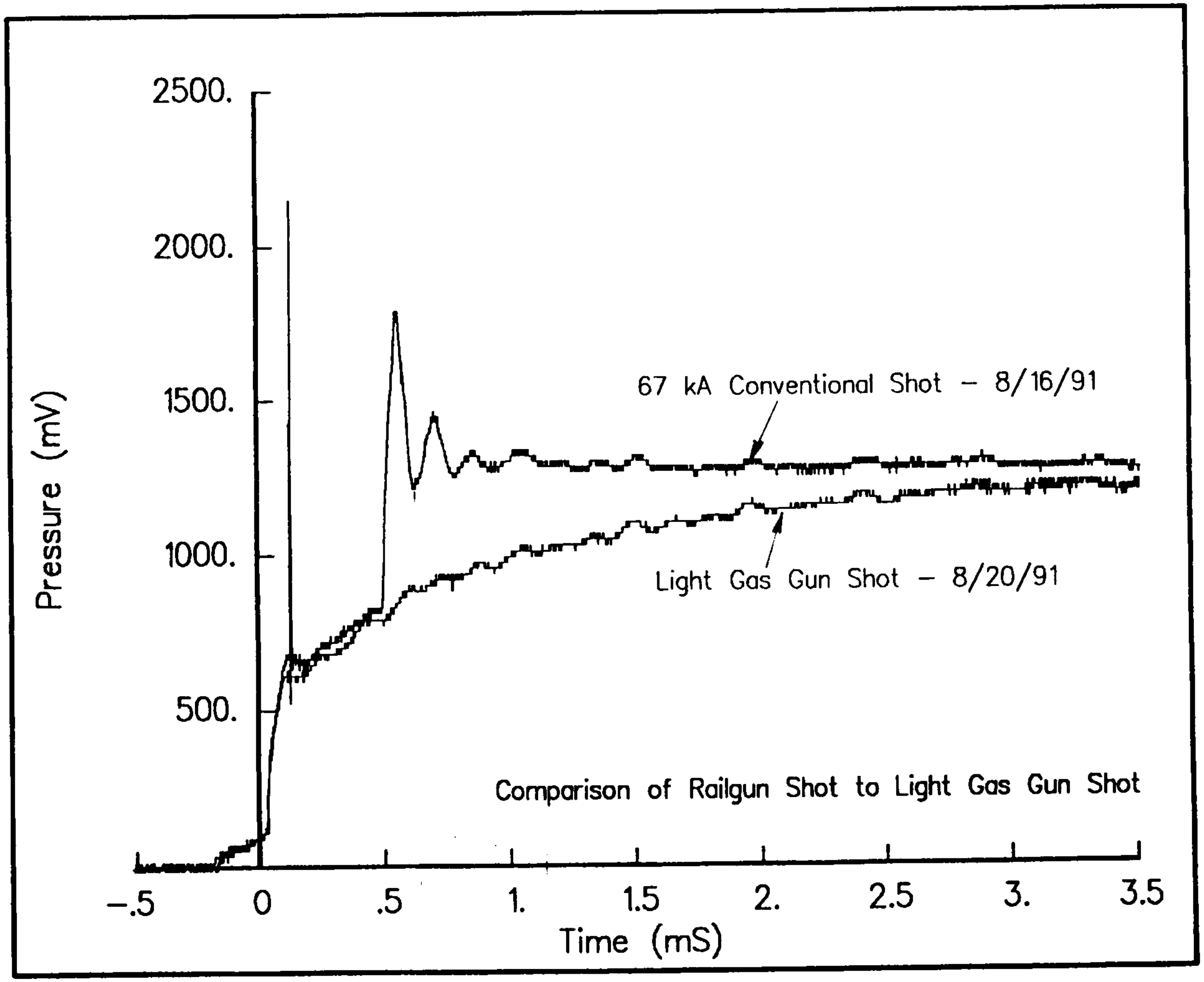

Figure 8. Comparison of Light Gas Gun and Railgun PT2 Pressure Data

railgun shot compared to the pressure found in a light gas gun of equal injection velocity. Figure 9 shows an empirical model of the pressure increase induced by the fusing transient.

As can be seen in the figure, the pressure in the railgun shot underwent a sharp increase in pressure after armature fusing as compared to the light gas gun shot. When the fuse on the back face of the projectile was initially vaporized into a high temperature plasma, a strong shock wave was formed which proceeded rearward through the driving gas.[8] This strong shock affected the flow in several ways: 1) it increased the pressure behind the shockwave, 2) it increased the flow temperature, thereby, increasing the speed of sound in the medium, and 3) it decreased the flow velocity behind the shock.[8,14]

It was believed that this pressure increase continued influencing the projectile motion but eventually decayed as the projectile proceeded down the bore. Taylor developed an empirical model of the fusing transient pressure pulse which assumed that the "fusing pressure pulse" behaved according to the equation:

$$P_t = (\omega t)^{\eta - 1} e^{-\theta t}\,, \tag{5}$$

where θ is an experimental decay constant, and ω and η are shape parameters used to determine the strength and length of the pressure pulse.[7] Figure 9 shows this empirical pressure pulse model compared to the pressure obtained by the PT2 probe during an actual railgun shot.

It should be remembered that the pressure port measured pressure obtained at a stationary position, whereas, the pressure pulse simulated the pressure directly behind the moving projectile. Even though this was not necessarily an equivalent comparison, the overall increase in both values should still be similar.

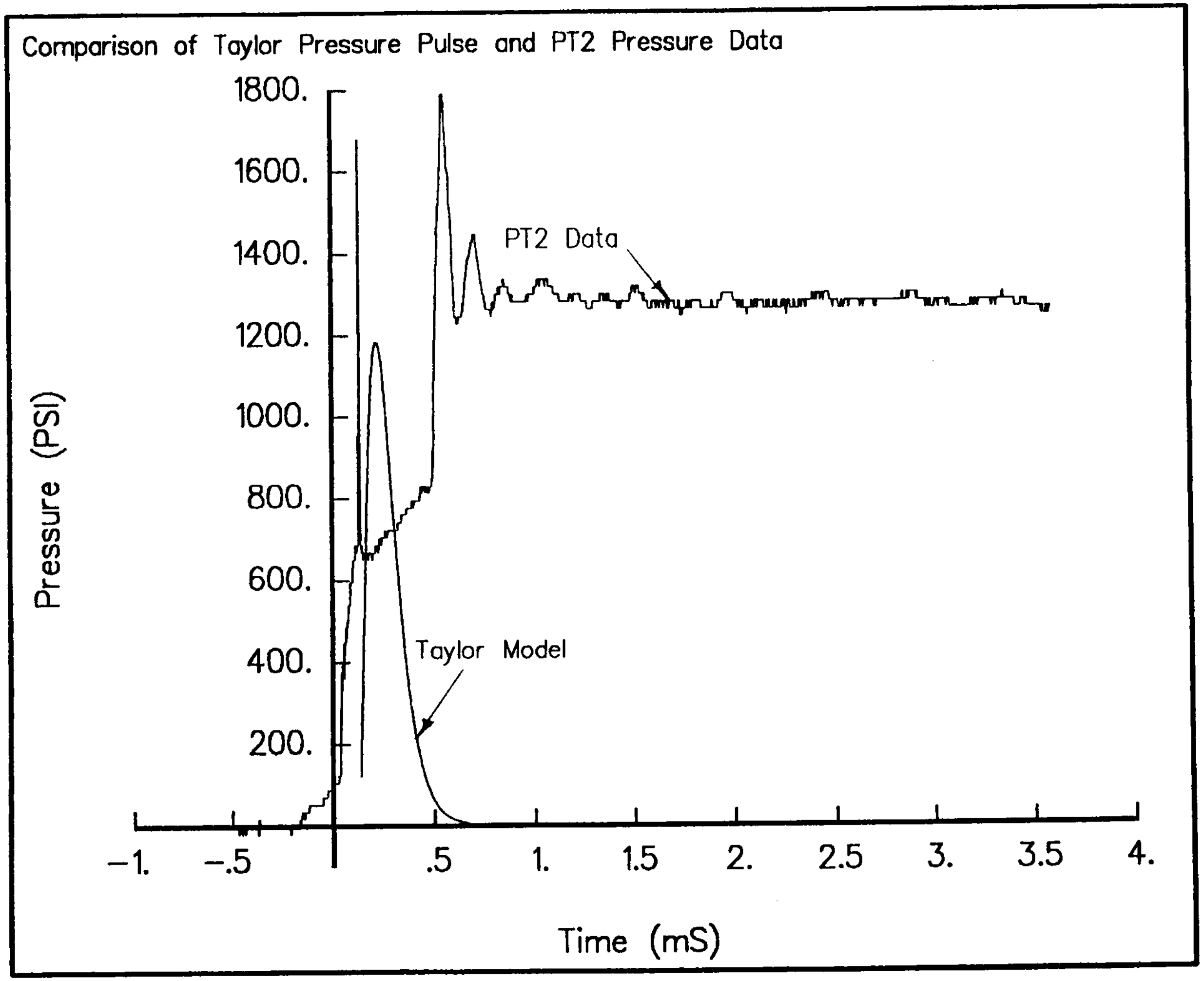

Figure 9. Comparison of Taylor Pressure Pulse Model and PT2 Pressure Data[7]

III. DEVELOPMENT OF THE RAILGUN MODEL

In previous railgun models, electromagnetic theory and circuit models usually were the primary focus. However, when trying to ascertain the effects of the gas dynamics and ablation, it was necessary to approach the problem from a different direction.

Determining the velocity of a projectile within the railgun simply involved implementing Newton's force equation:

$$\Sigma F = \frac{d}{dt}(mv) = m\frac{dv}{dt} + v\frac{dm}{dt} \qquad (6)$$

where m was the projectile mass and v was velocity. This equation stated that the sum of forces, ΣF, acting on the projectile was equal to the time rate of change of the linear momentum. The only problems were identifying and modeling correctly all of the pertinent forces and properly tracking the armature, projectile, and ablated mass.

Figure 10 shows a schematic of the projectile during railgun operation with all important forces labeled. The electromagnetic force, F_L, otherwise known as the Lorentz force is the force caused by the magnetic pressure induced by the current passing through the rail and plasma armature. F_P is the driving gas pressure on the rear of the armature acting on the projectile. The in-bore gas pressure force on the front face of the projectile, F_{IB}, was the force caused by the entrainment of gas ahead of the projectile. The drag force, F_D, was caused by the viscous interaction of the armature with the wall. In this model, projectile sliding friction was neglected and assumed to be zero.[11] Another important term in determining projectile motion was the calculation of the vdm/dt term in the right-hand side of equation (6). Once all of these terms were identified, the projectile acceleration could be calculated directly.

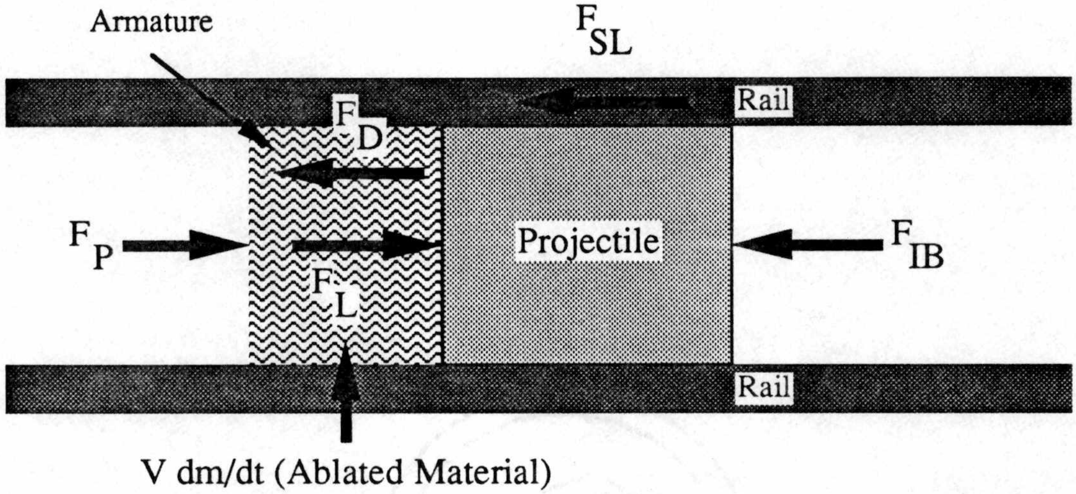

F_P — Driving Gas Pressure Force

F_L — Lorentz Force

F_D — Viscous Drag Force

F_{IB} — In-bore Gas Force

F_{SL} — Projectile Sliding Friction Force (Assumed to be Negligible)

Figure 10. Diagram of Pertinent Forces Acting on Railgun Projectile

This chapter discusses the theory, development process, and the governing equations used to develop the railgun model. Each of the various forces and effects which impact performance are identified and discussed.

Gas Dynamic Model

This section discusses the procedure used to calculate the base pressure and in-bore gas pressure within the railgun. The procedure used for the railgun model was an extension of the model proposed by Seigel[15,16] for determining projectile motion for conventional and pre-burned propellant guns.

In developing the gas dynamic equations, Seigel made several assumptions. The flow is assumed to be frictionless, reversible, and adiabatic, therefore, the flow is isentropic. The flow is considered to be one-dimensional and occurs within a constant area duct.[15]

It is assumed that as the projectile proceeds down the bore, it "sheds" two series of infinitesimal disturbances. The first series was shed from the rear face of the projectile and the waves proceeded rearward through the propellant gas. The second series was shed from the front face of the projectile, and the waves proceeded forward ahead of the projectile. Figure 11 shows a schematic of the process of wave generation asscociated with projectile motion.

By applying the momentum and continuity equations across the wave, it could be shown that the pressure change associated with an upstream disturbance, i.e., a wave travelling in the direction opposite of the flow, was related by the equation:

$$dP = -a\,\rho\,du\,. \tag{7}$$

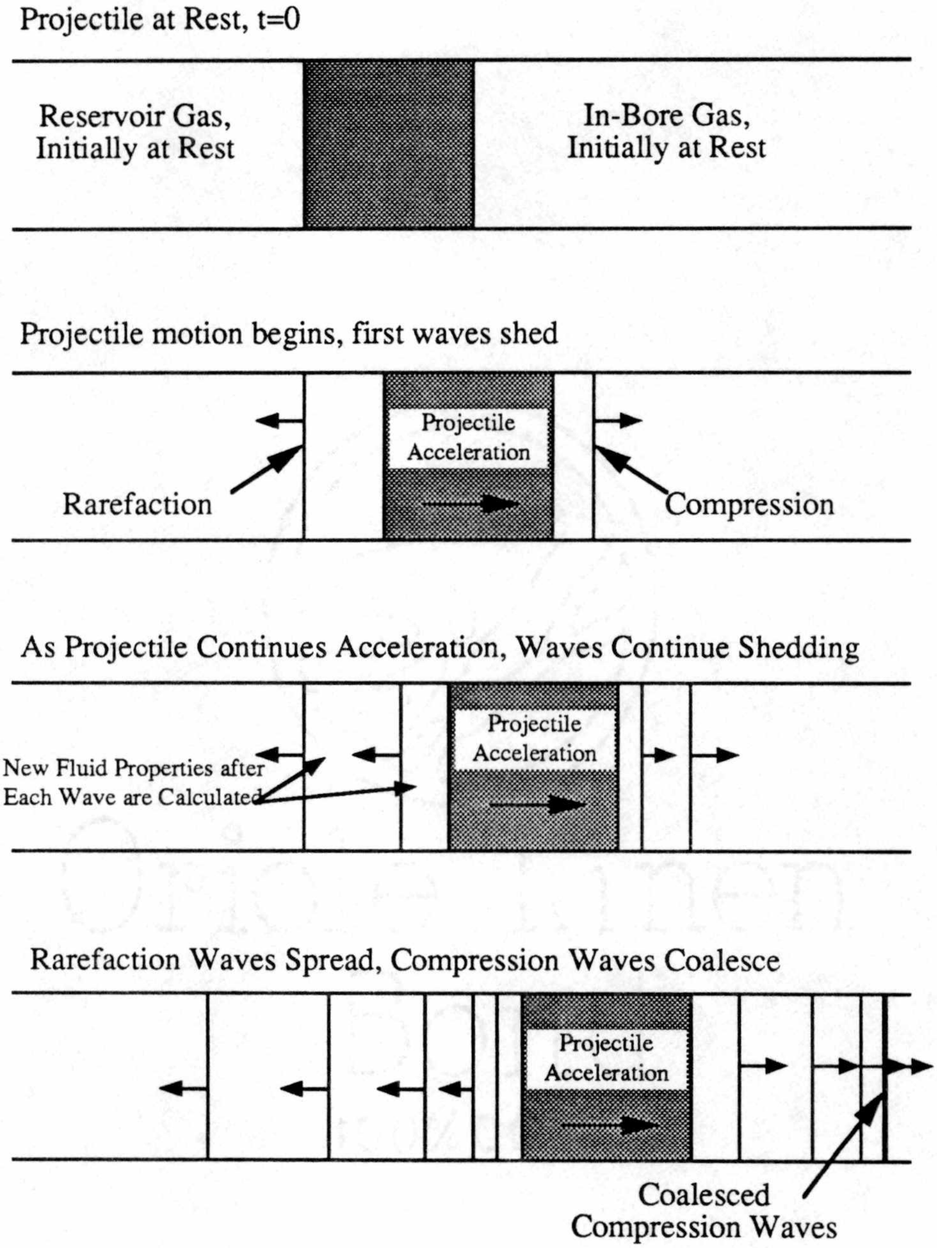

Figure 11. Schematic of Characteristic Wave Generation in Railgun Model

As can be seen, an increase in velocity caused a decrease in pressure, and a velocity decrease caused an increase in pressure. It can also be shown that for a downstream disturbance, or a wave travelling in the same direction of the flow, the pressure change was governed by the equation:

$$dP = a \rho \, du \, . \tag{8}$$

A velocity increase in (8) produced a pressure increase, and a velocity decrease produced a pressure decrease.[16]

Equations (7) and (8) are known as the characteristic wave equations. These equations were used to obtain numerical solutions for the railgun's gas dynamics. As long as these disturbances were small enough to be considered infinitesimal, these characteristic wave equations were valid for both rarefaction and compression waves. As each new set of waves was created, a new cell was created directly ahead and behind the projectile with the new flow conditions associated with each wave. The development of equations (7) and (8) is shown in Appendix A.

It was assumed that the railgun model has an infinite length breech. This assumption simplified the wave accounting system by eliminating the need to account for wave reflection from the breech wall.[16]

It was also assumed that railgun's breech was of the same diameter as the bore. This assumption again simplified the model's complexity since the problem of wave interaction in chambered guns is not fully understood and is difficult to model using just the wave equations. These assumptions tended to compute higher values of performance than expected, but these changes were generally very small and the results were still very usable.[16]

The wave velocity for infinitesimal disturbance was governed by the wave's ability to propagate through its medium. In this model, it assumed that the small disturbances travel through the gas at the speed of sound, a, relative to the flow where:

$$a^2 = \left(\frac{\partial P}{\partial \rho}\right)_s . \tag{9}$$

For the one-dimensional, thermally and calorically perfect gas, this could also be stated as:

$$a^2 = \gamma RT , \tag{10}$$

where γ was the ratio of specific heats for the light gas and R was the gas constant.

If the gas was flowing in the +x direction with the velocity u, then wave velocity, V_W, relative to the wall was given by:

$$V_w = u - a \tag{11}$$

for an upstream wave, and:

$$V_w = u + a. \tag{12}$$

for a downstream wave.[15]

Since the model had an infinite length breech, all waves shed from the rear facing surface were upstream travelling waves and were governed by equation (11). Since the railgun bore was open ended and no reflections occurred, all waves shed from the forward facing surface are downstream disturbances and were governed by equation (12).

As was mentioned, equations (11) and (12) apply when the change in velocity was infinitesimal. However, with the high acceleration rates expected within the railgun, it was determined that these equations overestimated the pressure change associated with compression waves with large values of du associated with them. Therefore it was necessary to find an equation which would apply to finite changes in pressure. In other words, an equation to find the dP across a finite shock wave was needed.

Siegel[16] showed a development first introduced by Lukasiewicz for the pressure change across a shock wave moving through an ideal gas which took the form:

$$\frac{P_2}{P_1} = 1 + \frac{\gamma_1(\gamma_1+1)}{4}\left(\frac{u_2}{a_1}\right)^2 + \frac{\gamma_1 u_2}{a_1}\sqrt{1+\left(\frac{(\gamma_1+1)}{4}\right)^2\left(\frac{u_2}{a_1}\right)^2} \quad . \tag{13}$$

Assuming $P_2=P_1+dP$, $u_2=du$, and solving equation (13) for dP yielded the following equation:

$$dP = P_1\left[\frac{\gamma(\gamma+1)}{4}\left(\frac{du}{a_1}\right)^2 + \frac{\gamma du}{a_1}\sqrt{1+\left(\frac{(\gamma+1)}{4}\right)^2\left(\frac{du}{a_1}\right)^2}\,\right]. \tag{14}$$

By taking the limit of equation (14) for very small du, equation (14) reduces to the original wave equation, equation (8). Therefore equation (14) was used to determine dP for all compression waves.

The temperature of the flow, T, could be found by implementing the energy equation. From the assumption that the flow was adiabatic, this yielded the equation:

$$T_2 = T_1 + \frac{u_1^2 - u_2^2}{2Cp}\,, \tag{15}$$

where Cp was the light gas's specific heat and where the subscripts 1 and 2 denoted flow before and after wave which had been transformed from a moving reference frame to a stationary reference frame, respectively. An increase in velocity caused a decrease in temperature, and a decrease in velocity caused an increase in temperature. This equation applied for both of the wave equations.

Flow density, ρ, could be determined by using the perfect gas equation:

$$\rho = \frac{P}{RT}\,, \tag{16}$$

where R was the gas constant for the light gas (Helium).

Compression waves posed a problem in the calculation of flow conditions because a series of compression waves tends to coalesce into a single compression wave. If enough waves coalesce, the assumption that the dP across the wave is infinitesimal is no longer valid. Therefore, the compression wave becomes a finite shock wave. Flow across the shock is no longer isentropic, but this does not affect the original assumptions since they only applied to the original creation of the compression waves.

A relationship could be developed which determined the shock waves velocity through the medium. It was assumed that the ΔP across the wave was the sum of the dP's of the compression waves which formed the shock wave. Using one-dimensional shock relations[14], the following equations could be shown:

$$V_w = V_{sw} = u \pm a\sqrt{\frac{(\gamma+1)}{2\gamma}\left(\frac{P_2}{P_1} - 1\right) + 1} \tag{17}$$

for an upstream shock wave and a downstream shock wave, respectively. The development of equation (17) is shown in Appendix A.

Since flow across the shock wave was still adiabatic, equation (15) was still valid to calculate flow temperature. Equation (16) was still used to calculate flow density.

Wave positions, x_w, can be found by integrating each wave's velocity according to the equation using a finite difference scheme:

$$x_{w_2} = x_{w_1} + V_w\, dt\,. \tag{18}$$

Figure 12 shows the characteristic wave generation for a light gas gun shot. Figure 13 shows a representation of the characteristic wave positions for a 70 kA conventional railgun shot simulation.

Figure 12 shows the characteristic wave generation for a light gas gun shot. Figure 13 shows a representation of the characteristic wave positions for a 70 kA conventional railgun shot simulation.

This ideal gas dynamics model can be applied to the non-adiabatic, ablating railgun model since this model deals only with the light gas as it expands from the reservoir. Since all of the ablation occurs ahead of the light gas, then this model can be used to approximate the behavior of the driving gas.

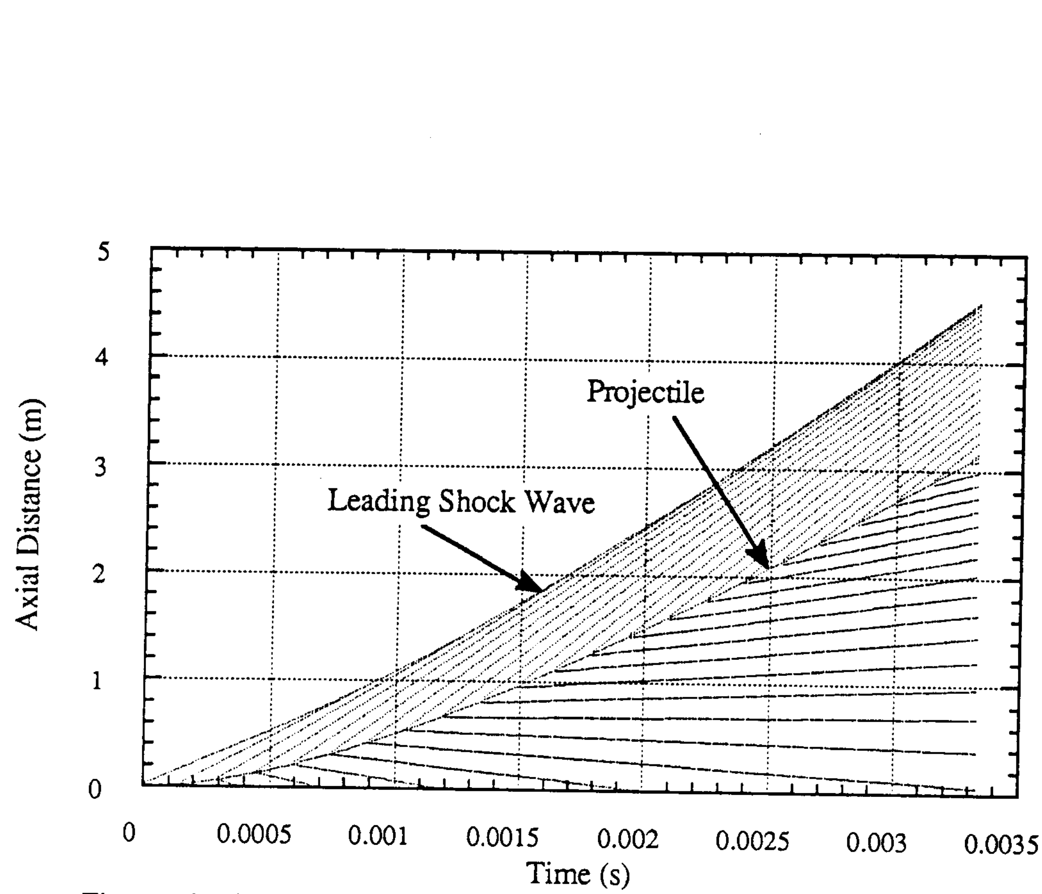

Figure 12. Characteristic Wave Generation in a Light Gas Gun Simulation

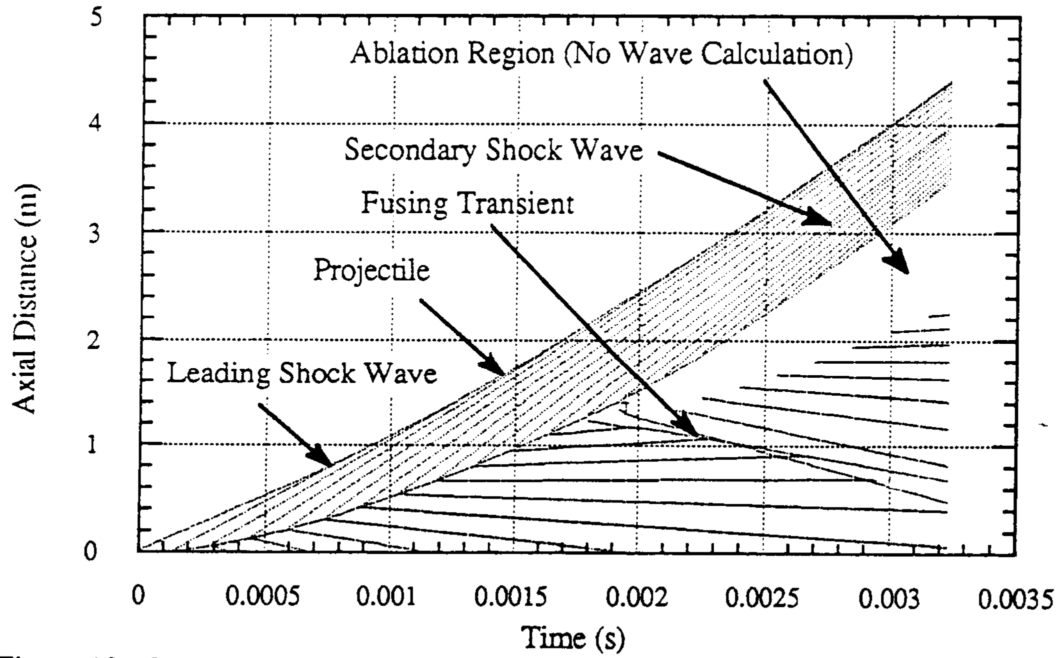

Figure 13. Characteristic Wave Generation in a 70kA Conventional Railgun Simulation

Electromagnetic Model

During the course of the development of the railgun model, simple empirical rail current and armature voltage models were used to determine Lorentz forces and armature power dissipation. Figures 14 and 15 show the simplified rail current and armature voltage models compared to experimental data. The rail current model linearly increased to a maximum value then decreased linearly to simulate the actual current as it decreased past the peak value, as seen in the figure. The voltage model was simply a step function which assumed a constant value at the time of fusing. The models are shown with data from a 70 kA conventional shot for comparison. In an attempt to improve the accuracy of the Lorentz force calculation, it was decided that a more rigorous scheme should be incorporated in order to more closely approximate the rail current and armature voltage. Also, a model was needed to simulate augmented shots. The simplified models could have been extended, but other methods already existed which could be directly inserted into the model.

Actual experimental data could have been used for specific cases, but it was decided that an LRC (Inductance-Resistance-Capacitance) model developed by Taylor could accurately model the actual values of the experimental data and provide more flexibility than using just experimental data. Taylor combined classical electromagnetic theory and empirical relationships to model the rail current and armature voltage within the railgun.[7]

From his analysis for the transaugmented railgun, the Lorentz force, F_L, could be given by the equation:

$$F_L = \frac{1}{2} L_1' I_1^2 + M_{12}' I_1 I_2, \tag{18}$$

where L' was the self-inductance, I was the rail current, M' was the mutual inductance, and 1 and 2 denoted the inner and outer rails, respectively.[7]

Mutual inductance, M'_{12} could be found by using the relation:

$$M_{12}' = k \sqrt{L_1' L_2'}, \tag{19}$$

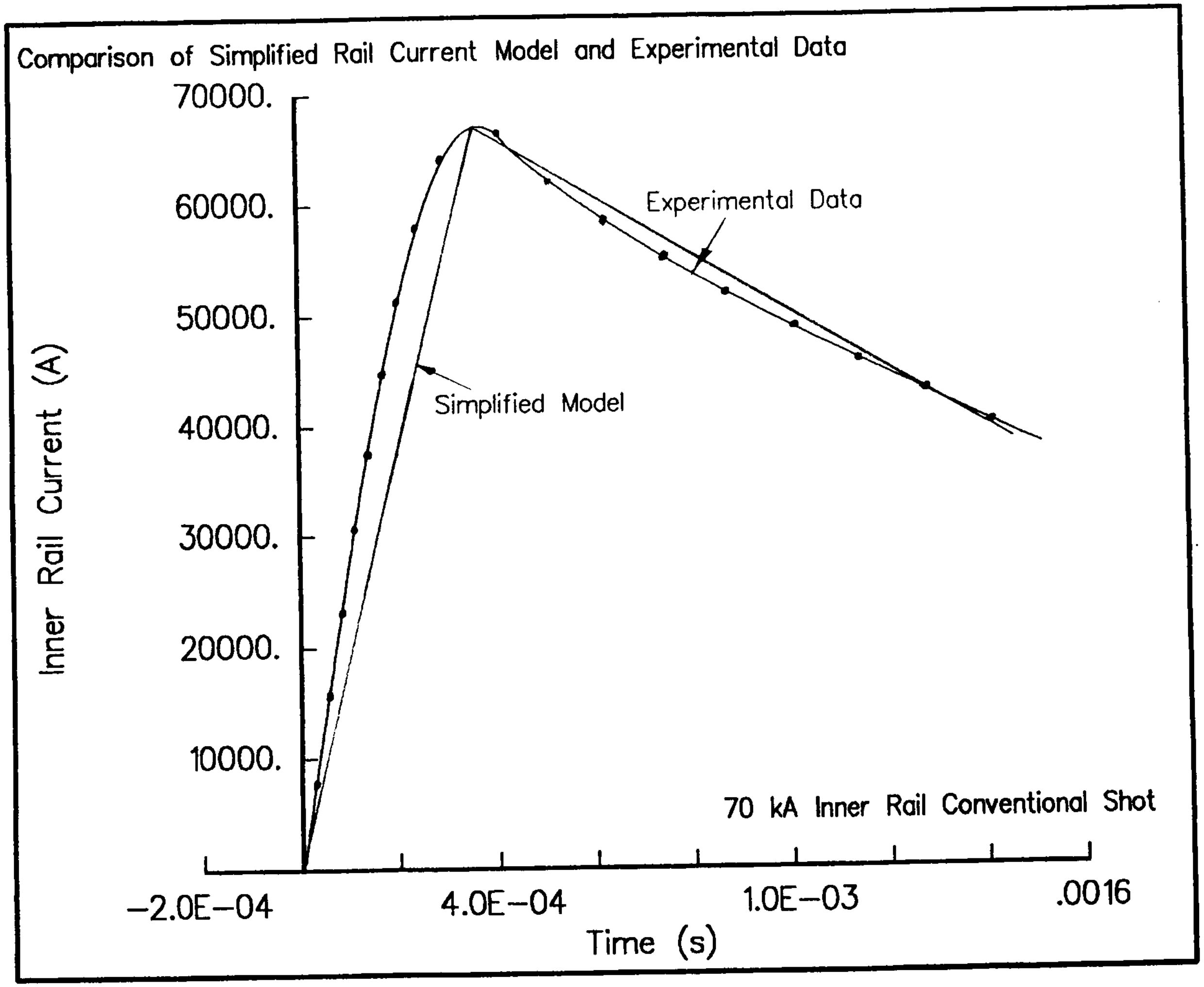

Figure 14. Simplified Inner Rail Current Model in Railgun Simulation

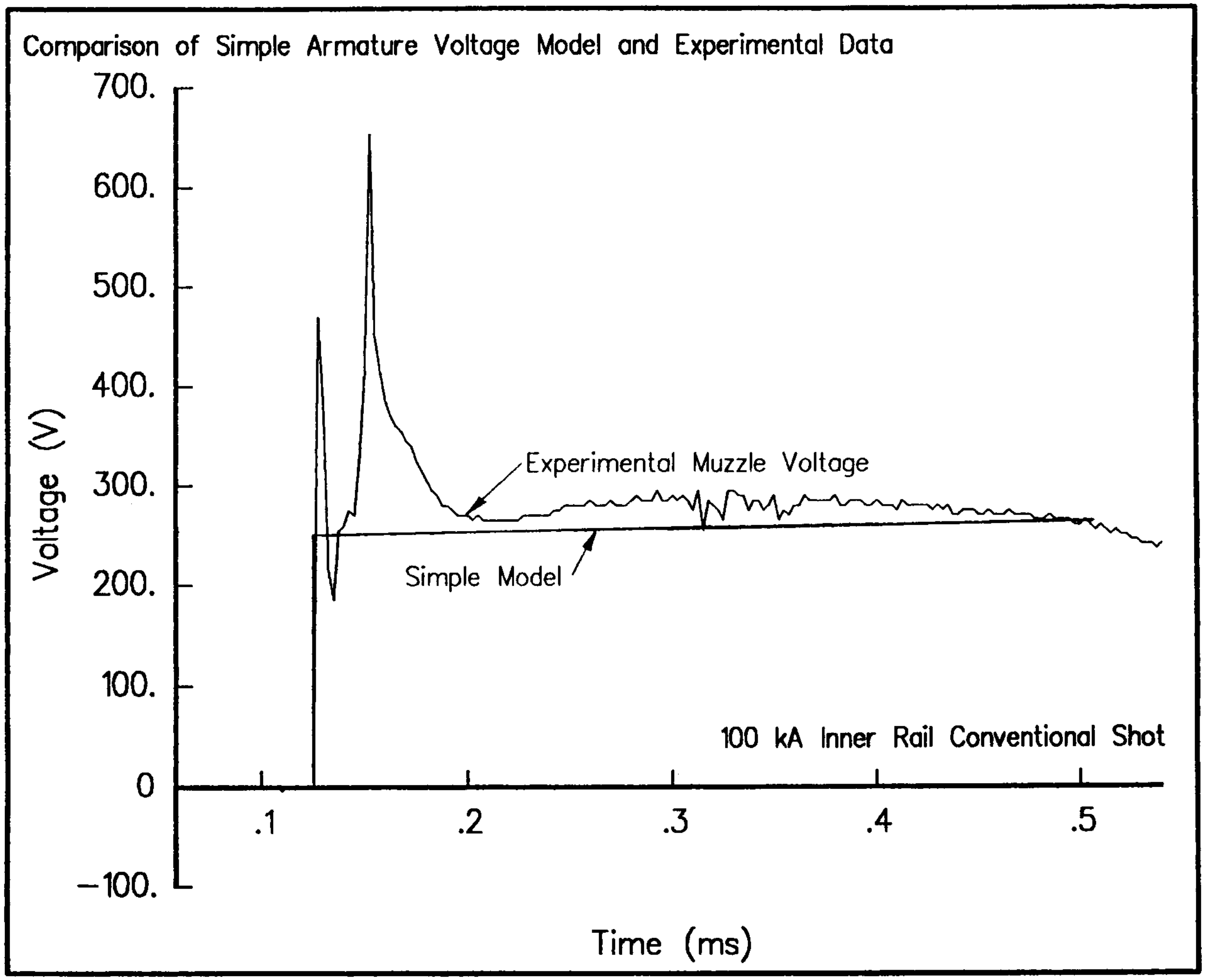

Figure 15. Simplified Voltage Model in Railgun Simulation

where k was the rail coupling coefficient. L'_1, L'_2, and k were found experimentally.

The time rate of change of mutual inductance was given by the equation:

$$\frac{dM_{12}}{dt} = M'_{12}\, V_p, \tag{20}$$

where V_p was the velocity of the projectile.

The time rate of change of the self inductance of the inner rail was given by the equation:

$$\frac{dL_1}{dt} = L'_1\, V_p. \tag{21}$$

The voltage within the capacitors, V_{C1} (inner), and V_{C2} (outer), as a function of time were found from the equations:

$$V_{C_1} = V_{0_1} - \frac{1}{C_1}\int I_1\, dt, \tag{22}$$

and:

$$V_{C_2} = V_{0_2} - \frac{1}{C_2}\int I_2\, dt\ . \tag{23}$$

V_{01} and V_{02} were the initial charges placed on the inner and outer capacitors, respectively. C_1 and C_2 were the total capacitance of the inner and outer rails, respectively.[7]

Summation of the voltages around the inner and outer rail circuit loops yielded the equation:

$$V_{C_1} - \frac{d}{dt}(I_1 L_{T_1} + I_2 M_{12}) - I_1 R_1 - V_a = 0 \tag{24}$$

for the inner rail, and:

$$V_{C_2} - \frac{d}{dt}(I_2 L_{T_2} + I_1 M_{12}) - I_2 R_2 = 0 \tag{25}$$

for the outer rail. L_{T1} and L_{T2} were the total self-inductance of the inner and outer rails, respectively. L_{T1} was found from the equation:

$$L_{T_1} = L_1'(x_p - L_{LGG}) , \tag{26}$$

where x_p was the projectile position within the railgun and L_{LGG} was the length of the light gas gun. L_{T2} was calculated by using the equation:

$$L_{T_2} = L_2'(L_{RG}) , \tag{27}$$

where L_{RG} was the length of the railgun.

Solving equations (24) and (25) for dI_1/dt and dI_2/dt yielded the following results:

$$\frac{dI_1}{dt} = \frac{V_{C_1} - I_1\left(R_1 + \frac{dL_1}{dt}\right) - I_2\frac{dM_{12}}{dt} - M_{12}\frac{dI_2}{dt} - V_a}{L_{T_1}} , \tag{28}$$

and:

$$\frac{\frac{dI_2}{dt} = V_{C_2} - I_2R_2 - I_1\frac{dM_{12}}{dt} - \frac{M_{12}\left[V_{C_1} - I_1\left(R_1 + \frac{dL_1}{dt}\right) - I_2\frac{dM_{12}}{dt} - M_{12}\frac{dI_2}{dt} - V_a\right]}{L_{T_1}}}{L_{T_2} - \frac{M_{12}^2}{L_{T_1}}} . \tag{29}$$

Equations (28) and (29) were solved by a finite difference method to determine values of the rail currents. Figures 16 and 17 show the inner and outer rail current compared to experimental data. As can be seen, the current model very accurately modeled the experimental measurements. The rail current values calculated by equations (28) and (29) were then placed into equation (18) to determine the Lorentz force.

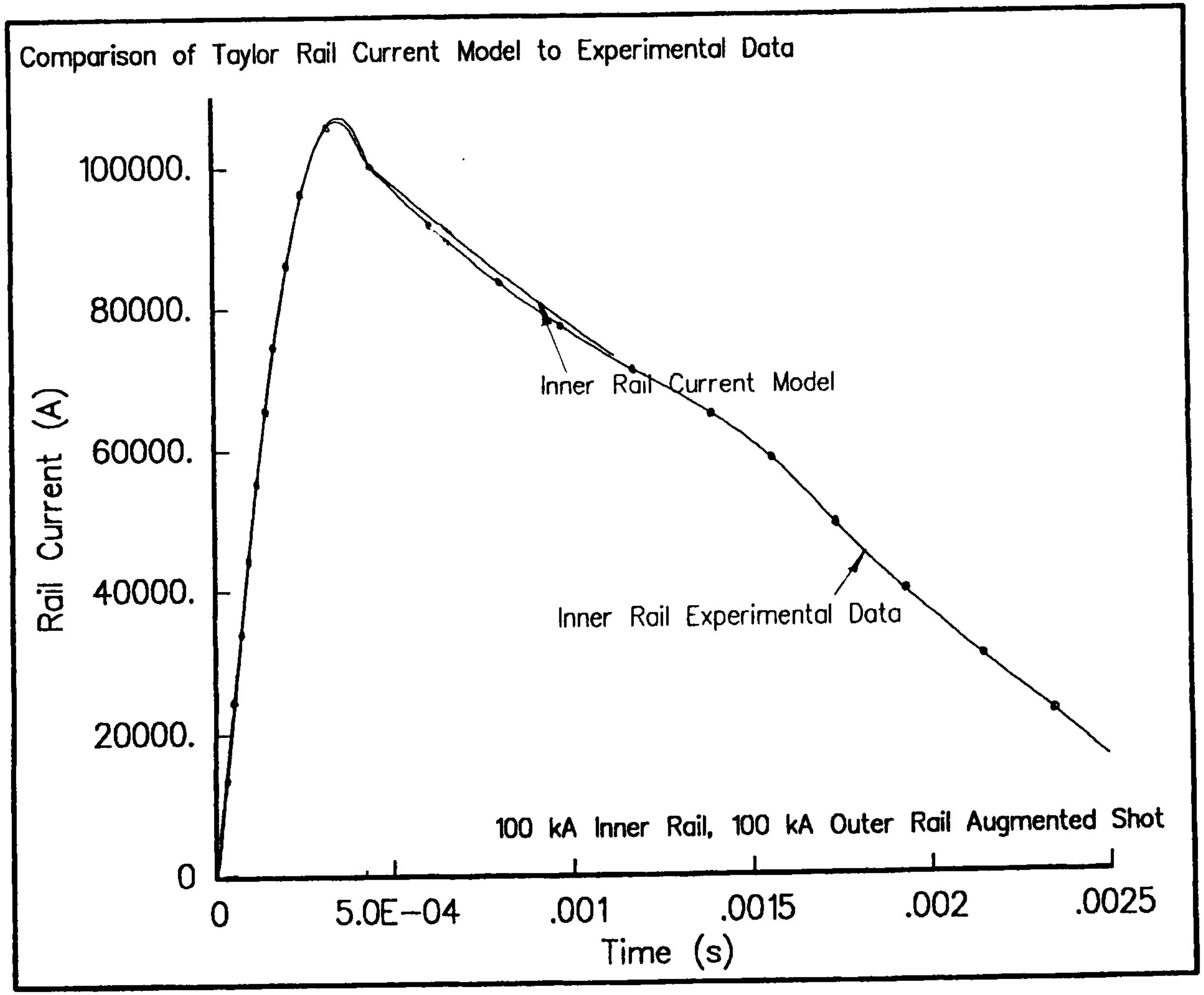

Figure 16. Taylor Inner Rail Current Model Compared to Experimental Data[7]

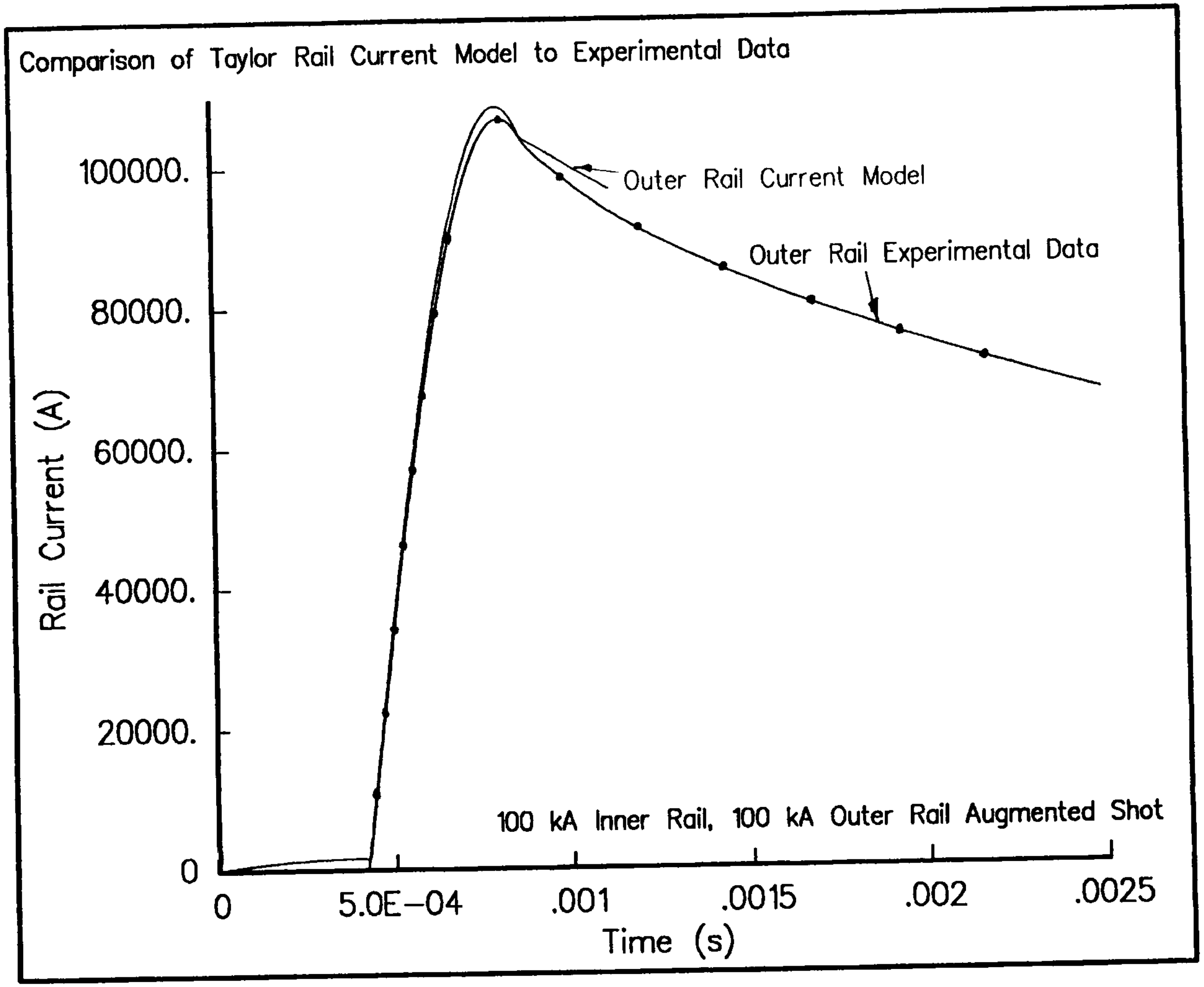

Figure 17. Taylor Outer Rail Current Model Compared to Experimental Data[7]

Considering just the conventional railgun arrangement, setting the values of V_{C2}, $I_2(t=0)$ and M_{12} to zero in equations (28) and (29) allow these equations to reduce to:

$$\frac{dI_1}{dt} = \frac{V_{C_1} - I_1\left(R_1 + \frac{dL_1}{dt}\right) - V_a}{L_{T_1}}, \tag{30}$$

and:

$$\frac{dI_2}{dt} = 0\,. \tag{31}$$

Equation (30) was the equation of time rate of change of current for a classical railgun model. Therefore, (28) and (29) were valid for both conventional and augmented simulations.

The armature voltage was empirically modeled by Taylor with the logarithmic curve:

$$V_a = V_{0_{11}} \ln\left(I_1\right), \tag{32}$$

where V_{011} was a parametric value which was set to match the experimental values of V_a.[7] Figure 18 shows a comparison of the Taylor voltage model with the experimental data; however, this voltage model did not accurately model the fusing transient.

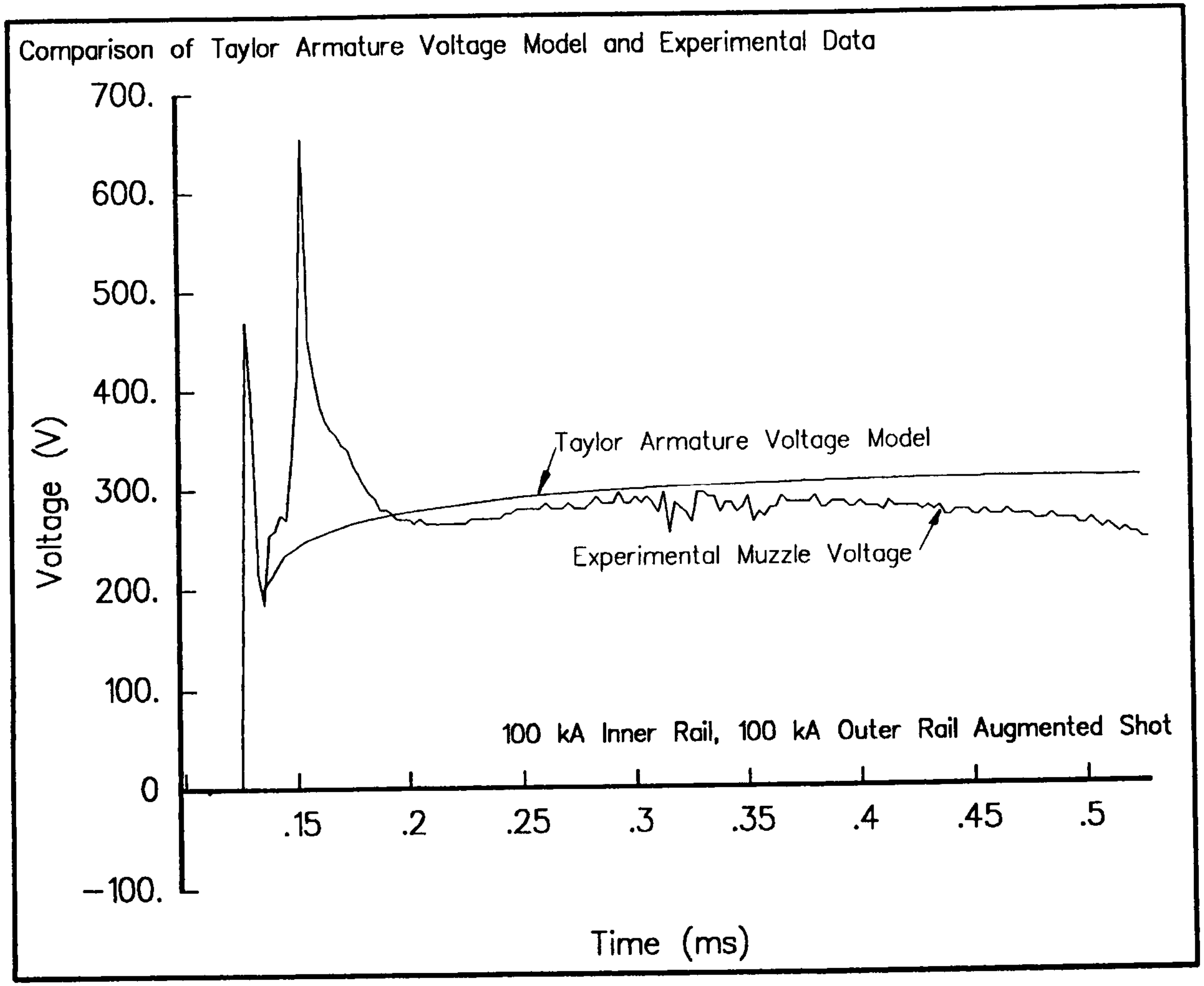

Figure 18. Taylor Voltage Model Compared to Experimental Data[7]

Ablation Model

In order to obtain an understanding of the physical nature of the electrothermal effects that occurred within the region of mixed ablated and neutral gas, an effort was made to account for the modes of energy transfer by applying an energy balance to the overall system. Figure 19 shows a schematic of the various energy modes that were present within the system during railgun operation. As can be seen in the figure, the primary input of energy is the electrical energy dissipated by the armature, $I_1 V_a dt$. This energy was then 1) stored as internal energy within the armature or ablated material, 2) transferred as thermal energy to the rails and insulation, and 3) used to vaporize material from the rail and insulators which was then added to the control volume. Therefore, not only was energy crossing the system's boundaries, but mass was as well.

The part of the system following the projectile is made up of three primary regions. The first is the high temperature armature region which according to experimental evidence[11] obtains a steady state temperature, T_{arm}, of the order of 10000°K. Another region was the neutral gas region which was modeled by the previously discussed gas dynamics model. The final region is the mixture of ablated material and neutral gas, otherwise known as the ablation region. It is this region in which most of the ablation model calculations are involved.

Since the temperature of the armature was very high, radiation heat transfer was important. Radiated energy lost by the armature was determined from the equation:

$$E_{Rad\,(Arm)} = \varepsilon\, \sigma\, \pi\, D\, L_{arm}\left(T_{arm}^4 - T_{amb}^4\right) dt \tag{33}$$

where ε was the emissivity of the armature, σ was the Stephan-Boltzmann radiation constant, D was the bore diameter, Tarm was the temperature of the armature, and T_{amb} was an assumed ambient temperature. For this model, L_{arm} was assumed to be the length of the armature as dictated by experimental evidence, approximately 6 cm.[11]

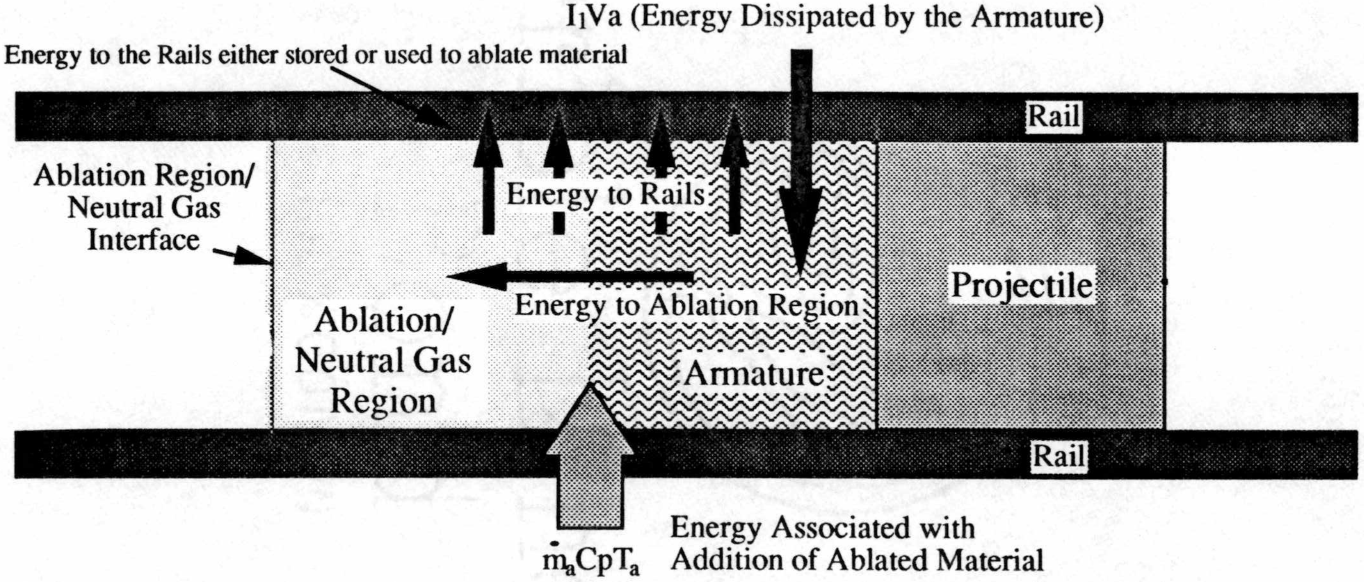

Figure 19. Energy Balance for Ablation Model

It was assumed that a fraction, β, of the power dissipated by the armature through radiation was dissipated directly into the ablation region. The remainder of the energy dissipated by the armature, $(1-\beta)E_{rad\,(Arm)}$, was deposited directly into the rails and side walls where it either melted and vaporized the rail and insulator material or it remained as stored energy. This assumed fraction, β, could be modulated to increase or decrease the amount of energy entering the ablation region. This fraction became known as the power dissipation parameter, and its use will be described in greater detail in subsequent sections.

Radiated energy lost by the ablation region can be calculated by using the equation:

$$E_{Rad\,(Abl)} = \varepsilon\,\sigma\,\pi\,D\,L_{abl}\left(T_a^4 - T_{amb}^4\right)dt \tag{34}$$

where T_a is the temperature of the ablation region and L_{abl} is the calculated length of that region. Since T_a is generally of the magnitude of 1000-2000°K, radiation lost by the ablation region is much less than the radiation lost by the armature.

For the one-dimensional model, the calculation of the extreme three-dimensional gradients which occur within ablation region was not included in this exercise. Therefore, it was necessary to assume that the properties within the ablation region changed in a uniform manner. It was recognized that it was possible for this region to be highly nonuniform, but these assumptions greatly reduced the complexity of the model, and reasonable results could still be obtained from the model.

The amount of rail material ablated into the bore was assumed to be proportional to the electrical power dissipated by the armature, after Parker:

$$\frac{dm_a}{dt} = \alpha\,I_1\,V_a = \dot{m}_a\,, \tag{35}$$

where α was the characteristic ablation rate coefficient for the rail material.[1] Various values of ablation rates for several different materials commonly used in railguns can be found in Reference [1].

It was also determined that it would be difficult to quantify actual temperatures of the ablated material as it entered the bore. Therefore, it was necessary to assume an initial temperature, T_{abl}, and determine the energy associated with the mass addition with the equation:

$$E_{abl} = \dot{m}_a Cp_{a_1} T_{a_1} dt \,. \tag{36}$$

From experimental data, T_{a1} was considered to be between 1000-2000°K. The remainder of the energy originally lost to the rail remained as stored energy.

The total amount of rail material ablated into the so-called ablation region was found by applying the following relationship:

$$m_{a_2} = m_{a_1} + \dot{m}_a \, dt \,. \tag{37}$$

Concerning the mass of the armature, it was assumed that only a certain fraction, λ, of the ablated material could be ionized and entrained by the plasma armature which would result in an increase in armature mass. Therefore, the time rate of change in mass of the armature, m_{arm}, with respect to time was:

$$\frac{dm_{arm}}{dt} = \lambda \dot{m}_a \,. \tag{38}$$

Total mass of the armature was then found with the equation:

$$m_{arm_2} = m_{arm_1} + \lambda \dot{m}_a \, dt \,. \tag{39}$$

For this particular model, it was assumed that even though the ablated rail material was accelerated by the armature, none of material was entrained by the armature; therefore, the armature mass remained constant. This assumption could be made based upon the fact that experimental evidence obtained at UTSI indicated that ablated material entering the armature was ejected rearward and was not entrained.[6] Therefore λ was set to zero.

Applying the energy equation to the armature only yields the relation:

Applying the energy equation to the armature only yields the relation:

$$I_1 V_a - E_{Rad\,(Arm)} + m_{arm} Cp_{arm} T_{arm_1} = m_{arm} Cp_{arm} T_{arm_2} \tag{40}$$

From this equation, it was possible to determine a new armature temperature, T_{arm2}.

Then, applying the energy equation to the ablation region, the following relation evolved:

$$\beta E_{Rad\,(Arm)} - E_{Rad\,(Abl)} + \dot{m}_a Cp_a T_{abl} dt + m_{a_1} Cp_a T_{a_1} = m_{a_2} Cp_a T_{a_2} \tag{41}$$

Now, the new temperature in the ablation region T_{a2}, could be calculated.

Using the assumption that the ablation region maintained uniform properties and that m_a was the total mass of material within the ablation region, the density of material, ρ_a, could be calculated by using the following relationship:

$$\rho_a = \frac{m_a}{A_{cs}\,L_{abl}}\,, \tag{42}$$

where A_{cs} is the cross-sectional area of the bore.

Pressure was then found by assuming that the vaporized material within the ablation region was in a single phase, and that it behaved as a perfect gas, i.e., by using the perfect gas relation:

$$P_a = \rho_a\,R_a\,T_a\,, \tag{43}$$

where R_a was an effective gas constant for the ablated material. It should be noted that the pressure indicated by this relationship is the thermal pressure of the material within the ablation region and does not include the pressure due to the Lorentz force present within the armature.

It was assumed that the ablation region and the neutral driving gas were separated by a free surface interface. Although it was possible that mass might be exchanged between the two regions, it was assumed in this model that the mass flow across the interface was equal to zero.

Figures 20 and 21 show the position and velocity of the interface during the railgun simulation, respectively. Since it was assumed that no flow occurred across the interface, it then had to move at the flow velocity directly behind the interface in order to maintain continuity. Therefore, the interface moved at a velocity, v_Z, which was equal to the most recently calculated flow velocity in the most recently created cell behind the interface. The position of the interface, x_Z, was found by integrating the following equation using a finite difference relationship:

$$x_{Z_2} = x_{Z_1} + v_Z \, dt \,. \tag{44}$$

The pressure difference across the interface was the primary factor in determining the interaction of the ablation region and the driving gas. Once the ablation region's pressure was calculated, the change in pressure associated with the wave shed at the interface was determined by the equation:

$$dP = -a\rho \, du + dP_Z \,, \tag{45}$$

where dP_Z was the difference between the ablation region pressure, Pa, and the flow pressure in the most recently created cell. If $dP_Z - a\rho du > 0$, then the shed wave was a compression wave, otherwise it was a rarefaction wave.

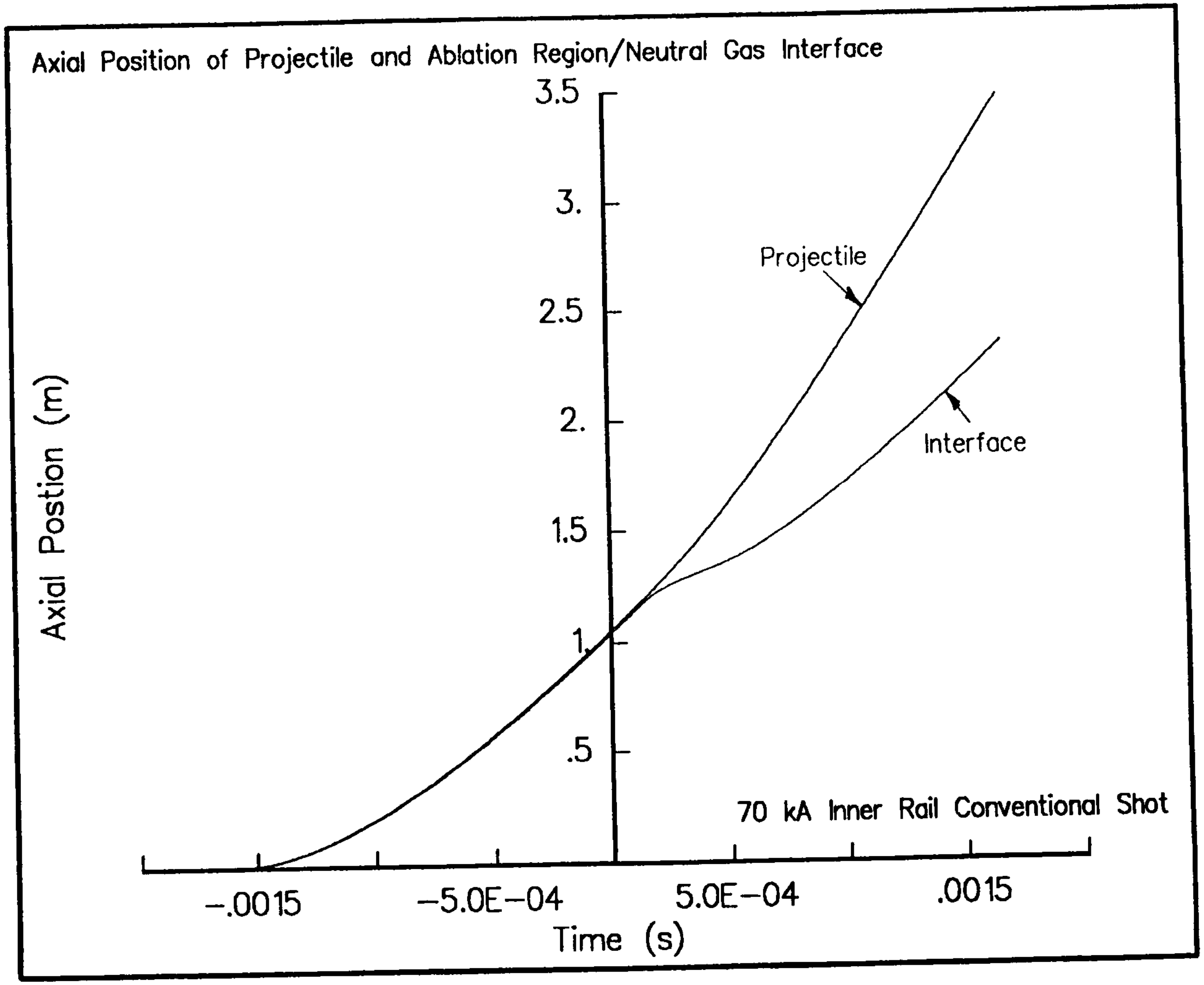

Figure 20. Position of Projectile and Ablation Region/Driving Gas Interface

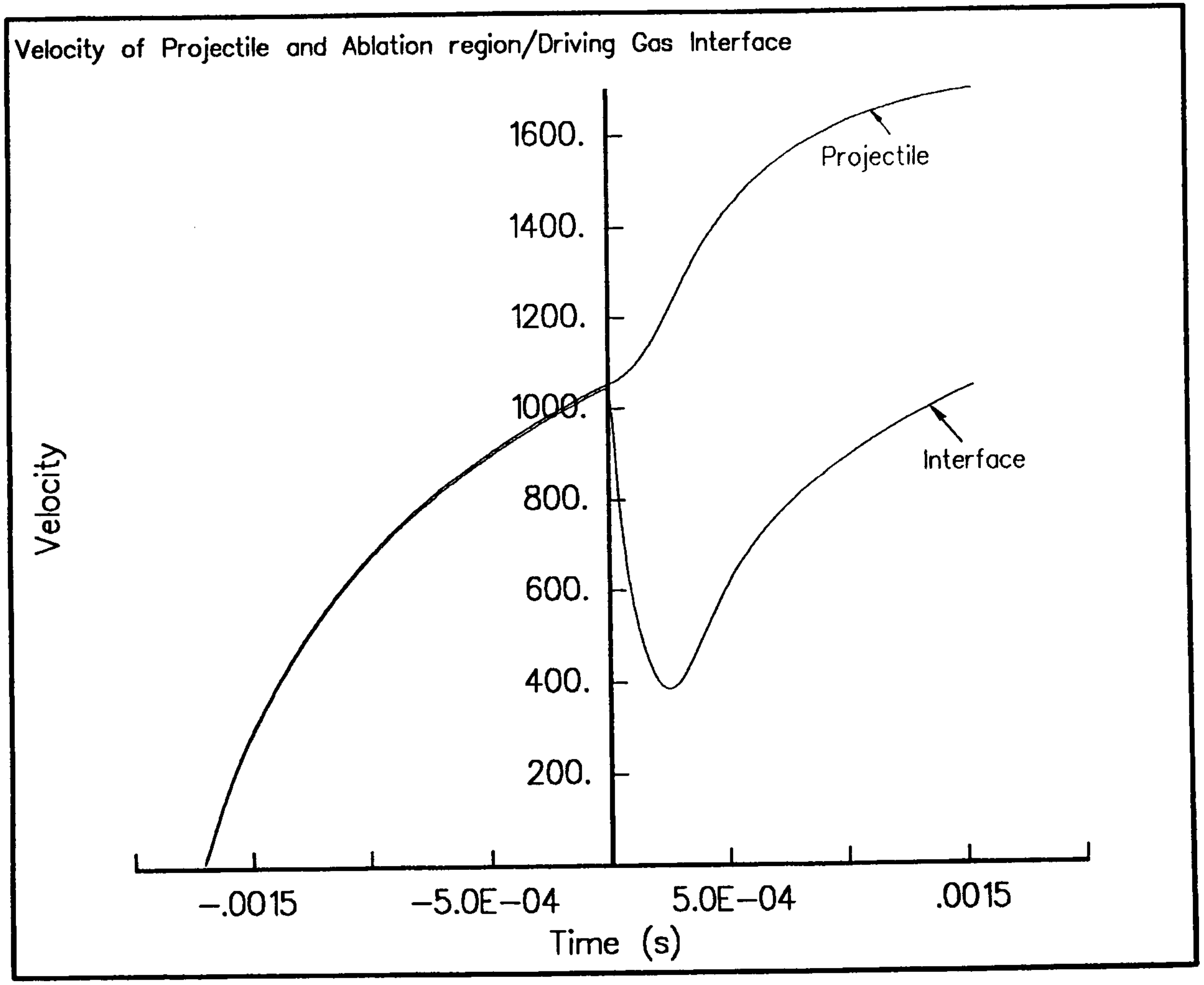

Figure 21. Velocity of Projectile and Ablation Region/Driving Gas Interface

Armature Viscous Drag Model

It was assumed that the armature was undergoing highly turbulent flow with very thin boundary layers. As previously discussed, Parker stated that these effects were caused by the intense MHD effects present within the armature. Thin boundary layers caused the viscous gradients to be much greater than would normally be expected.[1,17]

In order to model the viscous drag of the armature, it was estimated that a coefficient of friction, Cf_{arm}, ranging from 0.001 to 0.003 adequately determines the friction within the armature. Therefore, the drag force, F_D, was found using equation[1]:

$$F_D = \frac{1}{2} \rho_{arm} u^2 C_{f_{arm}} \pi D L_{arm} . \tag{46}$$

where ρ_{arm} was a calculated density of the armature material.

Experimental evidence indicated that the length of the armature grew fairly rapidly to a steady state value and remained at that value down the remainder of the bore. For the UTSI railgun, the armature length was a nominal 6 cm for both conventional and augmented shots. Therefore, once the armature length reached this nominal value, the values of ρ_{arm} and L_{arm} remained constant throughout the rest of the bore travel. This value was used to determine viscous friction within the armature for the remainder of the simulation.

Flow Friction Model

An attempt was made to incorporate a frictional model into the flow condition calculation routine. In order to do this, it was assumed that even though the flow crossed the waves isentropically, flow between the waves incurred losses from viscous interaction with the wall. From these assumptions, a one-dimensional model was developed to simulate the flow friction.

It was assumed that the viscosity of the gas, μ, obeyed the Sutherland Power Law of viscosity which was represented by the equation:

$$\mu = \mu_0 \left(\frac{T}{T_0}\right)^{\frac{3}{2}} \left(\frac{T_0 + S}{T + S}\right), \tag{47}$$

where μ_0 is the reference viscosity, T_0 is the reference temperature, and S is the characteristic temperature of the gas. Reference values of μ_0, T_0 and S for Helium are found in White's Viscous Fluid Flow.[19]

The diameter Reynold's number, Re_D, was found from the familiar equation:

$$Re_D = \frac{\rho\, u\, D}{\mu}, \tag{48}$$

where ρ was the flow density, u is the flow velocity, and D was the bore diameter.

The coefficient of friction was estimated by assuming that the bore walls were smooth, and by taking an empirical curve-fit of the Moody chart for pipe flows. One such curve-fit was the explicit formula given by Haaland[8] as:

$$C_f = \left(-3.6 \log\left(\frac{6.9}{Re_D}\right)\right)^{-2}. \tag{49}$$

The flow was assumed to be flowing at a uniform velocity with uniform flow conditions. It was assumed that the pressure in a particular cell was decreased by friction which occurred along the wall. The friction force, f_d, which occurs between successive waves was estimated by the equation:

$$f_d = \frac{1}{2} \rho \, u^2 \, C_f \, \pi \, D \, (X_{w_{i+1}} - X_{w_i}) \,, \tag{50}$$

where X_{wi+1} and X_{wi} were successive wave positions.

Taking the momentum equation:

$$P_1 + \rho_1 u_1^2 - \frac{f_d}{A_{cs}} = P_2 + \rho_2 u_2^2 \,, \tag{51}$$

and solving for P_2:

$$P_2 = P_1 - \frac{f_d}{A_{cs}} + \rho_1 u_1^2 - \rho_2 u_2^2 \ . \tag{52}$$

It was assumed that $\rho_1 u_1 = \rho_2 u_2$ for continuity and that velocity change in the flow was negligible; therefore, equation (52) reduced to:

$$P_2 = P_1 - \frac{f_d}{A_{cs}} \ . \tag{53}$$

After the new cell pressure was calculated, the dP associated with that cells wave now became the difference between the new cell pressure, P_i, and the pressure calculated for the previous cell, P_{i-1}, or otherwise stated:

$$dP = P_i - P_{i-1} \ . \tag{54}$$

The flow velocity change, du, associated with this dP was given by the equation:

$$du = -\frac{dP}{(u - V_w)\,\rho} \,, \tag{55}$$

Flow temperature, T, was calculated by using the perfect gas equation:

$$T = \frac{P}{R\,\rho}\,. \tag{56}$$

From this new temperature a new speed of sound was calculated by using equation (10) which is restated here for convenience:

$$a^2 = \gamma RT\,. \tag{10}$$

The next wave's velocity was calculated based on the new flow conditions. The same equations were used to determine wave velocity as were previously shown in the original gas dynamics model, equations (11) - (17).

One problem was later found in the assumption to reduce equation (52). If Δu is small then ΔP is small, and the assumption that Δu is negligible is not a valid assumption. Therefore, for the model no flow friction values were calculated. According to previous work, this should account for an approximate increase of 2% in performance.

Model Integration and Build-up of Effects

The particular models shown were selected to simulate the various electrothermal effects which were believed to occur within the railgun during railgun operation. The individual models were integrated in a manner which would most accurately duplicate the physical nature of the railgun. This section identifies the procedure used within the computer program to integrate the various models in order to simulate the electrothermal effects. The importance of the particular models is discussed, and the various impacts which these models have on the predicted performance are identified.

In modeling the electrothermal effects that occur within the railgun, the gas dynamic model was the most important of the ones mentioned in the previous sections, and it eventually became the basic foundation upon which the other models were then added.

Figure 22 shows a simulation of the railgun model with only the gas dynamic model operating. In essence, this simulated a light gas gun shot and predicted an exit velocity of 1278 m/s using the reservoir pressure of 22.06 MPa (3200 PSI) and 25°C (77°F). This simulation assumed that there was no flow friction and that there was no in-bore gas pressure.

The electromagnetic model was the primary model used to predict the performance within the railgun itself. Figure 23 shows the effects of the electromagnetic model with the inner rail operating at a maximum of 70 kA. The figure shows a simulation with electromagnetic model only compared to a simulation with both the electromagnetic effects and driving gas models included. The electromagnetic model operating alone predicted an ideal velocity of 1696 m/s. As can be seen in the figure, the gas dynamic model predicted a signficant boost in overall performance to this particular railgun as indicated by calculating a higher exit velocity of 1832 m/s.

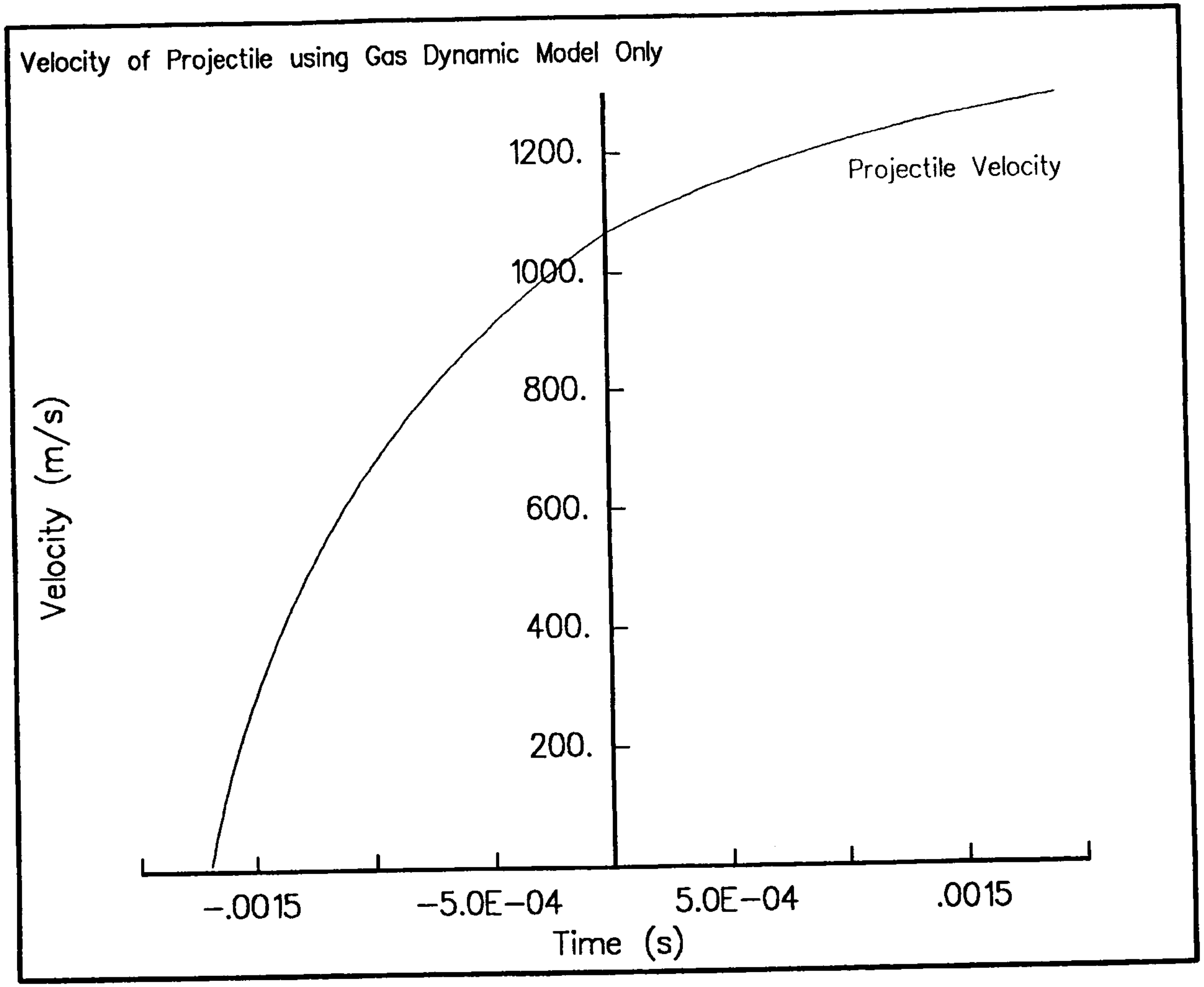

Figure 22. Projectile Velocity of Gas Dynamic Model

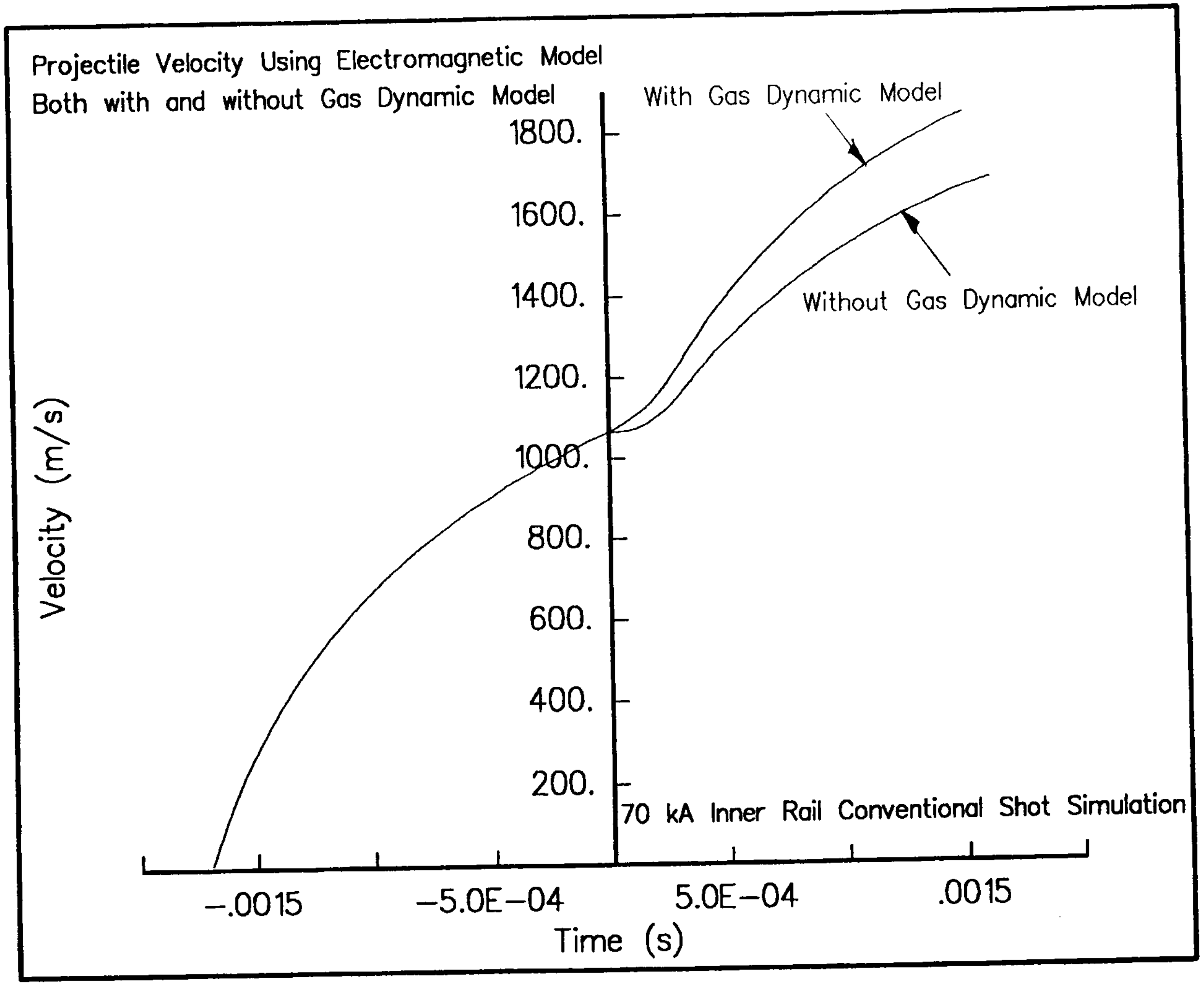

Figure 23. Projectile Velocity of Inner Rail Electromagnetic Model

Figure 24 shows simulations with the augmented rails also operating at 70 kA. Although the increment between the electromagnetic only and the electromagnetic and gas dynamic model still existed, the increment was smaller because the higher accelerations present in the augmented case reduce the driving potential of the injection gas. The electromagnetic model alone predicted an augmented velocity of 2490 m/s while the combined electromagnetic and driving gas model predicted an exit velocity of 2585 m/s.

Figure 25 shows the impact of in-bore gas pressure on the 70 kA conventional railgun simulation and 70-70 kA augmented railgun simulation. Using a background pressure of 0.506 MPa (7.35 PSI), the in-bore gas ahead of the projectile caused only a slight decrease in exit velocity in the conventional shot, but the impact of in-bore gas was greater in the augmented case because of the higher values of dP which occurred with the higher accelerations..

The next effects to be accounted for were the electrothermal effects of ablation. Figure 26 shows a parametric study of the effects of various rates of ablation coming off the inner rail into the bore. In these simulations it was assumed that all of the ablated material was accelerated by the armature to the projectile's velocity creating a momentum loss but was immediately lost by the armature. Therefore the rate of mass addition into the armature was assumed to be zero. Based on work by Parker, the ablation coefficient of 3 g/MJ, which was the median point of the parametric study, was considered to be adequate in simulating the rate of ablation from the rail surface so this value was used in subsequent calculations.

Figure 27 shows several projectile velocities based on various rates of mass addition into the armature. For all of the cases shown in the figure, an ablation rate coefficient of 3 g/MJ was used. As can be seen, the higher the amount of entrainment of material into the armature, the more significant the decrease in performance of the railgun.

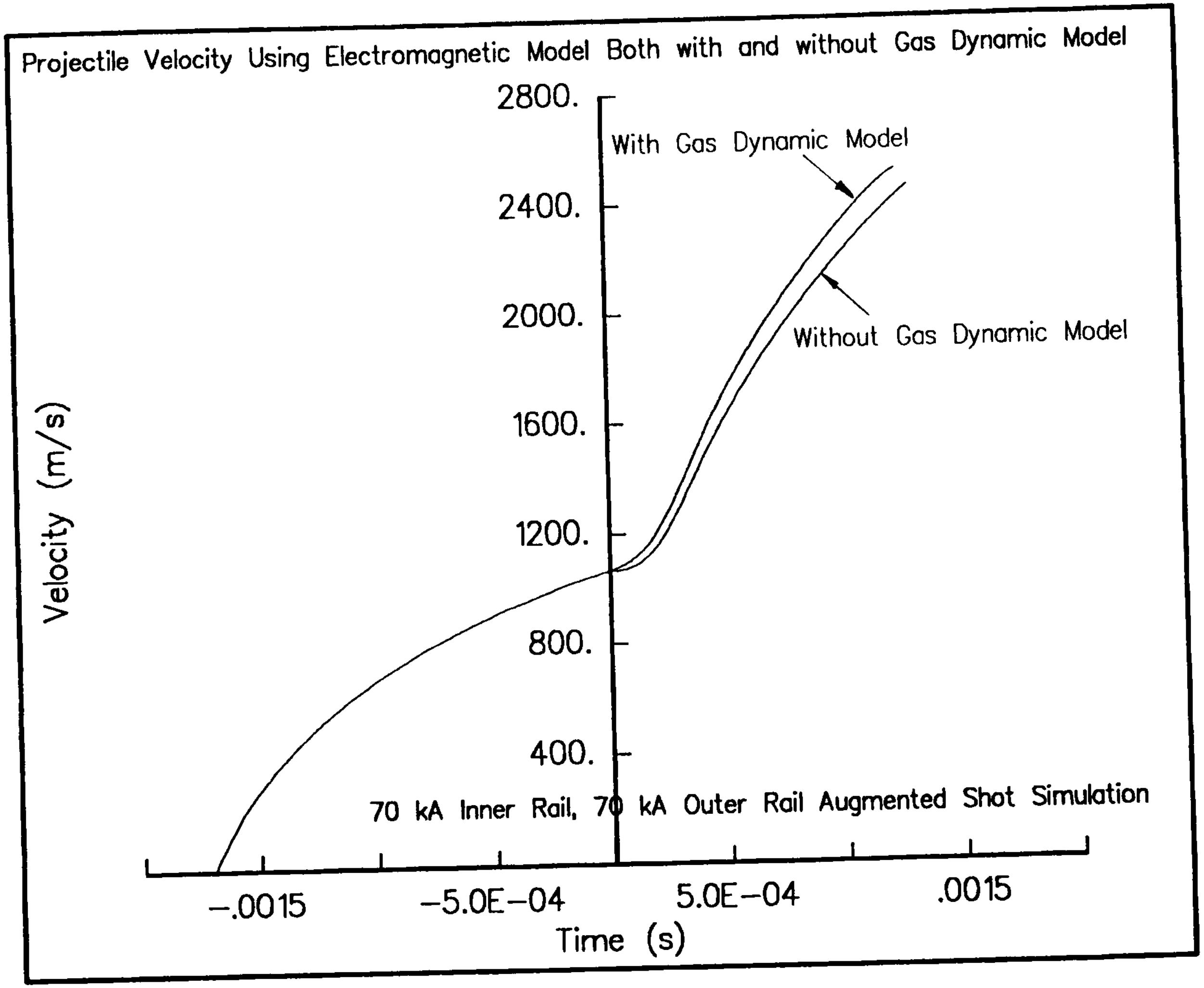

Figure 24. Projectile Velocity including Augmented Rail Electromagnetic Model

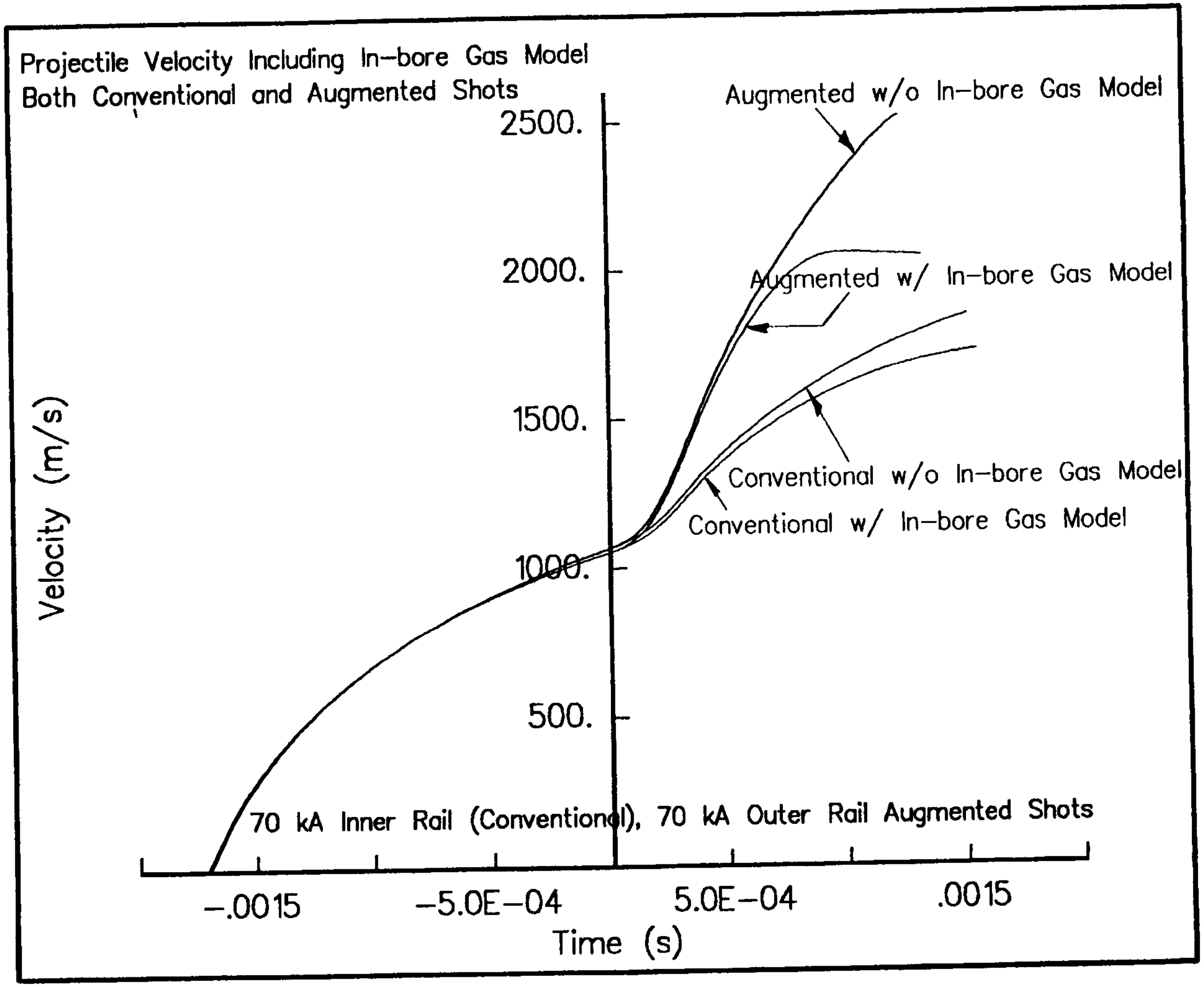

Figure 25. Projectile Velocity including In-bore Gas Model

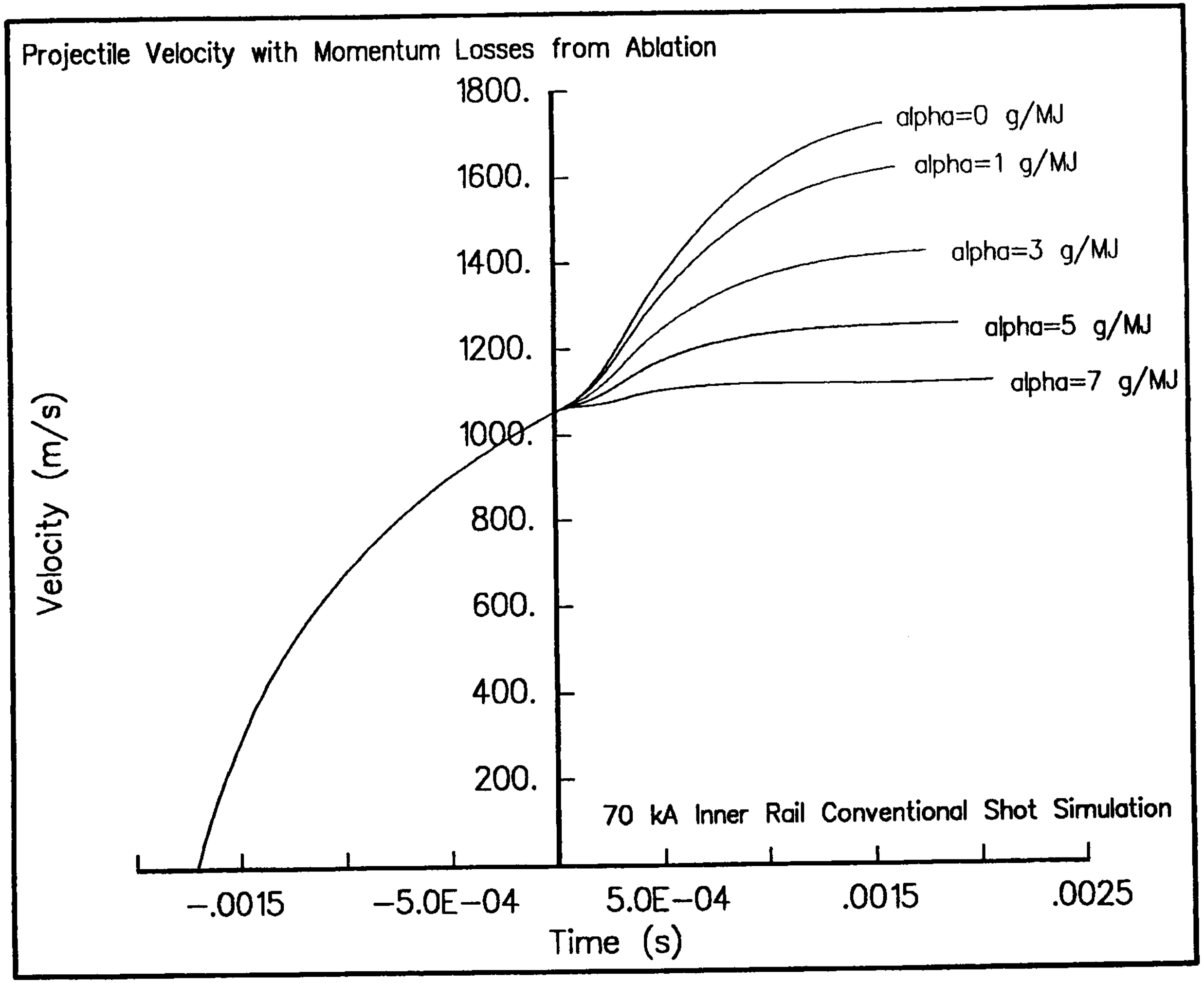

Figure 26. Projectile Velocity including Ablation Momentum Losses

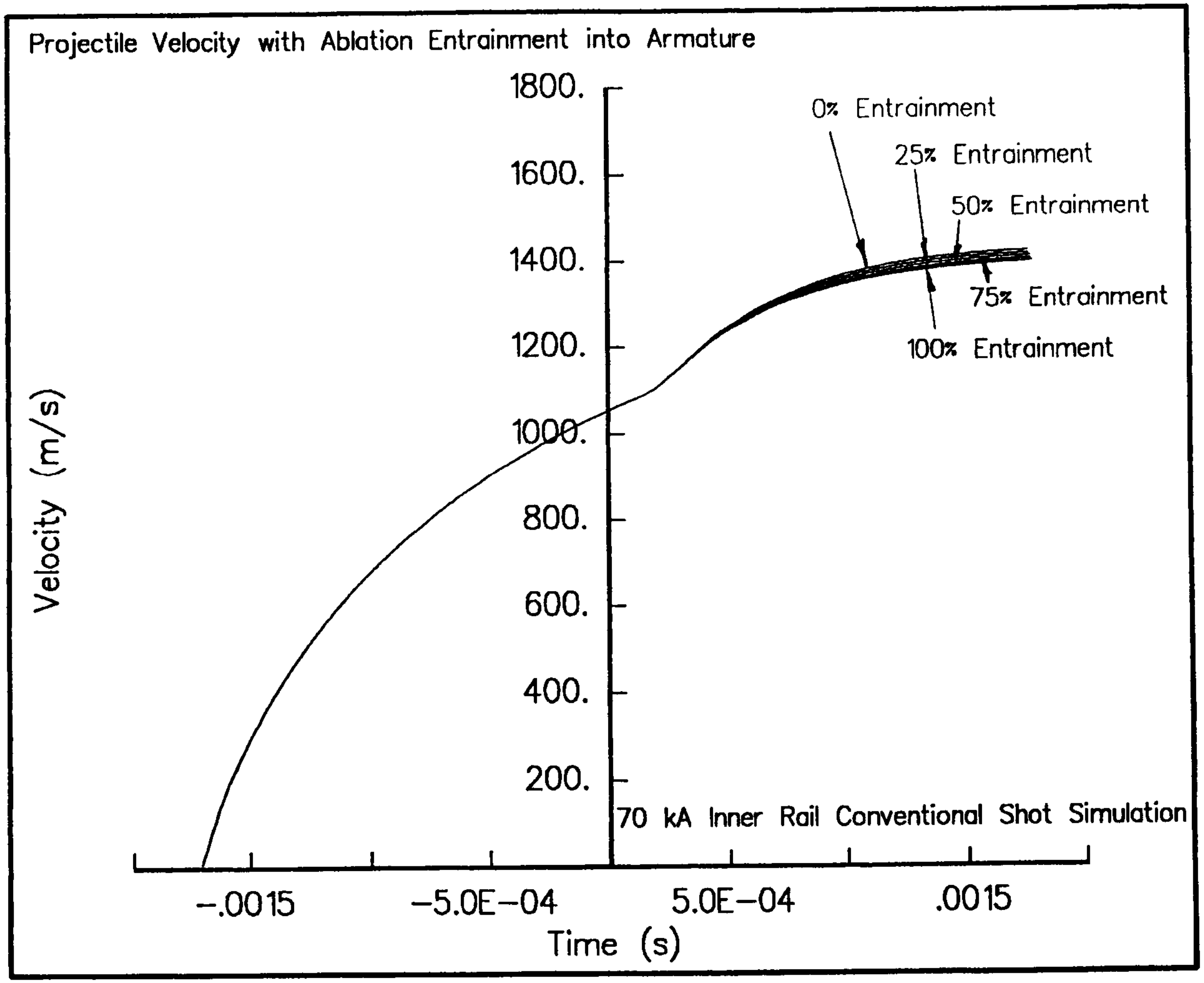

Figure 27. Projectile Velocity including Ablation Entrainment into Armature

However, according to the figure, the effect was smaller than was expected. This small difference reflects the difference between accelerating the ablated mass with the armature or accelerating it in the ablation region. Fortunately, experimental evidence indicated that the rate of mass addition into the armature was zero[11] so this value of mass addition was selected for subsequent simulation.

Previous theoretical work[16] indicated that flow friction within the bore would decrease performance by approximately 2% as compared to ideal analysis. The flow friction model severely overpredicted the effects of friction within the driving and in-bore gas. The impact imparted by the friction model was deemed to be too great to provide realistic performance results. It was determined that an error was made in the derivation of the friction model. Therefore, in subsequent simulations, the flow friction model was not used. This decision tended to produce performances slightly greater than expected, but according to previous work by Siegel[16], the frictionless assumption in ballistic analysis still provided reasonable results.

IV. COMPARISON OF RAILGUN MODEL AND EXPERIMENTAL DATA

The integrated model presented in the previous section was used to simulate the performance of the railgun under different operating conditions. The various parameters were modified in order to match numerical results to experimental data. Once the parameters were matched, attempts were made to determine trends that might indicate some predictable physical behavior which occur during railgun operation. The different railgun modes simulated included light gas gun, conventional and transaugmented plasma armature railgun, and conventional and transaugmented hybrid armature railgun.

During each railgun simulation, the entrainment parameter was set to zero and the ablation coefficient was set to 3 g/MJ. The power dissipation parameter for each shot was modulated in order to match the pressure increase measured by the PT2 pressure transducer. Once the pressure increase was matched, the simulated and experimental velocities were compared to determine if the measured pressure increase provided the same performance as was actually seen. For the light gas gun case, the ablation coefficient, and entrainment coefficient, and power dissipation parameter were all set to zero to simulate its actual operation.

Light Gas Gun

Several light gas gun shots were performed on the railgun to help calibrate the pressure transducers and to ascertain the performance of the gun with only the driving gas of the injector. Since no armature existed within the bore, no position data could be acquired by the B-dot probes. The velocity measurement of the MAVIS was the only data available for comparison to numerical simulation. Figure 28 shows the simulated velocity profile of a light gas gun shot with an initial reservoir pressure and temperature of 22.06 MPa and 25°C along with the experimentally obtained MAVIS velocity. The predicted exit velocity at 1256 m/s as compared to the MAVIS velocity of 1243 m/s shows that the gas dynamic model produces accurate results for light gas gun analysis; this provided confidence in its ability to predict gas dynamic performance during railgun operation.

Figure 29 shows a comparison of the experimentally obtained PT2 pressure probe data as compared to numerical results of the pressure at the PT2 axial station. As can be seen, the magnitude of the simulated results were not exactly the same as the experimental data, but the numerical results followed the same trends and closely followed the behavior of the experimental data. It was assumed that the difference in magnitude could be accounted for by the absence of the flow friction model in the simulation.

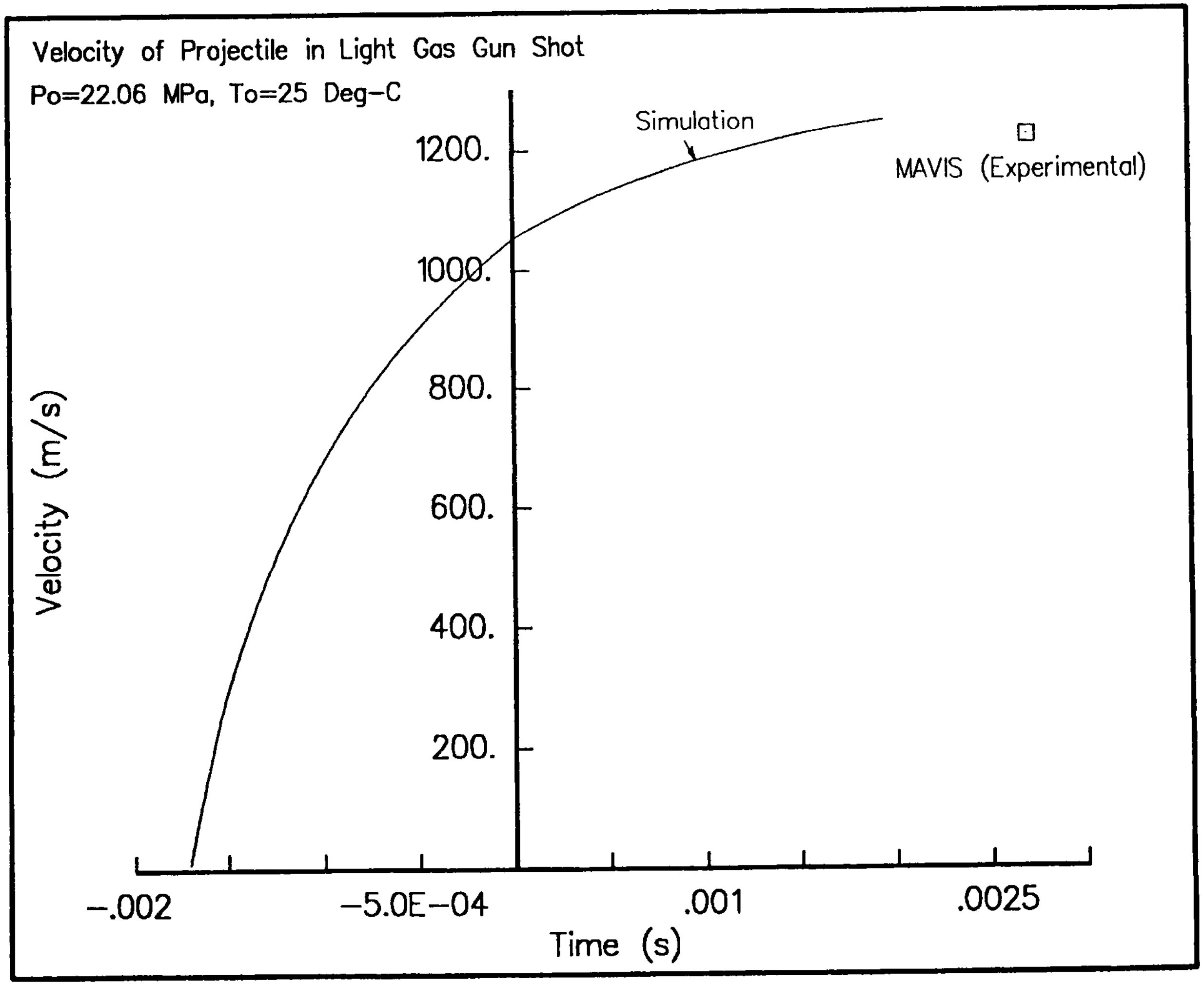

Figure 28. Numerical and Experimental Velocity of Light Gas Gun Shot

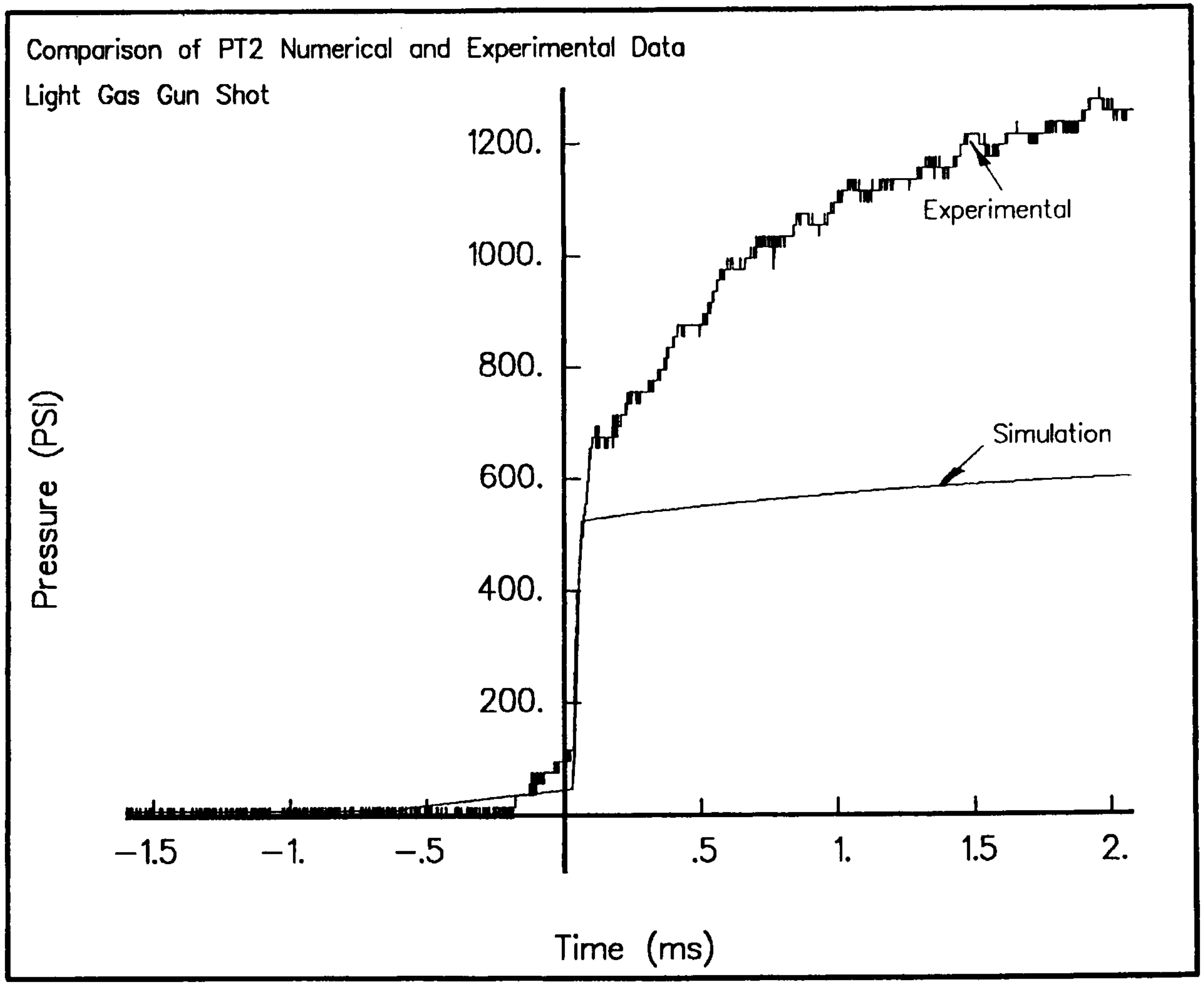

Figure 29. Numerical and Experimental PT2 Pressure of Light Gas Gun Shot

Figure 30 shows the magnitude of the various forces calculated during the simulation of the light gas gun shot. As expected, the driving gas pressure decayed smoothly from the reservoir pressure toward the background pressure The in-bore gas pressure increased as the projectile underwent the higher rates of acceleration at the beginning of the simulation, but eventually leveled toward the end of the simulation. For this simulation, the Lorentz force, ablation momentum loss, and armature viscous drag were all equal to zero since the railgun section was inoperative.

Conventional Plasma Armature Railgun

The railgun was configured as a conventional railgun and fired to maximum currents of 70, 100, and 140 kA on the inner rail. During each shot the position data from the B-dot probes and pressure data from the pressure transducers were recorded. For each of these shots both in-bore and MAVIS velocity data were available for comparison with numerical results since the B-dot probes were able to sense the passage of the armature as it passed.

Figure 31 shows a comparison of numerical and experimental velocity data for a 70 kA conventional shot. As can be seen in the figure, the experimental velocity appeared to increase to a maximum value of 1690 m/s and then began to decrease. The reason for this was that the B-dot data from which the velocity profile was derived by sensing the position of the armature and not the projectile. The appearance of deceleration in the velocity profile could be explained by separation of the armature from the rear face of the projectile near the end of the railgun where Lorentz forces were no longer strong enough to maintain the high pressures. The main point was that the numerical velocity and experimental velocity maintain similar profiles during primary acceleration sequence in the railgun.

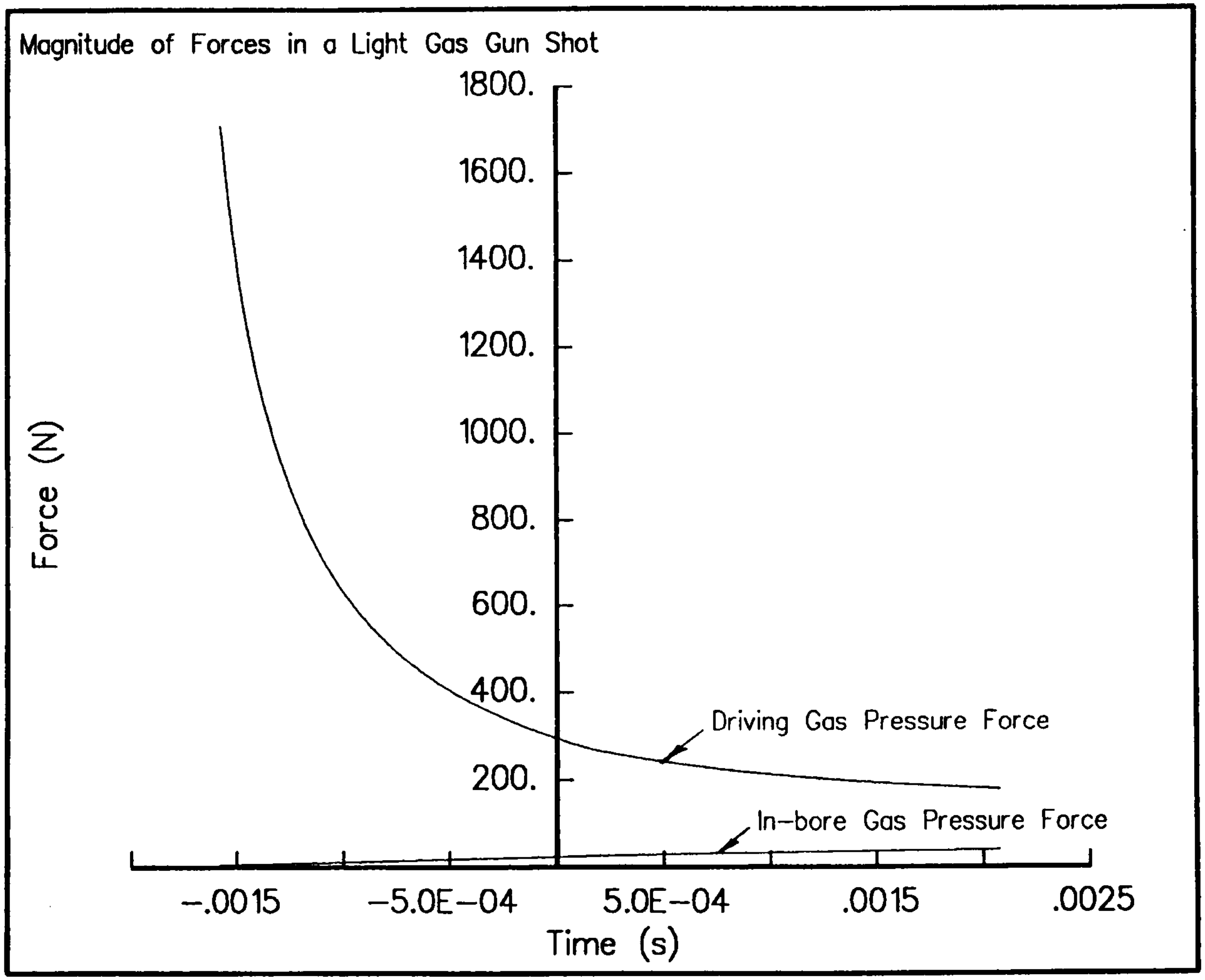

Figure 30. Magnitude of Forces for Light Gas Gun Simulation

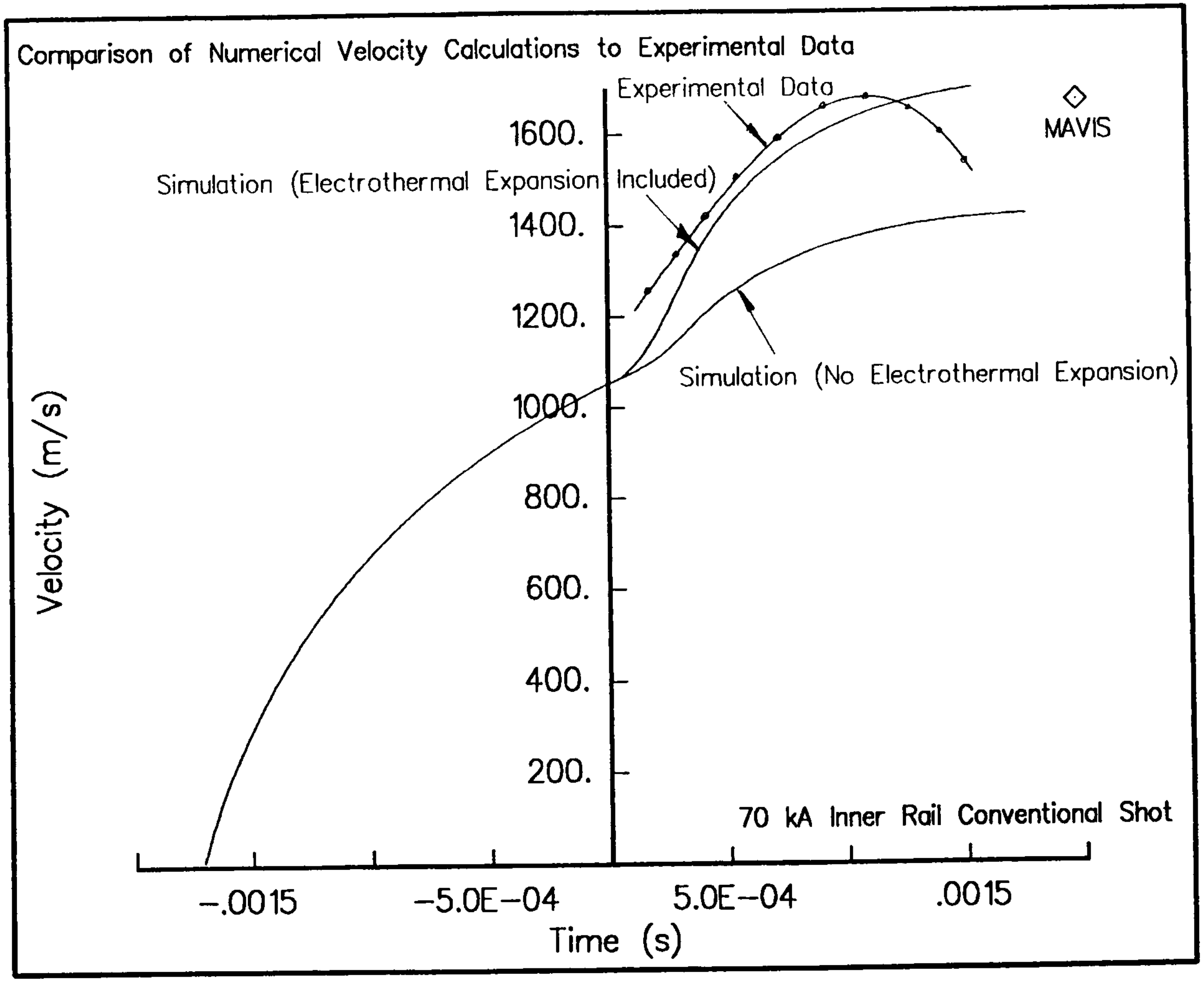

Figure 31. Numerical and Experimental Velocity for 70 kA Conventional Shot

The numerical simulation determined an exit velocity of 1710 m/s where as the MAVIS measured a velocity of 1662 m/s. This indicated that the model closely predicted the performance of the railgun at this power setting. Notice that without the electrothermal expansion accounted for, the simulation only predicted an exit velocity of 1405 m/s. This electrothermal expansion accounted for a 16.9% increase in performance.

Figure 32 shows a comparison of the numerical and experimental PT2 pressure data. The thermal expansion parameter was modulated until the pressure increase from the fusing transient shock wave was matched. Modulating the parameter indicated that 35% of the energy dissipated by the armature went directly into creation of the fusing transient. As can be seen, this amount of thermal expansion provided very similar velocity profiles for this relatively low powered railgun shot.

Figure 33 shows the magnitude of the forces as they were calculated by the railgun model. For this case, the driving gas pressure and electromagnetic forces were of similar magnitude while the remaining forces were relatively small in comparison. The only other force which provided any significant impact on performance was the ablation momentum loss term. The momentum loss term was equal to the vdm/dt term in equation (6) where dm/dt was assumed to be proportional to the power dissipated by the armature.

The next case studied was the 100 kA conventional railgun shot. Figure 34 shows the experimental PT2 data compared to PT2 values calculated by the program. The PT2 pressure data was matched with the numerical results by modulation of the power dissipation parameter and revealed that 30% of the dissipated energy went to support the creation of the fusing transient and subsequent thermal expansion behind the projectile. Figure 35 shows a comparison of the numerical velocity compared to the experimental data. Again, the numerically derived projectile velocity of 2425 m/s matched closely with the

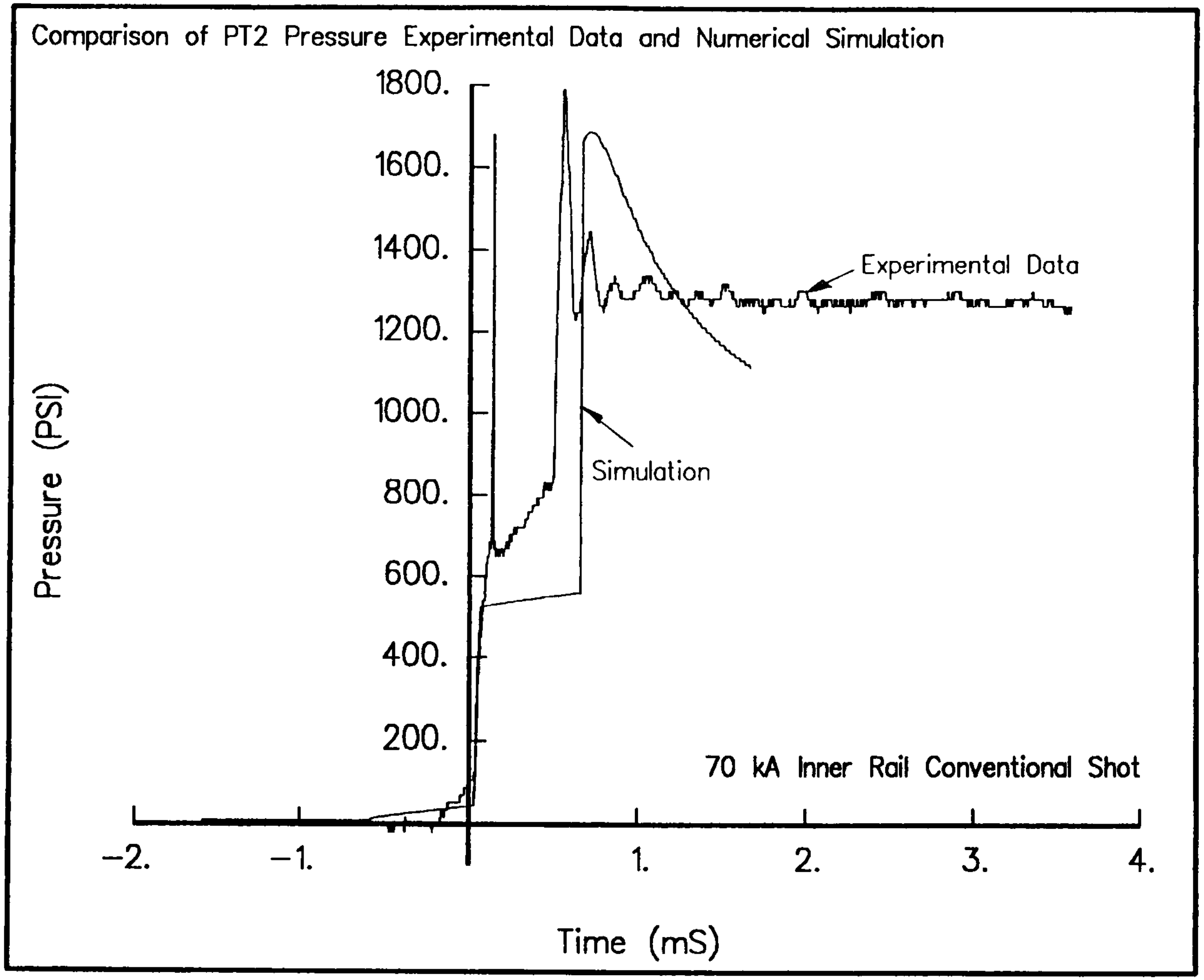

Figure 32. Numerical and Experimental PT2 Data for 70 kA Conventional Shot

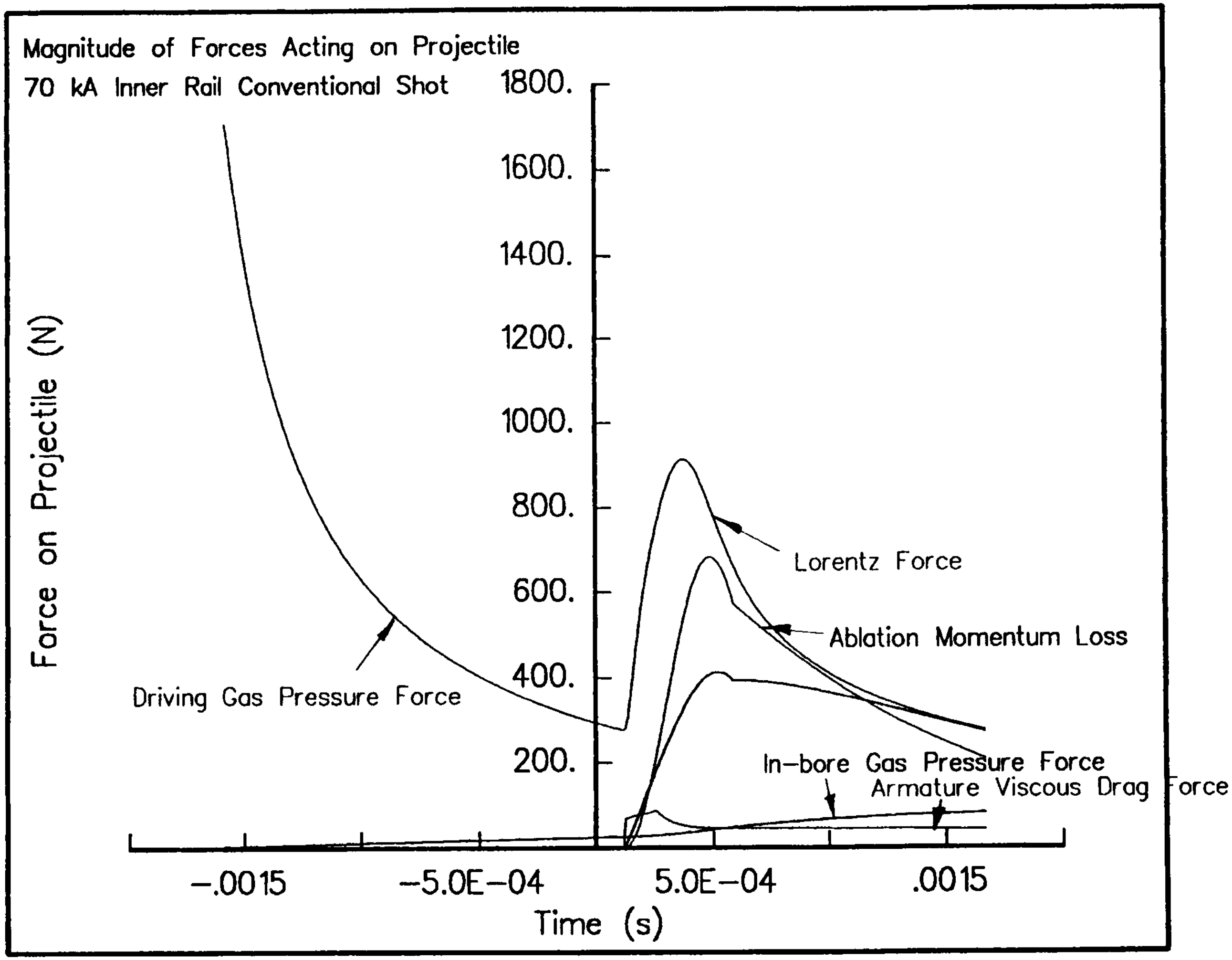

Figure 33. Magnitude of Forces for 70 kA Conventional Railgun Simulation

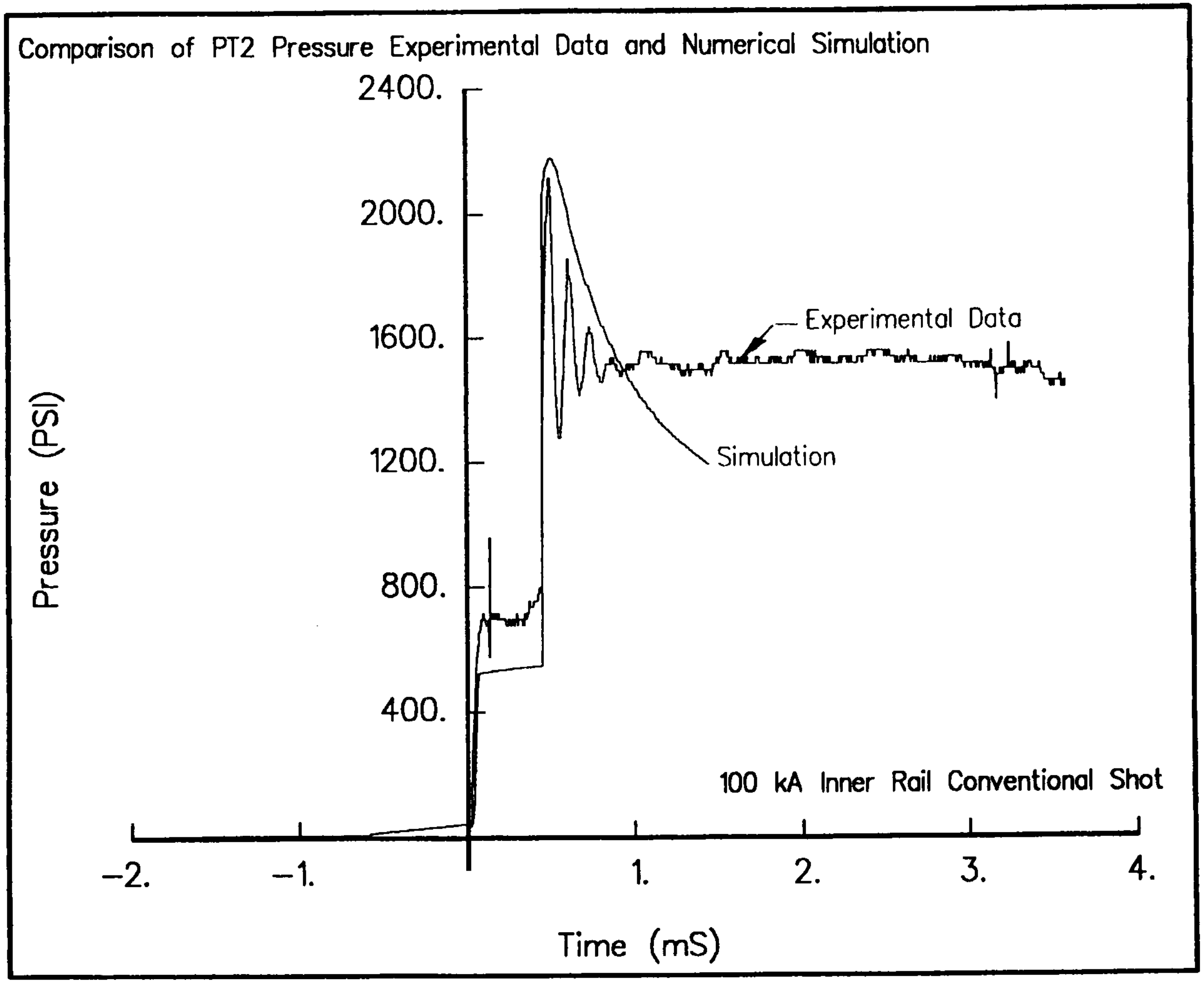

Figure 34. Numerical and Experimental PT2 Data for 100 kA Conventional Shot

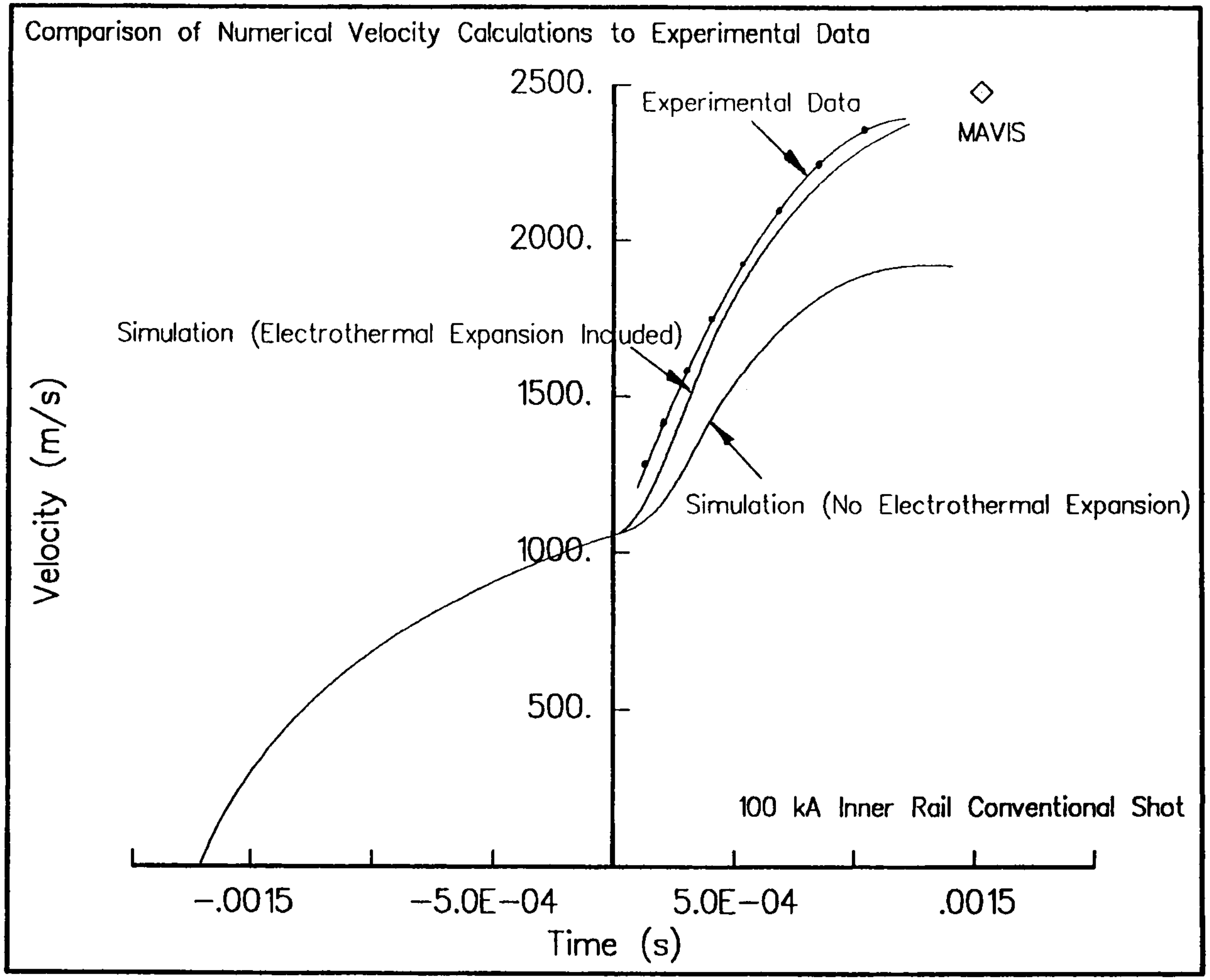

Figure 35. Numerical and Experimental Velocity for 100 kA Conventional Shot

experimentally measured velocity of 2436 m/s. Without electrothermal effects, the simulation predicted an exit velocity of 1926 m/s, a difference of 20.6% in performance.

Figure 36 shows that Lorentz force dominated over the other forces throughout most of the railgun for the 100 kA shot. However, the impulse given to the driving gas by the fusing transient still made it a major contributor to the overall performance. The ablation momentum loss term increased proportionally with the increase in Lorentz force (both ablation and Lorentz force in this model depend directly on current). In-bore gas pressure showed an increase because of the increase in acceleration during railgun operation.

The final case studied for the conventional railgun configuration was the 140 kA inner rail current shot. Figure 37 shows a comparison of the experimental and numerical pressure data. Again, the power dissipation parameter was adjusted in order to match the observed pressure increase sensed by the PT2 pressure probe. Modulation of the thermal expansion parameter revealed that 15% of the power was dissipated into the expanding products. Figure 38 shows the calculated velocity profile compared to the experimental velocity. The figure shows a velocity profile calculated with no electrothermal effects and a velocity profile with electrothermal effects included. Again, the numerical velocity of the case with the fusing transient included matched the experimental data. The program estimated an exit velocity of 2522 m/s while the MAVIS indicated an exit velocity of 2491 m/s. The simulated magnitude of forces can be seen in figure 39. The Lorentz force again dominated all of the other forces and the thermal expansion boost to the driving potential of the gas still provided significant thrust. However, the in-bore gas pressure intensified because of the increased acceleration and the ablation momentum loss term grew, thereby becoming significant impedances to further acceleration.

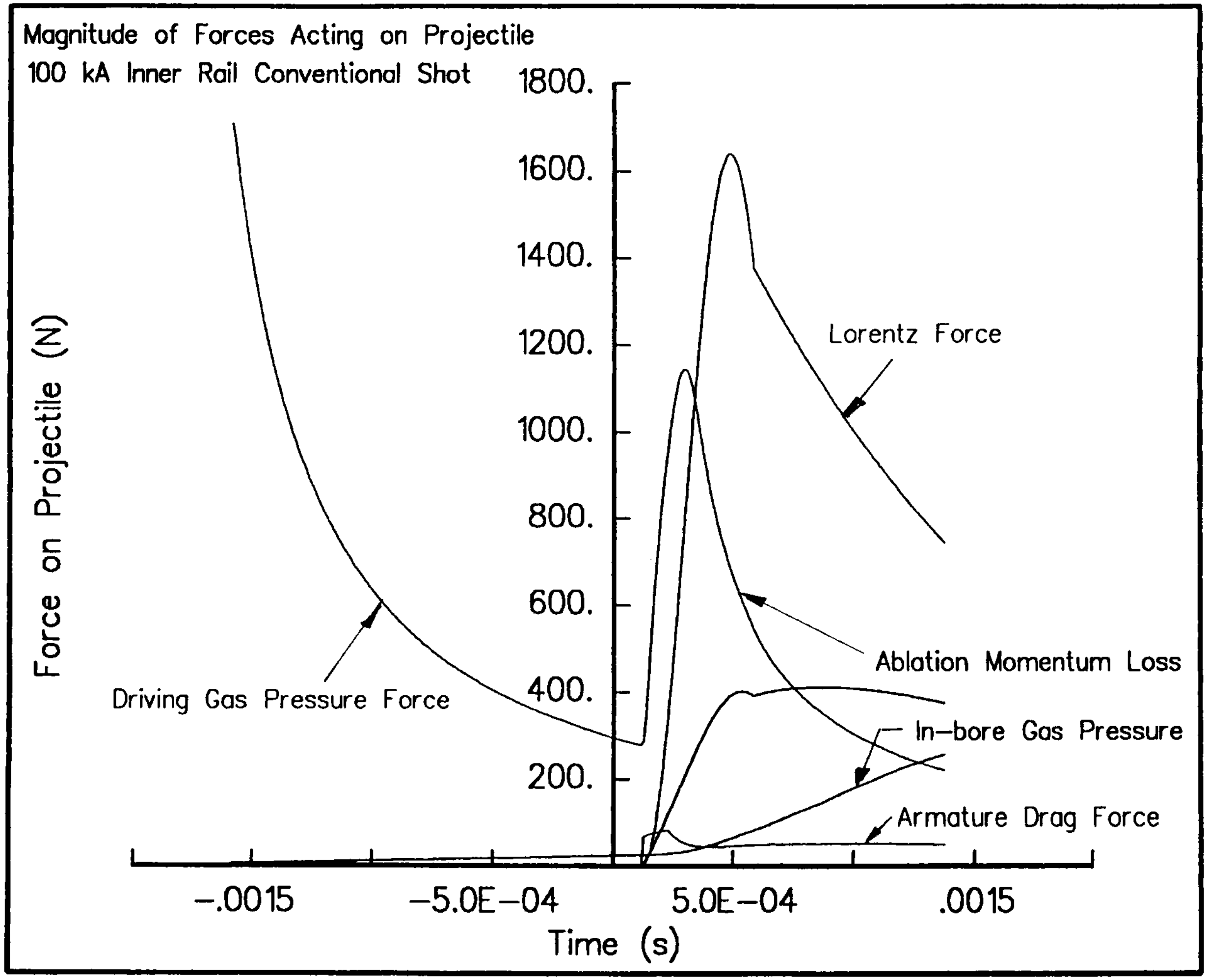

Figure 36. Magnitude of Forces for 100 kA Conventional Railgun Simulation

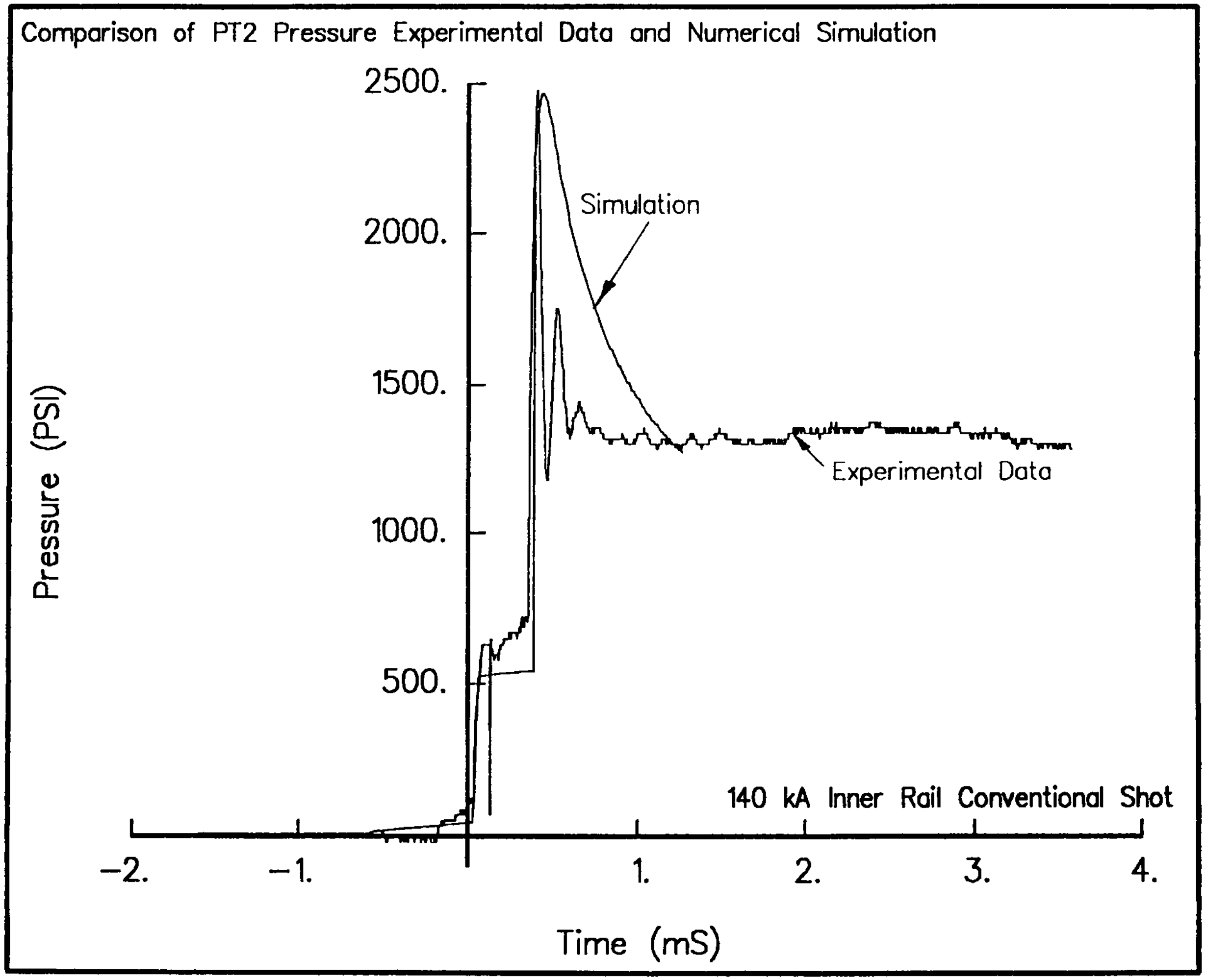

Figure 37. Numerical and Experimental PT2 Data for 140 kA Conventional Shot

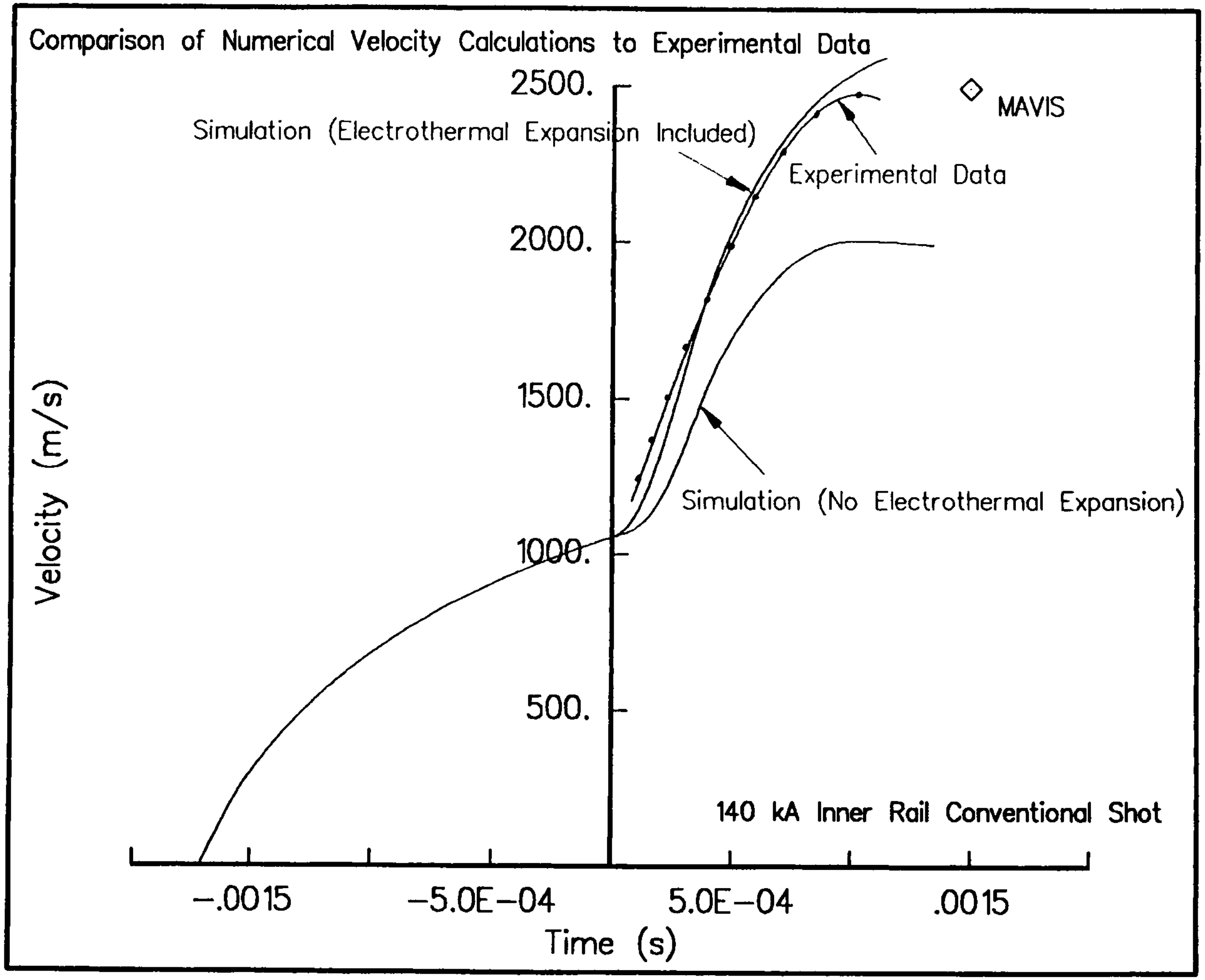

Figure 38. Numerical and Experimental Velocity for 140 kA Conventional Shot

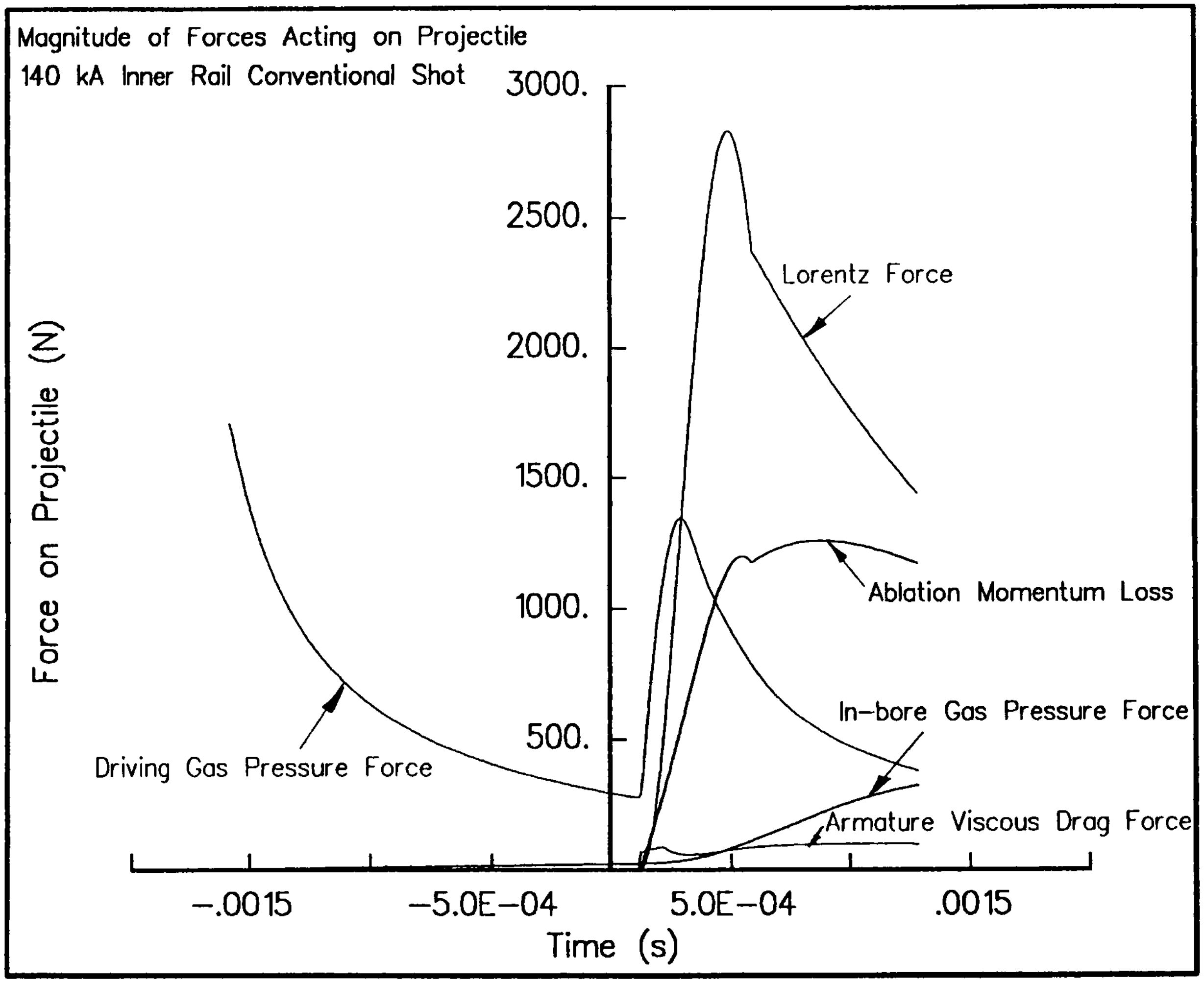

Figure 39. Magnitude of Forces for 140 kA Conventional Railgun Simulation

Augmented Plasma Armature Railgun

The railgun was then configured as a transaugmented railgun with a set of outer rails used to increase magnetic pressure without increasing power dissipated by the armature. The railgun was fired at several power levels, the 70 kA inner rail, 70 kA outer rail shot and 100 kA inner rail, 100 kA outer rail shot are the only two discussed in this section.

Figure 40 shows a comparison of numerical and experimental velocity data for the 70-70 kA (inner rail current-outer rail current) augmented shot. As can be seen in the figure, the experimental velocity appeared to increase to a maximum value of 2255 m/s and then began to decrease. Again, this was probably caused by separation of the armature from the rear face of the projectile. The numerical simulation calculated an exit velocity of 2450 m/s which was very close to that detected by the MAVIS. Again, this indicated that the railgun model closely predicted the performance at these power settings. Without the electrothermal expansion accounted, the simulation only predicted an exit velocity of 1910 m/s. This resulted in a difference in performance of this electrothermal expansion accounted for a 20.4% increase in performance.

Figure 41 shows the experimental and numerical data for the PT2 pressure probe for the 70-70 kA shot. The thermal expansion parameter finally predicted that 35% of the power was dissipated into the bore. Note that this was the same as with the 70 kA conventional shot. Figure 42 shows the magnitude of forces for the 70-70 kA railgun shot. As can be seen the Lorentz force dominated the other forces, with the thermal expansion force of the driving gas next in line. The other forces were relatively small.

Figure 43 shows both the numerical and experimental data of a 100-100 kA augmented railgun shot. For this shot, the experimental data closely matched the simulation throughout the entire shot. This is probably due to the fact that augmentation at

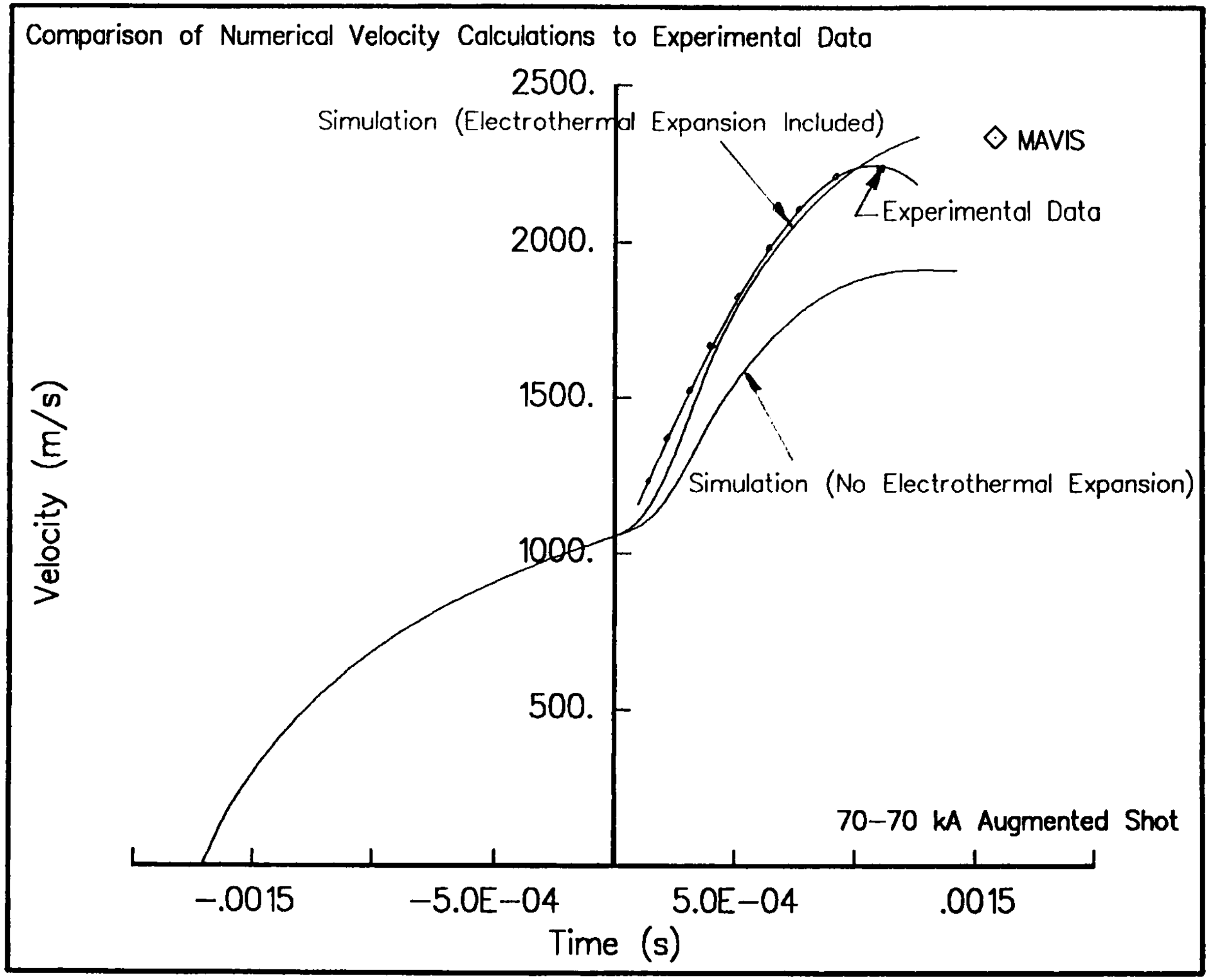

Figure 40. Numerical and Experimental Velocity for 70-70 kA Augmented Shot

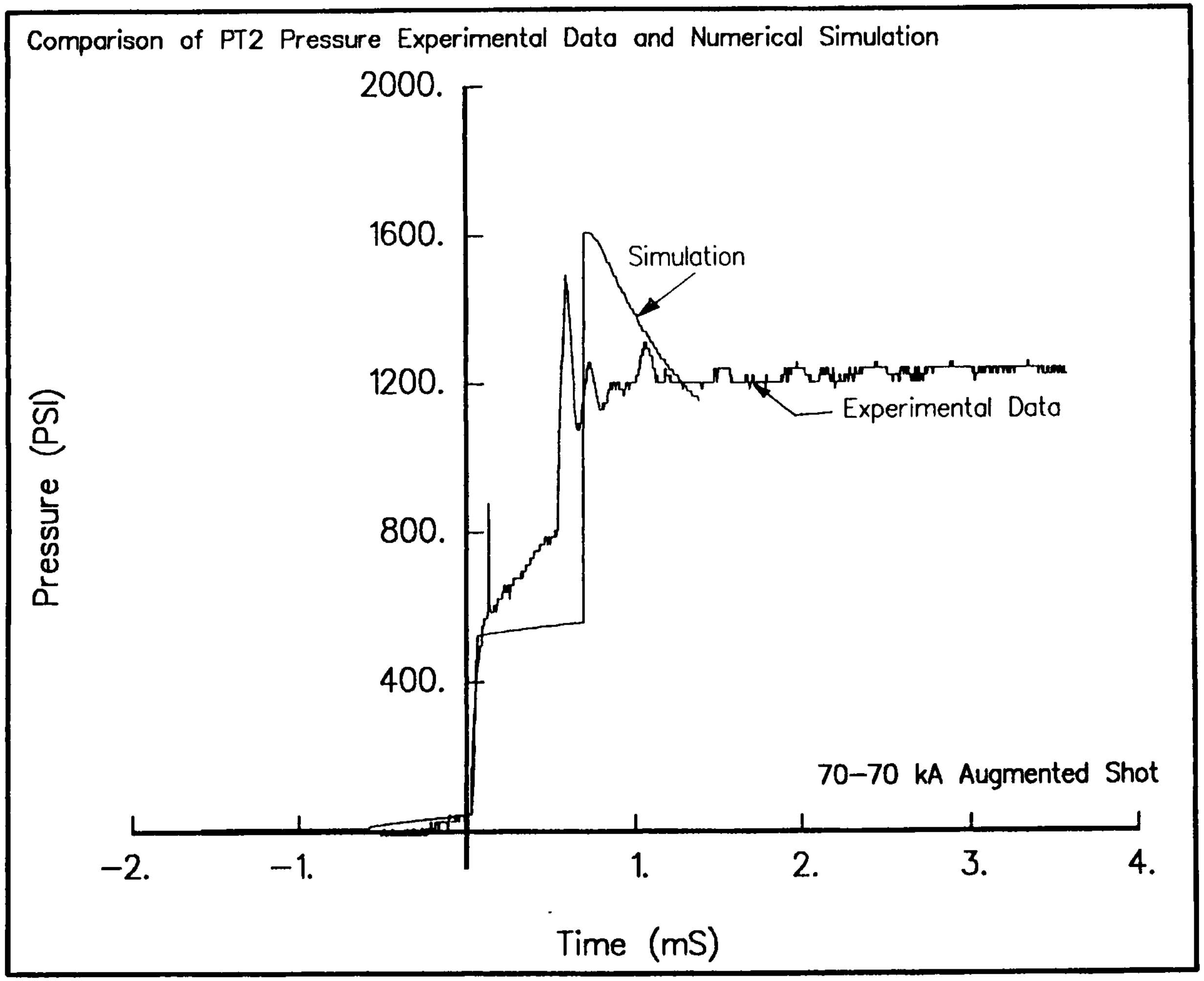

Figure 41. Numerical and Experimental PT2 Data for 70-70 kA Augmented Shot

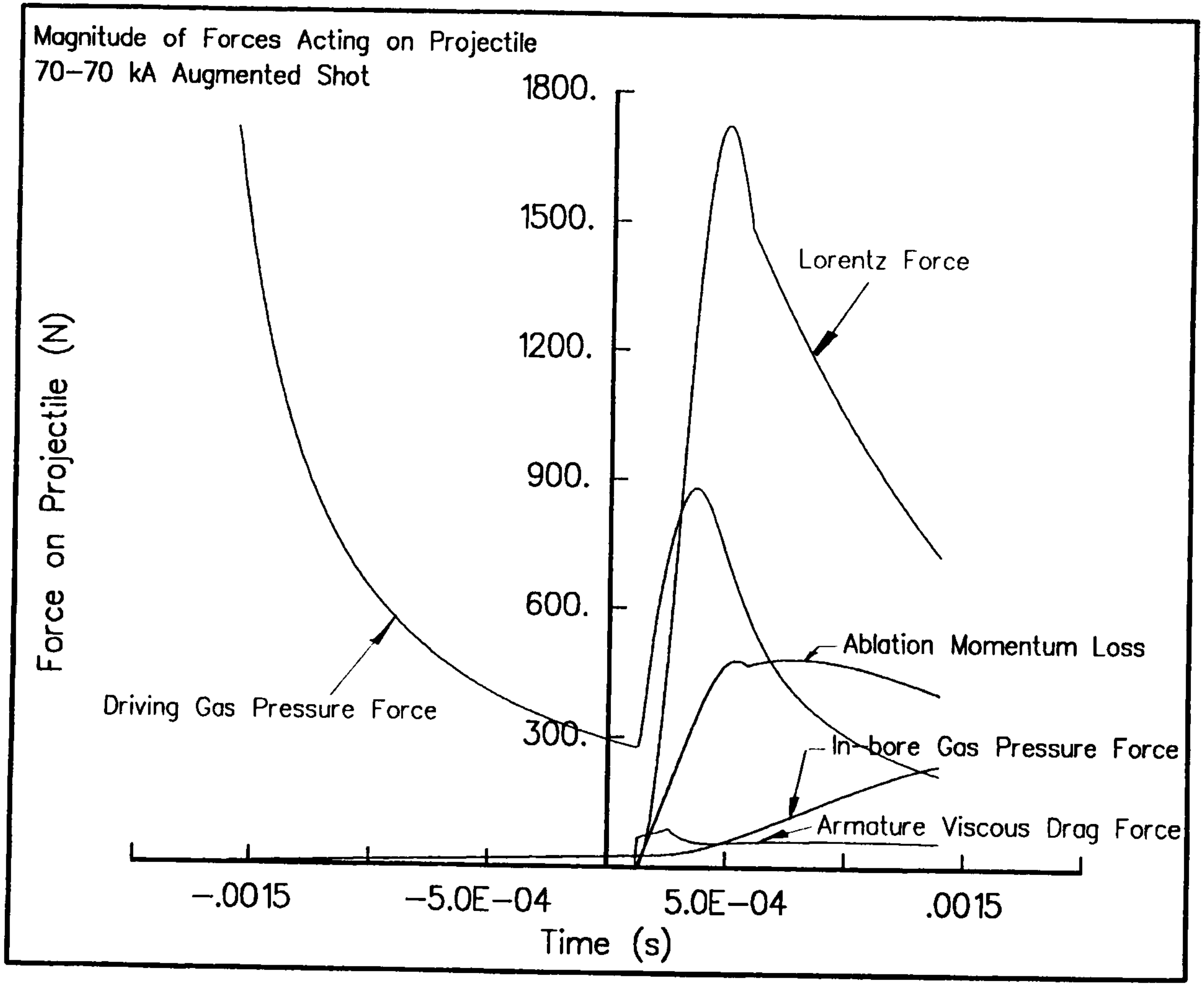

Figure 42. Magnitude of Forces for 70-70 kA Augmented Railgun Simulation

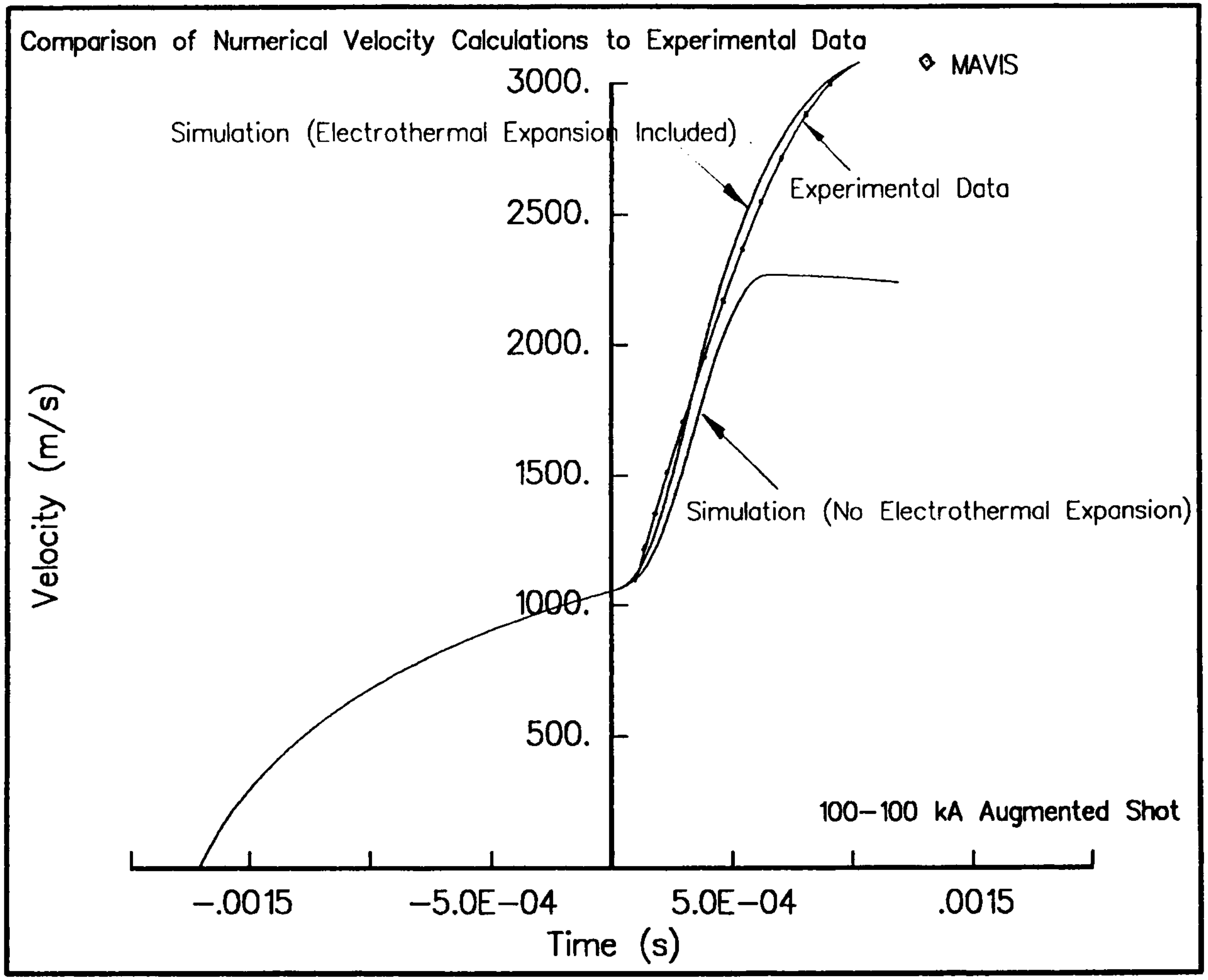

Figure 43. Numerical and Experimental Velocity for 100-100 kA Augmented Shot

this power level probably inhibited the separation of the armature from the rear face of the projectile. The simulation, experimental B-dot data, and MAVIS all predicted an exit velocity around 3025 m/s. However, without the electrothermal expansion, the simulation predicted an exit velocity of 2250 m/s, an increase of 25.6% in performance. Modulating the thermal expansion parameter in order to input 30% of the power of the inner rail provided the match in PT2 pressure as indicated in figure 44.

Figure 45 gives the magnitude of forces acting on the projectile for the 100-100 kA shot. As can be seen, the Lorentz force is the dominant force. The driving gas force with electrothermal expansion is now of the same order of magnitude as the ablation momentum loss term, and in-bore gas pressure.

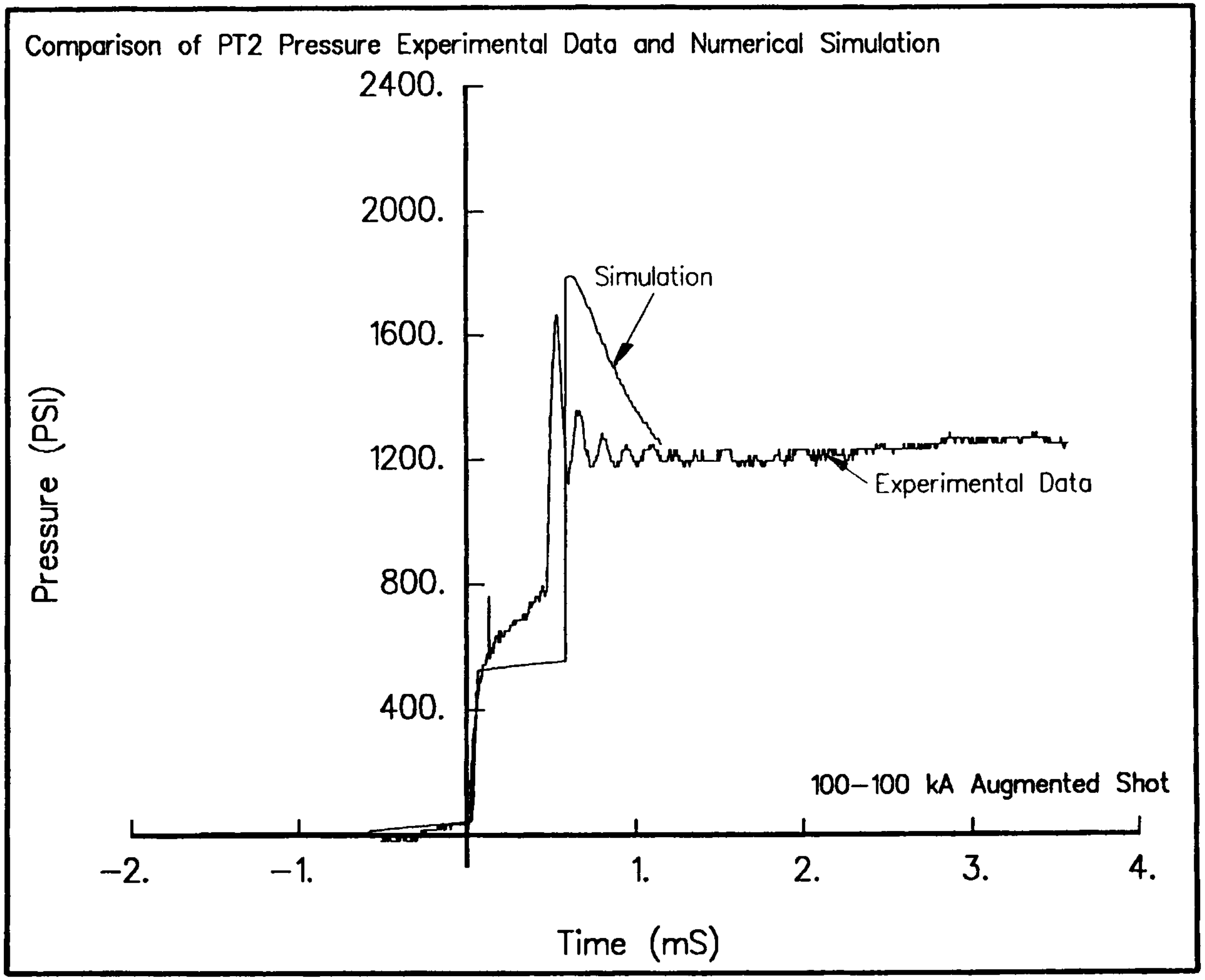

Figure 44. Numerical and Experimental PT2 Data for 100-100 kA Augmented Shot

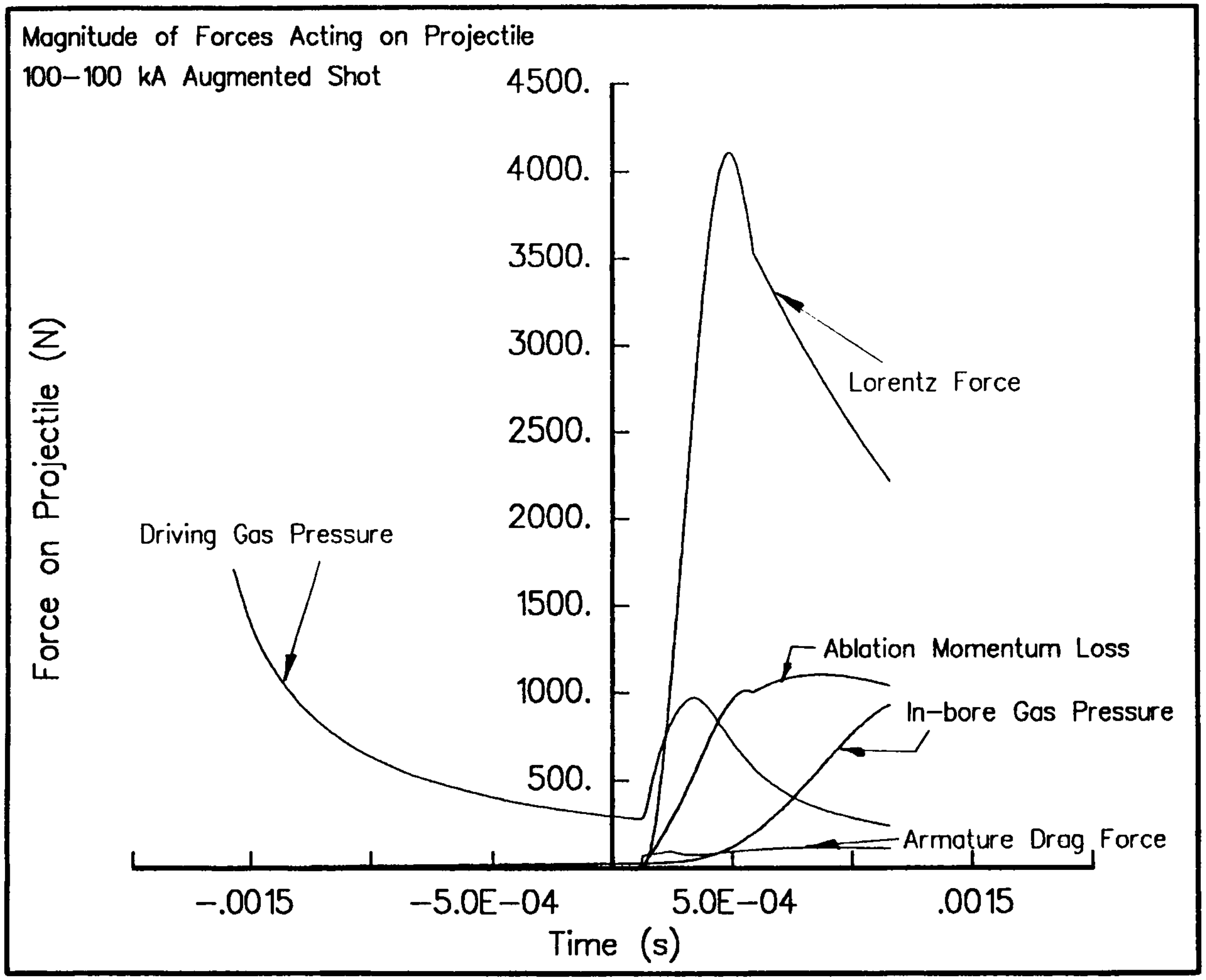

Figure 45. Magnitude of Forces for 100-100 kA Augmented Railgun Simulation

IV. CONCLUSIONS AND RECOMMENDATIONS

Numerical simulations were performed based on experimental data for various shots using both conventional and augmented configurations. For each of the cases mentioned previously, the fusing pressure pulse increased performance as compared to the non-electrothermal cases.

Table 3 shows the percentage increase in performance caused by the electrothermal effects for both the conventional and augmented shots. As can be seen, the ΔV_{exit} caused by the electrothermal interactions increases as the rail current increases. The reason for this can be attributed to the fact that as rail current increases, the proportion of energy transferred to the ablated material behind the projectile increases. The electrothermal expansion of the ablated material creates stronger pressure pulses as rail current increases. Since the numerical simulations with the electrothermal interactions included agreed closely with the experimental data, it can be concluded that the one-dimensional railgun model was able to predict reasonably the electrothermal effects that occurred during railgun operation.

Railgun Configuration	Rail Current (A) Inner/Outer	ΔV_{Exit} from Electrothermal Effects (m/s)	% Increase in V_{Exit} from Electrothermal Effects
Conventional	70/-	250	16.9%
Conventional	100/-	510	20.6%
Conventional	140/-	600	24.1%
Augmented	70/70	540	20.4%
Augmented	100/100	775	25.6%

Table 2. Impact of Electrothermal Effects on Railgun Performance

For the cases presented, the driving gas pressure force was on the order of or greater than the momentum loss term from the acceleration of the ablation for inner rail currents less than or equal to 140 kA. Without the electrothermal interaction with the ablated material, the driving gas pressure would continue decreasing and eventually become negligible. In this case, the momentum loss term would cause a severe decrease in performance. However, based on the experimental data and numerical results, it can be concluded that the electrothermal interactions actually occur, thereby decreasing the significance of the momentum loss incurred by the ablated material.

Based on experimental evidence and numerical results, the viscous drag of the armature is small compared to the other forces acting on the control volume. In-bore gas pressure is also small but increases in importance as projectile velocities increase.

The railgun model presented in this thesis was developed in order to gain insight into the physical behavior of plasma aramture railguns using simple schemes whenever possible. This railgun model reasonably predicted the electrothermal interaction of the ablation and the driving gas. However for future analysis, there are several areas in which improvements would greatly increase the accuracy of the model.

First, this model is a one-dimensional model which by its very nature depends upon assumptions of uniformity within the various parts. It has been recognized that the fluid dynamics which occur within the armature itself are highly three-dimensional and extremely turbulent. Incorporation of a multi-dimensional model of the armature into the simulation would be an obvious step toward the development of a more realistic model. This model should probably incorporate a 3-D MHD method in analysis of the armature.

Even though the flow friction model was not needed to obtain reasonable results, greater accuracy requires the incorporation of a realistic flow friction scheme. The present model needs to be examined and modified to improve its behavior, or a new scheme needs to be devised which would replace the current one.

The ablation model used a simplified energy balance in its analysis. In future models, a more rigorous scheme should be used to properly account for the energy transmitted to and from the rails. The present scheme involves one-dimensional blackbody radiation analysis. The high armature temperatures present indicate that radiation heat transfer is a dominating factor. However, the highly turbulent flow within the armature indicate that high rates of convective heat transfer may also exist. Future schemes should probably include the ability to account for convective heat transfer from the armature and ablation region to the rail.

The ablation momentum loss model which was selected did not explicitly account for the viscous losses that the ablated material encounters as it accumulates and proceeds down the bore. However, since the proportionality parameter, α, was selected to best match the experimental data, it is assumed that the viscous loss terms are somewhat accounted for in the present model. In future studies, if viscous forces are calculated, the term α should be reduced accordingly.

The expansion of the ablation region was calculated using simple gas relations and several simplifying assumptions. A more rigorous model might determine expansion in the ablation region using the same characteristic model used to determine the expansion of the driving gas. The inherent non-uniformity of the ablation region made this type of analysis too complicated for this present model, but for more accurate results, this type of analysis undoubtably would improve the simulated results.

Improved realism could be found be including relations for imperfect gases. A scheme to account for heat transfer from or to the gas also needs to be developed.

LIST OF REFERENCES

LIST OF REFERENCES

[1] Parker, J. V., "Why Plasma Armature Railguns Don't Work (and What Can Be Done About It)", IEEE Transactions on Magnetics, Vol. 25, No. 1, January 1989, pp. 418-424.

[2] Aigner, S., and E. Igenbergs, "Friction and Ablation Measurements in a Round Bore Railgun", IEEE Transactions on Magnetics, Vol. 25, No. 1, January 1989, pp. 33-38.

[3] Pyatt, K. D. and Ian R. McNab, "Limiting Physics Effects in Hypervelocity Railguns", 6th Symposium on Electromagnetic Launcher Technology, Austin, TX, April, 1992.

[4] Rolader, Glenn E., and Jad H. Batteh, "Effects of In-bore Gas on Railgun Performance", IEEE Transactions on Magnetics, Vol. 27, No. 1, January 1991, pp. 120-125.

[5] Batteh, Jad H., et. al.,"A Time-Dependent Model for Railgun Plasma Armatures", IEEE Transactions on Magnetics, Vol. 25, No. 1, January 1989.

[6] Crawford, Roger, Dennis Keefer, and Robert Tipton, "Velocity Limited Magnetohydrodynamic Effects in Railgun Plasma Armatures", 6th Symposium on Electromagnetic Launcher Technology, Austin, TX, April, 1992.

[7] Taylor, Jaime R., A Study of the UTSI Transaugmented and Classical Railgun, M.S. Thesis, University of Tennessee, December 1991.

[8] White, Frank M., Fluid Mechanics, New York: McGraw-Hill Book Company, 1986.

[9] Egeland, A. "Birkeland's Electromagnetic Gun: A Historical Review", IEEE Transactions on Plasma Science, Vol. 17, No. 2, April 1989, pp. 73-82.

[10] Hawke, R. S., et. al., "Railgun Performance with a Two-Stage Light Gas Gun Injector", 5th Symposium on Electromagnetic Launch Technology, Destin, FL, April 2-5, 1990.

[11] Crawford, Roger, Professor of Mechanical and Aerospace Engineering, The University of Tennessee Space Institute, Personal Communication, 1991-1992.

[12] Parker, J. V., et. al., "Performance Loss due to Wall Ablation in Plasma Armature Railguns", AIAA 18th Fluid Dynamics and Plasmadynamics and Lasers Conference, Cincinnati, Ohio, July 16-18, 1985.

[13] Ikuta, K., " A Study of Ablation Effects for an Axisymmetric Electromagnetic Accelerator", IEEE Transactions on Magnetics, Vol. 25, No. 1, January 1989, pp. 249-251.

[14] Anderson, John D., Modern Compressible Flow, New York: McGraw-Hill Book Company, 1982.

[15] Seigel, A. E., "Theory of High-Muzzle Velocity Guns", Progress in Aeronautics and Aeronautics: Interior Ballistics of Guns, Washington, D.C.: American Institute of Aeronautics and Astronautics,Vol. 66, pp. 135-175.

[16] Seigel, A. E., Theory of High Speed Guns, AGARDograph 91 Technical Report, Alexandria, VA: Defense Technical Information Center, May 1965.

[17] Kang, S. W. and R. McCallen, "Plasma Behavior in the Boundary Layer Near a Railgun Surface", IEEE Transactions on Magnetics, Vol. 25, No. 1, January 1989, pp. 277-279.

[18] Parker, J. V., "Experimental Measurements of Ablation Effects in Plasma Armature Railguns", IEEE Transactions on Magnetics, Vol. 22, No. 6, June 1986, pp. 1633-1640.

[19] White, Frank M., Viscous Fluid Flow, New York: McGraw-Hill Book Company, 1991.

APPENDICES

APPENDIX A: Derivation of Pertinent Relationships

Velocity of a Shock Wave

The velocity of a normal shock through a gas medium, Vw, can be found by utilizing the continuity, momentum, and energy equations. First, transform the reference frame to be attached to the shock in order to make it a stationary shock by setting u1=Vw and u2=Vw-ug where ug is the absolute velocity of the flow behind the shock.

Now taking the continuity equation across the shock wave:

$$\rho_1 u_1 = \rho_2 u_2 \ . \tag{A-1}$$

With only the pressure forces acting on the control volume, the momentum equation is given by the relation:

$$P_1 + \rho_1 u_1^2 = P_2 + \rho_2 u_2^2 \ . \tag{A-2}$$

Assuming that the shock wave involves an adiabatic process, the energy equation for the now stationary shock is:

$$h_1 + \frac{u_1^2}{2} = h_2 + \frac{u_2^2}{2} \ . \tag{A-3}$$

Assuming that the gas medium is a calorically perfect gas, the speed of sound is given by the equation:

$$a^2 = \gamma R T = \frac{\gamma P}{\rho}, \tag{A-4}$$

and that the enthalpy of the gas h is given by the equation:

$$h = C_P T \ . \tag{A-5}$$

Knowing that M1=u1/a1, equation (A-3) can be restated as:

$$T_1\left(1+\frac{\gamma-1}{2}M_2^2\right)=T_2\left(1+\frac{\gamma-1}{2}M_1^2\right)\ . \tag{A-6}$$

The momentum equation (A-2) becomes:

$$P_1\left(1+\gamma M_1^2\right)=p_2\left(1+\gamma M_2^2\right)\ . \tag{A-7}$$

Substituting (A-6) and (A-7) into (A-1) gives the relationship:

$$\frac{M_1}{1+\gamma M_1^2}\sqrt{1+\frac{\gamma-1}{2}M_1^2}=\frac{M_2}{1+\gamma M_2^2}\sqrt{1+\frac{\gamma-1}{2}M_2^2}\ . \tag{A-8}$$

Solving (A-8) for M2 yields two solutions. One solution is the trivial solution M1=M2. The other solution takes the form:

$$M_2^2=\frac{M_1^2+\frac{2}{\gamma-1}}{\frac{2\gamma}{\gamma-1}M_1^2-1} \tag{A-9}$$

Placing (A-9) back into (A-7) and rearranging give the pressure ratio:

$$\frac{P_2}{P_1}=\frac{2\gamma}{\gamma+1}M_1^2+\frac{1-\gamma}{\gamma+1} \tag{A-10}$$

Solving (A-10) for M1 gives:

$$M_1=\sqrt{\frac{\gamma+1}{2\gamma}\left(\frac{P_2}{P_1}-1\right)+1} \tag{A-11}$$

Remembering that M1=u1/a1, and that u1=Vw, the following equation is given:

$$V_w = a\sqrt{\frac{\gamma+1}{2\gamma}\left(\frac{P_2}{P_1} - 1\right) + 1} \tag{A-12}$$

If the shock wave is moving into a medium with an initial flow velocity, ug1, in the + x direction, then the wave velocity becomes:

$$V_w = u_{g1} + a\sqrt{\frac{\gamma+1}{2\gamma}\left(\frac{P_2}{P_1} - 1\right) + 1} \tag{A-13a}$$

If the shock wave is moving into a medium in the + x direction, then the wave velocity becomes:

$$V_w = u_{g1} - a\sqrt{\frac{\gamma+1}{2\gamma}\left(\frac{P_2}{P_1} - 1\right) + 1} \tag{A-13b}$$

Characteristic Wave Equations

The characteristic wave equations can be found by taking the continuity equation (A-1) and momentum equation (A-2):

$$\rho_1 u_1 = \rho_2 u_2 \ . \tag{A-1}$$

$$P_1 + \rho_1 u_1^2 = P_2 + \rho_2 u_2^2 \ . \tag{A-2}$$

Substituting (A-1) into (A-2):

$$P_1 + \rho_1 u_1 u_1 = P_2 + \rho_1 u_1 u_2 \ . \tag{A-14}$$

$$P_2 - P_1 = -\rho_1 u_1 (u_2 - u_1)\,. \tag{A-15}$$

$$\Delta P = -\rho_1 u_1 \Delta u\,. \tag{A-16}$$

Remembering that u1=Vw:

$$\Delta P = -\rho_1 V_w \Delta u\,. \tag{A-17}$$

By examining (A-12), it can be seen that as:

$$\Delta P \rightarrow 0 = dP \tag{A-18}$$

$$V_w \rightarrow a\,, \tag{A-19}$$

Therefore:

$$\Delta u \rightarrow du. \tag{A-20}$$

Equation (A-17) then becomes:

$$dP = -a\,\rho\,du\,. \tag{A-21}$$

This is the characteristic change associated with a wave traveling in the + x direction. For a wave traveling in the - x direction:

$$dP = a\,\rho\,du\,, \tag{A-22}$$

Since Vw=-a.

Both of these relationship where derived using information from Anderson [14].

APPENDIX B: FORTRAN Code of Railgun Model

```
C *********************************************************************
C *                                                                   *
C *  One Dimensional Gas Dynamics Model of Railgun                    *
C *                                                                   *
C *  John K. Foster                                                   *
C *  Dr. Roger Crawford, Advisor                                      *
C *                                                                   *
C *  August 11, 1992 (PC Version) 4:30 P.M.                           *
C *                                                                   *
C *********************************************************************
C *                                                                   *
C * Variables:                                                        *
C *                                                                   *
C *     A()      -      Speed of Sound behind Wave (m/s)              *
C *     A2()     -      Speed of Sound ahead of Wave (m/s)            *
C *     AA       -      Term to calculate current                     *
C *     ALPHA    -      Ablation Coefficient                          *
C *     AO1      -      Initial Current Parameter                     *
C *     AREA     -      Bore Cross Sectional Area (m^2)               *
C *     AS1      -      Initial Current Parameter                     *
C *     AX1      -      Initial Current Parameter                     *
C *     BB       -      Term to calculate current                     *
C *     BDATA()  -      Input data array                              *
C *     C1       -      Capacitance of inner rail circuit (f)         *
C *     C2       -      Capacitance of outer rail circuit (f)         *
C *     CF       -      Coefficient of Friction                       *
C *     CP       -      Constant Pressure Specific Heat J/(kg-degK)   *
C *     CPR      -      CP of Copper (J/(kg-DegK))                    *
C *     CPLG     -      CP of Light Gas  (J/(kg-DegK))                *
C *     D1       -      Viscous Drag of the Armature (N)              *
C *     DL1      -      Change in inner rail inductance due to Vel.   *
C *     DM12     -      Change in Mutual rail inductance due to Vel.  *
C *     DIA      -      Diameter of Bore (m)                          *
C *     DP       -      Differential of Pressure behind Proj (Pa)     *
C *     DP2      -      Differential of Pressure ahead Proj (Pa)      *
C *     DPF      -      Differential of Pressure due to Friction(Pa)  *
C *     DRAG     -      Flow Drag Total (N)                           *
C *     DRI1     -      Rate of change of inner rail current (A/s)    *
C *     DRI2     -      Rate of change of outer rail current (A/s)    *
C *     DT       -      Differential of Time (s)                      *
C *     DT1      -      Differential of Time (s)                      *
C *     DTT      -      Differential of Time (s)                      *
C *     DUF      -      Differential of Velocity of Flow (m/s)        *
C *     DUP      -      Differential of Velocity of Projectile (m/s)  *
C *     DVDT     -      Acceleration (m/s^2)                          *
C *     F1       -      Total Electromagnetic Force (N)               *
C *     FD       -      Drag Force Behind Projectile (N)              *
C *     FD2      -      Drag Force ahead of Projectile (N)            *
C *     FM       -      Mutual Inductance Force (N)                   *
C *     GAMMA    -      Ratio of Specific Heats                       *
C *     KAPPA    -      Coefficient of Rail Coupling                  *
C *     L1       -      Inductance of Inner rail due to Proj Pos.(H)  *
C *     LLGG     -      Length of Light Gas Gun (m)                   *
C *     LO1      -      Inductance of inner rails (H)                 *
C *                                                                   *
C *********************************************************************
```

```
C ******************************************************************
C *                                                                *
C *     LP       -       Length of Projectile (m)                  *
C *     LP1      -       Inductance/length of inner rail (H/m)     *
C *     LP2      -       Inductance/length of outer rail (H/m)     *
C *     LRG      -       Length of Railgun (m)                     *
C *     LT1      -       Total Inductance of Inner Rail (H)        *
C *     LT2      -       Total Inductance of Outer Rail (H)        *
C *     M12      -       Mutual Inductance of the rails (H)        *
C *     MASS     -       Mass of Armature (kg)                     *
C *     MDOT     -       Rate of Mass Addition to armature (kg/s)  *
C *     MP12     -       Mutual Inductance/Length of the rails (H/m) *
C *     MZ       -       Mass of Fuse (kg)                         *
C *     P()      -       Pressure behind projectile (Pa)           *
C *     P2()     -       Pressure ahead of projectile (Pa)         *
C *     PB()     -       Pressure behind wave (Pa)                 *
C *     PB2()    -       Pressure behind wave (Pa)                 *
C *     PERI     -       Perimeter of railgun bore (m)             *
C *     PMASS    -       Projectile Mass (kg)                      *
C *     POSW()   -       Position of Wave behind projectile (m)    *
C *     POSW2()  -       Position of Wave ahead of projectile (m)  *
C *     PX()     -       Pressure at X Location (Pa)               *
C *     R        -       Gas Constant (m^2/(s^2*°K))               *
C *     R1       -       Resistance of inner rail circuit          *
C *     R2       -       Resistance of outer rail circuit          *
C *     RAD      -       Radius of Bore (m)                        *
C *     RES      -       Resistance of Armature(Ohms)              *
C *     RI1      -       Inner rail current (A)                    *
C *     RI2      -       Outer rail current (A)                    *
C *     RLG      -       Gas Constant of Light gas(m^2/(s^2*K))    *
C *     RHO()    -       Density of Gas behind Projectile (kg/m^3) *
C *     RHO2()   -       Density of Gas ahead of Projectile (kg/m^3) *
C *     RHOX()   -       Density of Gas at X Location (kg/m^3)     *
C *     RHOZ     -       Density of Armature (kg/m^3)              *
C *     RU       -       Universal Gas Constant (N*m/(kgmol*°K))   *
C *     T        -       Time (s)                                  *
C *     TCROW1   -       Crowbar Time for inner rail circuit (s)   *
C *     TCROW2   -       Crowbar Time for outer rail circuit (s)   *
C *     TDELAY   -       Delay time between PT1 initiation and fusing *
C *     TEMP()   -       Temperature behind projectile (K)         *
C *     TEMP2()  -       Temperature ahead of projectile (K)       *
C *     TFIRE    -       Time between firing of outer and inner rails *
C *     TFUSE    -       Time @ projectile passing PT1 (s)         *
C *     TTEMP    -       Temporary Holder (T-TFUSE)                *
C *     TX()     -       Temperature of Gas at X Location (°K)     *
C *     TZ       -       Temperature of Armature (K)               *
C *     UP()     -       Projectile Velocity (m/s)                 *
C *     UX()     -       Velocity of Gas at X Location (m/s)       *
C *     V1       -       Projectile Velocity (m/s)                 *
C *     VB       -       Breech Voltage (V)                        *
C *     VC1      -       Initial Voltage charge on inner rail circuit *
C *     VC2      -       Initial Voltage charge on outer rail circuit *
C *     VELW()   -       Velocity of Wave behind projectile (m/s)  *
C *     VELW2()  -       Velocity of Wave ahead of projectile (m/s) *
C *                                                                *
C ******************************************************************
```

```
C *********************************************************************
C *                                                                   *
C *     VF1      -      Firing Voltage (V)                            *
C *     VO1      -      Empirical Constant for Voltage Model          *
C *     VR1      -      Voltage of inner rail (V)                     *
C *     W        -      Molecular weight (kg/kgmol)                   *
C *     WLG      -      Molecular weight of Light Gas (kg/kgmol)      *
C *     WR       -      Molecular weight of Rail Material (kg/kgmol) *
C *     WTEMP    -      Temporary Holder of Wave Position (m)         *
C *     X1       -      Position of Projectile (m)                    *
C *     XT       -      Total length of Gun (LLGG+LRG) (m)            *
C *     XPT1     -      X Location of PT1 Pressure Probe (m)          *
C *     XPT2     -      X Location of PT2 Pressure Probe (m)          *
C *                                                                   *
C *********************************************************************
$STORAGE:2
C
C
      PROGRAM RAILGUN
C
C *** INITIALIZE VARIABLES
C
      PARAMETER (DIM=3500)
      REAL AA,ALPHA,AO1,AREA,AS1,AX1,BB,BDATA(100),BETA,C1,CF,CP,CPR,
     +     CPLG,D1,DL1,DM12,DIA,MDOT,DRI1,DRI2,DT,DT1,DTT,ERAD,DE,RED,
     +     DUF,DUP,EDIS,F1,FD,FD2,FM,LAMBDA,GAMMA,KAPPA,MU,MUREF,TREF,
     +     S,L1,LLGG,LO1,LO2,LP,LP1,LP2,LRG,LT1,LT2,M12,MASS,MP12,MZ,
     +     PERI,PI,PMASS,R,R1,R2,RES,RI1,RI2,RLG,RU,T,TCROW1,EPS,DPT,
     +     TCROW2,TDELAY,TFIRE,TFUSE,TTEMP,V1,VB,VC1,VC2,VF1,VO1,
     +     VR1,WLG,WR,WTEMP,X1,XPT1,XPT2,LARM,TAMB,CFARM,
     +     GMMZ,CF2,PZ,RHOZ,TZ,AZ,RZ,VELZ,POSZ,UTEMP
      CHARACTER INFIL*24,FN1(20)*15,FNAME(20)*24
      INTEGER I,II,IEXIT,IFLAG,J,JJ,K,KK,L,LL,M,N,JFLAG,ICROWB1,ICROWB2,
     +        IPT1,IPT2,IV
      COMMON A(DIM),A2(DIM),DP(DIM),DP2(DIM),P(DIM),P2(DIM),POSW(DIM),
     + POSW2(DIM),PX(DIM),RHO(DIM),RHO2(DIM),RHOX(DIM),TEMP(DIM),
     + TEMP2(DIM),TX(DIM),UF(DIM),UP(DIM),UX(DIM),VELW(DIM),VELW2(DIM),
     + PWP(DIM),PWP2(DIM)
      COMMON/PLOTS/DATA(20,2000),TT(2000)
      DATA FN1/'XP','VP','RI1','RI2','P1','P2','LF','AB','MZ','NRG',
     +         'RAD','TZ','D1','LAR','VZ','XZ','PW1','PW2','PT1','PT2'/
C
C *** OPEN INPUT FILE: USER SPECIFIED
C
      PRINT *,'INPUT DATA FILENAME?'
      READ(*,'(A)')INFIL
      OPEN (UNIT=2,FILE=INFIL,STATUS='OLD')
C
C ** OPEN OUTPUT FILE
C
      OPEN (UNIT=1,FILE='OUTPUT.DAT',STATUS='unknown')
C
C ** ASSIGN OUTPUT FILE NAMES
C
      DO 1100 I=1,20
         FNAME(I)=INFIL(1:3)//'.'//FN1(I)
```

```
            PRINT *,FNAME(I)
 1100 CONTINUE
C
C *** DEFINE ALL INITIAL VALUES
C
      DO 1110 I=1,3500
            A(I)=0.0
            A2(I)=0.0
            DP(I)=0.0
            DP2(I)=0.0
            P(I)=0.0
            P2(I)=0.0
            POSW(I)=0.0
            POSW2(I)=0.0
            PWP(I)=0.0
            PWP2(I)=0.0
            PX(I)=0.0
            RHO(I)=0.0
            RHO2(I)=0.0
            RHOX(I)=0.0
            TEMP(I)=0.0
            TEMP2(I)=0.0
            TX(I)=0.0
            UF(I)=0.0
            UP(I)=0.0
            UX(I)=0.0
            VELW(I)=0.0
            VELW2(I)=0.0
 1110 CONTINUE
      NW=30
      DO 1115 I=1,3500,NW
            PWP(I)=1.0
            PWP2(I)=1.0
 1115 CONTINUE
C
C *** READ DATA FROM INPUT.DAT
C
      N=1
 1120 CONTINUE
      READ (2,*)BDATA(N)
      IF (BDATA(N).EQ.999.)THEN
            CLOSE(2)
            GOTO 1130
      ENDIF
      N=N+1
      GOTO 1120
C
C *** DEFINE STARTING VALUES AND CONSTANTS FROM INPUT DATA
C
 1130 CONTINUE
      PMASS=    BDATA(1)
      MZ=       BDATA(2)
      LP=       BDATA(3)
      DIA=      BDATA(4)
      LLGG=     BDATA(5)
      LRG=      BDATA(6)
```

```
      XPT1=     BDATA(7)
      XPT2=     BDATA(8)
      WLG=      BDATA(9)
      WR=       BDATA(10)
      CPLG=     BDATA(11)
      CPR=      BDATA(12)
      GAMMA=    BDATA(13)
      GMMZ=     BDATA(14)
      TEMP(1)=  BDATA(15)
      TEMP2(1)=BDATA(16)
      P(1)=     BDATA(17)
      P2(1)=    BDATA(18)
      DT=       BDATA(19)
      INVIS1=   INT(BDATA(20))
      INVIS2=   INT(BDATA(21))
      LO1=      BDATA(22)
      LO2=      BDATA(23)
      LP1=      BDATA(24)
      LP2=      BDATA(25)
      KAPPA=    BDATA(26)
      RES=      BDATA(27)
      R1=       BDATA(28)
      R2=       BDATA(29)
      VF1=      BDATA(30)
      VO1=      BDATA(31)
      C1=       BDATA(32)
      C2=       BDATA(33)
      VC1=      BDATA(34)
      VC2=      BDATA(35)
      TCROW1=   BDATA(36)
      TCROW2=   BDATA(37)
      TDELAY=   BDATA(38)
      TFIRE=    BDATA(39)
      CFARM=    BDATA(40)
      TREF=     BDATA(41)
      S=        BDATA(42)
      MUREF=    BDATA(43)
      ALPHA=    BDATA(44)
      BETA=     BDATA(45)
      EPS=      BDATA(46)
      LAMBDA=   BDATA(47)
C
C *** INITIALIZE VARIABLES AND ASSIGN CONSTANTS
C
      PI=3.1415927
      SIGMA=5.67E-8
      RU=8314.4
      R=RU/WLG
      RZ=RU/WR
      RLG=R
      UTEMP=0.
      T=0.
      D1=0.
      F1=0.
      RI1=1.0D-8
      RI2=1.0D-8
```

```
      AREA=DIA**2.*PI/4.
      IV=INT(0.00001/DT)
      CP=CPLG
      DPT=0.
      MASS=0.
      PZ=0.
      RHOZ=0.
      AZ=0.
      X1=0.
      FD=0.
      FD2=0.
      MDOT=0.
      EDIS=0.
      L2=LP2*LRG
      LT2=L2+LO2
      MP12=KAPPA*SQRT(LP1*LP2)
      PERI=DIA*PI
      AS1=VO1/RES
      AX1=AS1*(VF1/VO1+LOG(AS1))
      AO1=AS1-AX1
      IPT1=INT(XPT1*1000.)
      IPT2=INT(XPT2*1000.)
      IEXIT=INT((LLGG+LRG)*1000.)
      ICROWB1=1
      ICROWB2=1
C
C *** ASSIGN INITIAL CONDITIONS TO THE AXIAL STATIONS
C
      DO 1140 J=INT(LP*1000),INT((LLGG+LRG)*1000)
         PX(J)=P2(1)
         TX(J)=TEMP2(1)
         RHOX(J)=PX(J)/RLG/TX(J)
 1140 CONTINUE
C
C ***BEGIN FIRST ITERATION
C
      I=1
      LL=1
      KK=1
      II=0
      IFLAG=0
      JFLAG=0
      PZ=P(1)
      TAMB=TEMP2(1)
      TZ=TAMB
      RHOZ=PZ/(RZ*TZ)
      LARM=MZ/AREA/RHOZ
      POSZ=X1-LARM
      RHO(1)=P(1)/(R*TEMP(1))
      RHO2(1)=P2(1)/(RLG*TEMP2(1))
      A(1)=(GAMMA*R*TEMP(1))**(.5)
      A2(1)=(GAMMA*RLG*TEMP2(1))**(.5)
 1150 CONTINUE
C
C *** DETERMINE TIME WHEN PROJECTILE PASSES PT1 STATION
C
```

```
      IF (IFLAG.EQ.0)THEN
         IF ((X1+LP).GT.XPT1)THEN
            TFUSE=T
            IFLAG=1
         ENDIF
      ENDIF
C
C *** DELAY TIME AFTER PT1 SENSES PROJECTILE PASSAGE
C
      IF (IFLAG.EQ.1.AND.JFLAG.EQ.0)THEN
         TTEMP=T-TFUSE
         IF (TTEMP.GE.TDELAY)THEN
            JFLAG=1
         ENDIF
      ENDIF
C
C *** JAIME TAYLOR LRC CIRCUIT MODEL FOR CURRENT AND VOLTAGE
C
 1154 IF (JFLAG.EQ.1)THEN
         M12 = MP12*(X1-LLGG)
         L1 = LP1*(X1-LLGG)
         LT1 = L1+LO1
         DL1 = LP1*V1
         DM12 = MP12*V1
         IF (LARM.GT.0.06)THEN
            D1 = .5*RHOZ*V1**2.*CFARM*0.06*PERI
         ELSE
            D1 = .5*RHOZ*V1**2.*CFARM*LARM*PERI
         ENDIF
         TRG=(T-TFUSE-TDELAY)
C
C *** CALCULATE INNER AND OUTER RAIL CURRENT
C
         IF (TRG.LT.TFIRE)THEN
            DRI1=0.
            DRI2=((VC2-RI2*R1)/LT1)*DT
         ELSE
            AA=VC1-VR1-RI1*(DL1+R1)-RI2*DM12
            BB=VC2-RI2*R2-RI1*DM12
            DRI2=((BB-M12*AA/LT1)*DT)/(LT2-M12*M12/LT1)
            DRI1=(AA*DT-M12*DRI2)/LT1
         ENDIF
         RI1=RI1+DRI1
         RI2=RI2+DRI2
C
C *** CALCULATE BREECH VOLTAGE
C
         VB = VR1+RI1*DL1+DRI1/DT*L1+RI2*DM12+DRI2/DT*M12
C
C *** CALCULATE VOLTAGE ACROSS ARMATURE
C
         CALL VOLTAGE(RI1,VR1,VF1,VO1,RES,AX1,AO1)
C
C *** CALCULATE THE VOLTAGE CHARGE REMAINING IN THE CAPACITORS
C
         CALL VCAPACITOR(ICROWB1,VC1,C1,RI1,DT,TRG,TCROW1)
```

```fortran
          CALL VCAPACITOR(ICROWB2,VC2,C2,RI2,DT,TRG,TCROW2)
C
C *** DETERMINE THE AMOUNT OF ABLATION
C
          MDOT = ALPHA*RI1*VR1
          MASS = MASS+LAMBDA*MDOT*DT
C
C *** CALCULATE THE LORENTZ ELECTROMAGNETIC FORCES
C
          F1 = 0.5*LP1*RI1**2 + MP12*RI1*RI2
          FM = MP12*RI1*RI2
       ENDIF
C
C *** CALCULATE CHANGE IN VELOCITY OF PROJECTILE AND FLOW
C
       DUP=(F1+(P(I)-P2(I))*AREA-MDOT*UP(I)-D1)/(PMASS+MASS)*DT
       V1=V1+DUP
       UP(I+1)=V1
C
C *** CALCULATE TEMP AND PRESSURE OF FLOW DUE TO POWER DISSIPATION
C
       EDIS=BETA*RI1*VR1*DT
       ERAD=EPS*SIGMA*LARM*PERI*(TZ**4.-TAMB**4.)*DT
       DE=EDIS-ERAD
       TZ=(MZ*CPR*TZ+DE)/((MZ+MDOT*DT)*CPR)
       IF (TZ.LT.1.)TZ=1.
       MZ=MZ+MDOT*DT
       RHOZ=MZ/(AREA*LARM)
       PZ=RHOZ*RZ*TZ
       AZ=(GMMZ*RZ*TZ)**(0.5)
C
C *** CALCULATE NEW WAVE POSITIONS
C
       POSW(I)=X1-LARM
       POSW2(I)=X1+LP
C
C *** CALCULATE CHARACTERISTIC WAVE PRESSURE
C
       DP(I)=-A(I)*RHO(I)*DUP+PZ-P(I)
       P(I+1)=P(I)+DP(I)
       IF (P(I+1).LE.0.0)P(I+1)=1.0E-6
       IF (DP(I).GT.0.)THEN
          VELW(I)=UF(I)-A(I)*((GAMMA+1.)/(2.*GAMMA)*
     +             (P(I+1)/P(I)-1.)+1.)**.5
       ELSE
          VELW(I)=UF(I)-A(I)
       ENDIF
       DUF=-DP(I)/((UF(I)-VELW(I))*RHO(I))
       UF(I+1)=UF(I)+DUF
       VELZ=UF(I+1)
       IF (DUP.GT.0.0)THEN
          DP2(I)=P2(I)*(GAMMA*(GAMMA+1.)/4.*(DUP/A(I))**2.+
     +     GAMMA*DUP/A(I)*(1+((GAMMA+1.)/4)**2.*(DUP/A(I))**2.)**0.5)
       ELSE
          DP2(I)=A2(I)*RHO2(I)*DUP
       ENDIF
```

```
 1156 IF (DP2(I).GT.0.)THEN
         VELW2(I)=UP(I)+A2(I)*((GAMMA+1.)/(2.*GAMMA)*
     +             ((P2(I)+DP2(I))/P2(I)-1.)+1.)**.5
      ELSE
         VELW2(I)=UP(I)+A2(I)
      ENDIF
      P2(I+1)=P2(I)+DP2(I)
      IF (P2(I+1).LE.0.0)P2(I+1)=1.0E-6
C
C *** CALCULATE TEMPERATURE OF FLOW
C
      TEMP(I+1)=TEMP(I)+((UF(I))**2.-(UF(I+1))**2.)/(2.*CP)
      IF (TEMP(I+1).LE.0.) TEMP(I+1)=1.
      TEMP2(I+1)=TEMP2(I)+((UP(I))**2.-(UP(I+1))**2.)/(2.*CPLG)
      IF (TEMP2(I+1).LE.0.) TEMP2(I+1)=1.
C
C *** CALCULATE SPEED OF SOUND IN DRIVING GAS AND IN-BORE GAS
C
      A(I+1)=(GAMMA*R*TEMP(I+1))**0.5
      A2(I+1)=(GAMMA*RLG*TEMP2(I+1))**0.5
C
C *** CALCULATE DENSITY OF FLOW AHEAD AND BEHIND PROJECTILE
C
      RHO(I+1)=P(I+1)/R/TEMP(I+1)
      RHO2(I+1)=P2(I+1)/RLG/TEMP2(I+1)
C
C *** CALCULATE PROJECTILE POSITION
C
      X1=X1+V1*DT
C
C *** CALCULATE ARMATURE-NEUTRAL GAS FREE SURFACE INTERFACE POSITION
C
      POSZ=POSZ+VELZ*DT
C
C *** CALCULATE ARMATURE LENGTH
C
      LARM=LARM+(V1-VELZ)*DT
C
C *** CALCULATE PREVIOUS WAVE POSITIONS AND VELOCITIES BEHIND PROJECTILE
C
      DO 1190 J=LL,I
cc          IF (DP(J).GT.0.0)THEN
             K=J-1
             DTT=DT
 1160        WTEMP=POSW(J)
             POSW(J)=POSW(J)+VELW(J)*DTT
             IF (J.GT.LL)THEN
                IF (POSW(J).LT.POSW(K))THEN
                   POSW(J)=POSW(K)
                   DT1=ABS((WTEMP-POSW(K))/VELW(J))
                   DTT=DTT-DT1
                   P(J)=P(K)
                   RHO(J)=RHO(K)
                   TEMP(J)=TEMP(K)
                   DP(J)=DP(J)+DP(K)
                   UF(J)=UF(K)
```

```
                  A(J)=A(K)
                  IF (PWP(K).NE.0.0)PWP(J)=PWP(K)
                  IF (DP(J).GT.0)THEN
                     VELW(J)=UF(J)-A(J)*((GAMMA+1.)/(2.*GAMMA)*
     +                       ((P(J)+DP(J))/P(J)-1.)+1.)**.5
                  ELSE
                     VELW(J)=UF(J)-A(J)
                  ENDIF
                  DO 1170 L=J-1,LL+1,-1
                     POSW(L)=POSW(L-1)
                     P(L)=P(L-1)
                     A(L)=A(L-1)
                     RHO(L)=RHO(L-1)
                     TEMP(L)=TEMP(L-1)
                     UF(L)=UF(L-1)
                     VELW(L)=VELW(L-1)
                     DP(L)=DP(L-1)
                     PWP(L)=PWP(L-1)
 1170             CONTINUE
                  LL=LL+1
                  GOTO 1160
                ENDIF
              ENDIF
cc          ELSE
cc             POSW(J)=POSW(J)+VELW(J)*DT
cc          ENDIF
 1190 CONTINUE
cc      write(3,*)'1190'
C
C *** CALCULATE PREVIOUS WAVE POSITIONS AND VELOCITIES AHEAD PROJECTILE
C
      DO 1230 J=KK,I
         IF (DP2(J).GT.0.0)THEN
            K=J-1
            DTT=DT
 1200       WTEMP=POSW2(J)
            POSW2(J)=POSW2(J)+VELW2(J)*DTT
            IF (J.GT.KK)THEN
               IF (POSW2(J).GT.POSW2(K))THEN
                  POSW2(J)=POSW2(K)
                  DT1=(POSW2(K)-WTEMP)/VELW2(J)
                  DTT=DTT-DT1
                  P2(J)=P2(K)
                  RHO2(J)=RHO2(K)
                  TEMP2(J)=TEMP2(K)
                  DP2(J)=DP2(J)+DP2(K)
                  UP(J)=UP(K)
                  A2(J)=A2(K)
                  IF (PWP2(K).NE.0.0)PWP2(J)=PWP2(K)
                  IF (DP2(J).GT.0)THEN
                     VELW2(J)=UP(J)+A2(J)*((GAMMA+1.)/(2.*GAMMA)*
     +                       ((P2(J)+DP2(J))/P2(J)-1.)+1.)**.5
                  ELSE
                     VELW2(J)=UP(J)+A2(J)
                  ENDIF
                  DO 1210 L=J-1,KK+1,-1
```

```
                  POSW2(L)=POSW2(L-1)
                  P2(L)=P2(L-1)
                  A2(L)=A2(L-1)
                  RHO2(L)=RHO2(L-1)
                  TEMP2(L)=TEMP2(L-1)
                  UP(L)=UP(L-1)
                  VELW2(L)=VELW2(L-1)
                  DP2(L)=DP2(L-1)
                  PWP2(L)=PWP2(L-1)
 1210          CONTINUE
               KK=KK+1
               GOTO 1200
            ENDIF
         ENDIF
      ELSE
         POSW2(J)=POSW2(J)+VELW2(J)*DT
      ENDIF
 1230 CONTINUE
cc      write(3,*)'1230'
C
C *** CALCULATE FLOW FRICTION BEHIND PROJECTILE
C
      FD=0.
      IF (INVIS1.EQ.0)GOTO 1236
      DO 1235 J=LL,I
         IF (POSW(J+1).LT.0.)GOTO 1235
         MU=MUREF*(TEMP(J)/TREF)**(1.5)*(TREF+S)/(TEMP(J)+S)
         RED=RHO(J)*UF(J)*DIA/MU
         IF (RED.LT.3500.)RED=3500.
         CF=(-3.6*LOG(6.9/RED))**(-2.)*INVIS1
         IF (J.NE.I)THEN
            IF (POSW(J).LT.0.)THEN
               FD=POSW(J+1)*PERI*CF*0.5*RHO(J+1)*UF(J+1)**2.
            ELSE
               FD=(POSW(J+1)-POSW(J))*PERI*CF*0.5*RHO(J+1)*
     +            UF(J+1)**2.
            ENDIF
         ELSE
            FD=(POSZ-POSW(J))*PERI*CF*0.5*RHO(J+1)*UF(J+1)**2.
         ENDIF
         P(J+1)=P(J+1)-FD/AREA
         IF(P(J+1).LE.0)P(J+1)=1.0E-6
         DP(J)=P(J+1)-P(J)
cc         write(3,*)j,cf,fd,p(j+1),p(j)
         IF (DP(J).GT.0.0)THEN
            VELW(J)=UF(J)-A(J)*((GAMMA+1.)/(2.*GAMMA)*
     +              ((P(J)+DP(J))/P(J)-1.)+1.)**.5
         ELSE
            VELW(J)=UF(J)-A(J)
         ENDIF
         UTEMP=UF(J+1)
         DUF=-DP(J)/(UF(J)-VELW(J))/RHO(J)
         UF(J+1)=UF(J)+DUF
         TEMP(J+1)=TEMP(J+1)+(UTEMP**2.-UF(J+1)**2.)/(2.*CP)+
     +             FD*UF(J+1)/CP*DT
         IF (TEMP(J+1).LE.0.) TEMP(J+1)=1.
```

```
cc          RHO(J+1)=RHO(J)*(UF(J)-VELW(J))/(UF(J+1)-VELW(J))
          RHO(J+1)=P(J+1)/(R*TEMP(J+1))
          IF (RHO(J+1).LT.0.0001)RHO(J+1)=0.0001
          A(J+1)=(GAMMA*R*TEMP(J+1))**0.5
 1235 CONTINUE
C
C *** CALCULATE FLOW FRICTION AHEAD OF PROJECTILE
C
 1236 IF (INVIS2.EQ.0)GOTO 1246
      FD2=0.0
      DO 1245 J=KK,I
cc          IF (POSW2(J+1).GT.(LLGG+LRG))GOTO 1245
         MU=MUREF*(TEMP2(J)/TREF)**(1.5)*(TREF+S)/(TEMP2(J)+S)
         RED=RHO2(J)*UP(J)*DIA/MU
         IF (RED.LT.3500.)RED=3500.
         CF2=(-3.6*LOG(6.9/RED))**(-2.)
         IF (J.NE.I)THEN
cc            IF (POSW(J).GT.(LLGG+LRG))THEN
cc               FD2=((LLGG+LRG)-POSW2(J+1))*PERI*CF2*0.5*
cc     +               RHO2(J+1)*UP(J+1)**2.
cc            ELSE
               FD2=(POSW2(J)-POSW2(J+1))*PERI*CF2*0.5*
     +               RHO2(J+1)*UP(J+1)**2.
cc            ENDIF
         ELSE
            FD2=(POSW2(J)-(X1+LP))*PERI*CF2*0.5*RHO2(J+1)*UP(J+1)**2.
         ENDIF
         P2(J+1)=P2(J+1)-FD2/AREA
         IF(P2(J+1).LE.0)P2(J+1)=1.0E-6
         DP2(J)=P2(J+1)-P2(J)
         IF (DP2(J).GT.0.0)THEN
            VELW2(J)=UP(J)+A2(J)*((GAMMA+1.)/(2.*GAMMA)*
     +               ((P2(J)+DP2(J))/P2(J)-1.)+1.)**.5
         ELSE
            VELW2(J)=UP(J)+A2(J)
         ENDIF
         UTEMP=UP(J+1)
         DUP=DP2(J)/RHO2(J)/(VELW2(J)-UP(J))
         UP(J+1)=UP(J)+DUP
         TEMP2(J+1)=TEMP2(J+1)+(UTEMP**2.-UP(J+1)**2.)/(2.*CPLG)+
     +               FD2*UP(J+1)/CP*DT
         IF (TEMP2(J+1).LE.0.) TEMP2(J+1)=1.
         RHO2(J+1)=RHO2(J)*(VELW2(J)-UP(J))/(VELW2(J)-UP(J+1))
         RHO2(J+1)=P2(J+1)/(RLG*TEMP2(J+1))
         IF (RHO2(J+1).LT.0.0001)RHO2(J+1)=0.0001
         A2(J+1)=(GAMMA*RLG*TEMP2(J+1))**0.5
 1245 CONTINUE
C
C *** ASSIGN FLOW CONDITIONS TO AXIAL STATION BEHIND PROJECTILE
C
 1246 DO 1250 J=LL,I
         K=INT(POSW(J)*1000.)
         IF (J.EQ.I) THEN
            L=INT((X1-LARM)*1000.)
         ELSE
            L=INT(POSW(J+1)*1000.)
```

```
         ENDIF
         IF (K.LT.0)K=0
         IF (L.LT.0) GOTO 1250
         DO 1240 M=K,L
            UX(M)=UF(J+1)
            PX(M)=P(J+1)
            TX(M)=TEMP(J+1)
            RHOX(M)=RHO(J+1)
 1240    CONTINUE
 1250 CONTINUE
cc      write(3,*)'1250'
C
C *** ASSIGN FLOW CONDITIONS TO AXIAL STATION IN FRONT OF PROJECTILE
C
      DO 1270 J=KK,I
         L=INT(POSW2(J)*1000.)
         IF (J.EQ.I) THEN
            K=INT((X1+LP)*1000.)
         ELSE
            K=INT(POSW2(J+1)*1000.)
         ENDIF
         IF (L.GT.IEXIT)L=IEXIT
         IF (K.GT.IEXIT) GOTO 1270
         DO 1260 M=K,L
            UX(M)=UP(J+1)
            PX(M)=P2(J+1)
            TX(M)=TEMP2(J+1)
            RHOX(M)=RHO2(J+1)
 1260    CONTINUE
 1270 CONTINUE
cc      write(3,*)'1270'
C
C *** ASSIGN P, T, RHO AND U PROPERTIES AT PROJECTILE
C
      K=INT((X1-LARM)*1000.)
      L=INT((X1+LP)*1000.)
      DO 1275 M=K,L
         UX(M)=UP(I)
         PX(M)=(P2(I+1)-P(I+1))/FLOAT(L-K)*FLOAT(M-K)+P(I+1)
         TX(M)=(TEMP2(I+1)-TEMP(I+1))/FLOAT(L-K)*FLOAT(M-K)+TEMP(I+1)
         RHOX(M)=(RHO2(I+1)-RHO(I+1))/FLOAT(L-K)*FLOAT(M-K)+RHO(I+1)
 1275 CONTINUE
cc      write(3,*)'1275'
      I=I+1
      PRINT *, I,ll,kk,X1,V1
C
C *** DETERMINE IF PROJECTILE HAS PASSED RAILGUN BORE EXIT
C
      IF (X1.GT.(LLGG+LRG))GOTO 1290
C
C *** STORE DATA IN DATA ARRAY FOR EVENTUAL OUTPUT
C
      IF (MOD(I,IV).EQ.0)THEN
         II=II+1
         TT(II)=T
         DATA(1,II)=X1
```

```
         DATA(2,II)=V1
         DATA(3,II)=RI1
         DATA(4,II)=RI2
         DATA(5,II)=P(I)*AREA
         DATA(6,II)=P2(I)*AREA
         DATA(7,II)=F1
         DATA(8,II)=MDOT*V1
         DATA(9,II)=MZ
         DATA(10,II)=EDIS
         DATA(11,II)=ERAD
         DATA(12,II)=TZ
         DATA(13,II)=D1
         DATA(14,II)=LARM
         DATA(15,II)=VELZ
         DATA(16,II)=POSZ
         DATA(17,II)=POSW(LL)
         DATA(18,II)=POSW2(KK)
         DATA(19,II)=PX(IPT1)/6891.1564
         DATA(20,II)=PX(IPT2)/6891.1564
      ENDIF
C
C *** OUTPUT TIME, POSITION, AND VELOCITY OF EACH WAVE WITHIN RAILGUN
C
cc       IF (MOD(I,IV).EQ.0)THEN
cc          DO 1280 N=LL,I
cc             IF (PWP(N).NE.0.0)THEN
cc                WRITE(1,2000) T,POSW(N),VELW(N),ll,n
cc             ENDIF
cc 1280     CONTINUE
cc          DO 1282 N=KK,I
cc             IF (PWP2(N).NE.0.0)THEN
cc                WRITE(1,2000) T,POSW2(N),VELW2(N)
cc             ENDIF
cc 1282     CONTINUE
cc          WRITE(1,2000)T,X1,V1,i
cc       ENDIF
C
C *** INCREMENT TIME BY DT AND PROCEED WITH NEXT ITERATION
C
      T=T+DT
      GOTO 1150
 1290 CONTINUE
C
C *** OPEN OUTPUT FILES, OUTPUT DATA, AND END PROGRAM
C
      DO 1300 J=1,20
         PRINT *,FNAME(J)
         OPEN (10,FILE=FNAME(J),FORM='UNFORMATTED',STATUS='UNKNOWN')
         IF (J.LE.18.AND.J.NE.2.AND.J.NE.3.AND.J.NE.4.AND.J.NE.15)THEN
            WRITE(10)II,(TT(JJ)-TFUSE,DATA(J,JJ),JJ=1,II)
         ELSE
            IF (J.EQ.2.OR.J.EQ.3.OR.J.EQ.4.OR.J.EQ.15)THEN
               WRITE(10)II,(TT(JJ)-TFUSE-TDELAY,DATA(J,JJ),JJ=1,II)
            ELSE
               WRITE(10)II,((TT(JJ)-TFUSE)*1000.,DATA(J,JJ),JJ=1,II)
            ENDIF
```

```
          ENDIF
          CLOSE(10)
 1300 CONTINUE
      CLOSE(3)
cc 2000 FORMAT (1X,F8.5,F8.3,F9.2,i4,i4)
 2100 FORMAT (1X,F8.5,F8.5,F9.4,i4,i4)
      END
C
C *** SUBROUTINE VCAPACITOR TO CALCULATE VOLTAGE WITH A CAPACITOR
C
      SUBROUTINE VCAPACITOR(ICROWBAR,VCI,C,RI,DT,T,TCROW)
         REAL VCI,C,RI,DT,T,TCROW
         INTEGER ICROWBAR
         IF (ICROWBAR.EQ.1)THEN
            IF (T.GE.TCROW)THEN
               ICROWBAR=-1
               VCI=0.0
            ELSE
               VCI=VCI-(1./C)*RI*DT
            ENDIF
         ENDIF
      RETURN
      END
C
C *** SUBROUTINE VOLTAGE TO CALCULATE VOLTAGE ACROSS ARMATURE
C
      SUBROUTINE VOLTAGE(RI,V1,VF,VO,RE,AX,AO)
         REAL VF,VO,RE,AO,AAA,AX,RI
         IF (RI.LE.AX) THEN
            V1=RE*RI
         ELSE
            AAA=RI+AO
            V1=VO*LOG(AAA)+VF
         ENDIF
      RETURN
      END
```

APPENDIX C: Sample Data File for Railgun Model Program

.00098	MASS OF PROJECTILE (KG)	- PMASS
.0001	MASS OF FUSE	- MZ
.015	PROJECTILE LENGTH (M)	- LP
.01	BORE DIAMETER (M)	- DIA
1.1	LENGTH OF LIGHT GAS GUN (M)	- LLGG
2.38	LENGTH OF RAILGUN (M)	- LRG
1.060	AXIAL POSITION OF PT1 (M)	- XPT1
1.100	AXIAL POSITION OF PT2 (M)	- XPT2
4.	MOLECULAR WEIGHT OF LIGHT GAS (AMU)	- WLG
63.54	MOLECULAR WEIGHT OF RAIL MATERIAL (AMU)	- WR
5192.6	COEFF OF SPECIFIC HEAT OF HE (J/KG/K)	- CPLG
411.2	COEFF OF SPECIFIC HEAT OF CU (J/KG/K)	- CPR
1.67	RATIO OF SPECIFIC HEATS FOR LIGHT GAS	- GAMMA
1.000	RATIO OF SPECIFIC HEATS FOR ARMATURE	- GMMZ
298.	INITIAL RESERVOIR TEMPERATURE (K)	- TEMP
298.	INITIAL IN-BORE GAS TEMPERATURE (K)	- TEMP2
22.06336E6	INITIAL RESERVOIR PRESSURE (Pa)	- P(1)
50.65E3	INITIAL INBORE GAS PRESSURE (Pa)	- P2(1)
.000005	TIME INCREMENT (SEC)	- DT
0.	INVISCID (0), VISCOUS (1) DRIVING GAS	- INVIS1
0.	INVISCID (0), VISCOUS (1) IN-BORE GAS	- INVIS2
11.7E-6	INDUCTANCE OF INNER RAIL CIRCUIT (H)	- LO1
11.7E-6	INDUCTANCE OF OUTER RAIL CIRCUIT (H)	- LO2
.289E-6	INNER RAIL SELF INDUCTANCE (H/M)	- LP1
.295E-6	OUTER RAIL SELF INDUCTANCE (H/M)	- LP2
0.0	RAIL COUPLING COEFFICIENT	- KAPPA
0.05	ARMATURE RESISTANCE (OHMS)	- RES
2.3E-3	RESISTANCE OF INNER CIRCUIT (OHMS)	- R1
3.4E-3	RESISTANCE OF OUTER CIRCUIT (OHMS)	- R2
1.0	FIRING VOLTAGE (V)	- VF1
13.3	FIRING VOLTAGE (V)	- V01
4.8E-3	CAPACITANCE OF INNER RAIL CIRCUIT (F)	- C1
4.8E-3	CAPACITANCE OF OUTER RAIL CIRCUIT (F)	- C2
3.69E+3	INITIAL CHARGE ON INNER RAIL CAPACITORS (V)	- VC1
0.0E+3	INITIAL CHARGE ON OUTER RAIL CAPACITORS (V)	- VC2
4.6E-4	TIME INNER RAIL CAPACITOR CROWBARS (SEC)	- TCROW1
4.13E-4	TIME OUTER RAIL CAPACITOR CROWBARS (SEC)	- TCROW2
.000125	DELAY TIME FROM WHEN PROJECTILE REACHES PT1 (SEC)	- TDELAY
0.00000	DELAY TIME BETWEEN OUTER AND INNER RAIL (SEC)	- TFIRE
0.000	ARMATURE FRICTION COEFFICIENT	- CFARM
273.	LIGHT GAS REFERENCE TEMPERATURE (K)	- TREF
144.	LIGHT GAS CHARACTERISTIC TEMPERATURE (K)	- S
1.97E-5	LIGHT GAS REFERENCE ABSOLUTE VISCOSITY (N*S/M^2)	- MUREF
3.E-8	ABLATION COEFFICIENT	- ALPHA
0.400	POWER DISSIPATION COEFFICIENT	- BETA
1.000	EMISSIVITY COEFFICIENT	- EPS
1.000	ABLATION ENTRAINMENT COEFFICIENT	- LAMBDA
999.	END FLAG	

VITA

John K. Foster was born in Lumberton, North Carolina on April 9, 1967. He attended elementary schools in Claxton, Madison, Hendersonville, and Morristown, Tennessee. He attended high school at Morristown-Hamblen High School East and graduated in 1985.

He then attended the University of Tennessee, Knoxville where he received his Bachelor of Science in Aerospace Engineering and graduated with high honors in May 1990. While attending the University of Tennessee, he participated in the cooperative education program with McDonnell Douglas in St. Louis and performed 8 industrial periods with that company. He then attended the University of Tennessee Space Institute where he worked as a graduate research assistant as he pursued his graduate work. He received his Master of Science degree in Aerospace Engineering in May 1993.

He is presently a design engineer and principle investigator of the Environmental Control System IRAD (Independent Research and Development) Task for McDonell Douglas Aerospace Company, St. Louis, Missouri.